

**HYPOXIC AND LOW PH WATER IN THE NEARSHORE  
MARINE ENVIRONMENTS OF MONTEREY BAY,  
CALIFORNIA: CHARACTERIZING A DECADE OF OXYGEN  
AND PH, AND DRIVERS OF VARIABILITY**

---

A Thesis

Presented to the

Faculty of the

Moss Landing Marine Laboratories

California State University Monterey Bay

---

In Partial Fulfillment

of the Requirements for the Degree

Master of Science

---

by

J. Ashley Tomer Booth

Summer 2011

**CALIFORNIA STATE UNIVERSITY MONTEREY BAY**

The Undersigned Faculty Committee Approves the

Thesis of J. Ashley Tomer Booth:

HYPOXIC AND LOW PH WATER IN THE NEARSHORE MARINE  
ENVIRONMENTS OF MONTEREY BAY, CALIFORNIA:  
CHARACTERIZING A DECADE OF OXYGEN AND PH, AND DRIVERS OF  
VARIABILITY



---

Erika McPhee-Shaw, Chair  
Moss Landing Marine Laboratories

---

Laurence Breaker  
Moss Landing Marine Laboratories



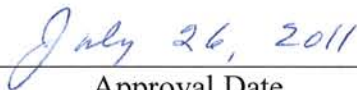
---

William Gilly  
Hopkins Marine Station of Stanford University, Pacific Grove



---

Marsha Moroh, Dean  
College of Science, Media Arts, and Technology



---

Approval Date

**CALIFORNIA STATE UNIVERSITY MONTEREY BAY**

The Undersigned Faculty Committee Approves the

Thesis of *J. Ashley Tomer Booth*:

**HYPOXIC AND LOW PH WATER IN THE NEARSHORE MARINE  
ENVIRONMENTS OF MONTEREY BAY, CALIFORNIA:  
CHARACTERIZING A DECADE OF OXYGEN AND PH, AND DRIVERS OF  
VARIABILITY**

---

Erika McPhee-Shaw, Chair  
Moss Landing Marine Laboratories



---

Laurence Breaker  
Moss Landing Marine Laboratories

---

William Gilly  
Hopkins Marine Station of Stanford University, Pacific Grove

---

Marsha Moroh, Dean  
College of Science, Media Arts, and Technology

---

Approval Date



Copyright © 2011

by

J. Ashley Tomer Booth

All Rights Reserved

Waves on top of waves  
Upwelling from the cold deep  
A breathless balance

## ABSTRACT

Hypoxic and low pH water in the nearshore marine environments of Monterey Bay, California: Characterizing a decade of oxygen and pH, and drivers of variability

by

J. Ashley Tomer Booth

In Partial Fulfillment of the Requirements for the Degree Master of Science

Moss Landing Marine Laboratories, California State University  
Monterey Bay, 2011

A decade-long time series recorded in southern Monterey Bay, California demonstrates that the shallow, near-shore environment (17 m depth) is regularly inundated with pulses of cold, hypoxic and low pH water. During these episodes, oxygen can drop to biologically threatening levels, and pH levels were lower than expected. Weekly water chemistry monitoring revealed that the saturation state of aragonite (the more soluble form of calcium carbonate) was often below saturation and had a moderate positive relationship with pH, however, analytical and human error could be high. Pulses of hypoxia and low pH water with the greatest intensity arise at the onset of the spring upwelling season, and fluctuations are strongly semidiurnal (tidal) and diurnal. Arrival of cold, hypoxic water on the inner shelf typically occurs 3 days after the arrival of a strong upwelling event and appears to be driven by upwelling modulated by internal tidal fluctuations. I found no relationship between the timing of low-oxygen events and the diel solar cycle nor with terrestrial nutrient input. These observations are consistent with advection of hypoxic water from the deep, offshore environment where water masses experience a general decline of temperature, oxygen and pH with depth, and inconsistent with biochemical forcing. Comparisons with concurrent temperature and oxygen time series taken ~20 km away at the head of the Monterey Canyon show similar patterns but even more intense hypoxic events due to stronger semidiurnal forcing there. Analysis of the durations of exposure to low oxygen levels establishes a framework for assessing the ecological relevance of these events. Increasing oceanic hypoxia and acidification of both surface and deep waters may increase the number, intensity, duration and spatial extent of future intrusions along the Pacific coast. Evaluation of the resiliency of nearshore ecosystems such as kelp forests, rocky reefs and sandy habitats, will require consideration of these events.

## TABLE OF CONTENTS

ABSTRACT .....	vi
LIST OF TABLES .....	ix
LIST OF FIGURES .....	x
ACKNOWLEDGEMENTS.....	xix
Introduction .....	19
Background .....	20
Marine Oxygen and pH.....	20
Climate Change and Increasing CO <sub>2</sub> .....	25
Internal tides, internal waves and Monterey Bay, California.....	26
Methods.....	28
Oceanographic Measurements.....	28
Water Monitoring at the Monterey Bay Aquarium and Moss Landing Marine Laboratories .....	28
Monterey Bay Aquarium Weekly Spot-Checks .....	33
Assessing Error.....	35
Error at the Monterey Bay Aquarium .....	35
Comparison between Monterey Bay Aquarium measurements and independent mooring and water profiles .....	37
Error at the Moss Landing Marine Laboratories.....	39
Quality Control .....	40
What has been the state of oxygen, pH and temperature in the nearshore environment of the southern Monterey Bay over the past decade? Do oxygen and pH levels drop to biologically stressful levels?.....	42
Results .....	42
A decade and a half of seawater monitoring in the nearshore habitat of southern Monterey Bay.....	42
Nearshore Oxygen in Southern Monterey Bay.....	46
Nearshore pH in Southern Monterey Bay .....	51
Comparing Dissolved Oxygen, Temperature and pH in Southern Monterey Bay.....	51

Seasonal Patterns of Variability.....	57
Carbonate Chemistry.....	59
Water Profiles.....	64
What are the dominant time scales of high variability in oxygen and pH? What are the relationships between the measured variables and underlying drivers of system variability? Are there any trends in the time series? .....	66
Analysis and Results.....	66
Seasonal Patterns.....	66
Spectral Analysis.....	68
Short-Term Variability.....	73
Empirical Mode Decomposition of MBA Time Series.....	75
MBA Temperature IMF 12 and ENSO.....	86
Long-term Trends at MBA.....	87
Comparison Between an Upwelling Index and MBA Measurements.....	87
Depth of Advected Offshore Source Waters.....	92
Are there differences between southern and central Monterey Bay? And if so, why? .....	95
Methods Review.....	95
Analysis and Results.....	95
Temperature and dissolved oxygen at MBA and MLML seawater intakes.....	95
EEMD of MLML Temperature.....	98
Conclusions and Discussion.....	107
REFERENCES.....	114

**LIST OF TABLES**

Table 1 Seawater monitoring start dates at the Monterey Bay Aquarium (MBA) and Moss Landing Marine Laboratories (MLML). .....	30
Table 2 High Resolution Water Monitoring Quality Control Limits.....	40
Table 3 Inter-lab comparison of carbonate chemistry. Total CO <sub>2</sub> (TCO <sub>2</sub> ) and pH samples measured at the Monterey Bay Aquarium (MBA) and by Dr. Jim Barry's lab at the Monterey Bay Aquarium Research Institution (MBARI). MBARI pH measurements measured converted from Total scale to NBS scale using CO2SYS. ....	61

## LIST OF FIGURES

Figure 1 Map of Pacific oxygen levels at 200 m depth. Dark purple indicates oxygen levels below 0.64 mg/L, the Oxygen Minimum Zone (OMZ). Black indicates no data. Data from World Ocean Database 2005 and map by J. A. T. Booth. ....	21
Figure 2 Diagram of dissolved oxygen concentrations in the Northeast Pacific and biological and physical forcing mechanisms. The Oxygen Minimum Zone (OMZ) is noted between 500-1,100 m. ....	22
Figure 3 Sublethal, lethal and Oxygen Minimum Zone (OMZ) oxygen levels as defined in the literature. ....	23
Figure 4 Map of California, USA and study region of Monterey Bay showing locations of sampling sites at Monterey Bay Aquarium (MBA) and Moss Landing Marine Laboratories (MLML) as well as NOAA tide sensor on the Monterey municipal wharf (NOAA) and meteorological sensors on National Data Buoy Center #46042 (NDBC). Other hydrographic data were recorded at MBARI's M1 buoy (M1), Partnership for Interdisciplinary Studies of Coastal Oceans (PISCO) mooring and at two location near the Hopkins Marine Station a CTD was moored (HMS 15 and HMS17). Bathymetric data from Seafloor Mapping Lab of California State University Monterey Bay and the California Department of Fish and Game. ....	29
Figure 5 Schematic of seawater intake plumbing and monitoring at the Monterey Bay Aquarium in Pacific Grove, California. Flow-through measurements record every 5 minutes and spot-check measurements were conducted weekly. ....	30
Table 1 Seawater monitoring start dates at the Monterey Bay Aquarium (MBA) and Moss Landing Marine Laboratories (MLML). ....	30
Figure 6 Seawater monitoring dates at the Monterey Bay Aquarium (MBA) and Moss Landing Marine Laboratories (MLML). ....	31
Figure 7 Example of several hours of MBA temperature (5 min sampling) drawn from 2 meters above bottom (m.a.b.) (black line) compared to temperature taken by several thermistors (20 sec sampling) on a PISCO mooring (36.6214°N, 121.8996°W, Figure 4). Note high frequency temperature fluctuations between 16:00 and 18:00 are not seen in mixed MBA water. ....	32
Figure 8 Schematic of MLML seawater intake system and instrumentation. ....	33
Figure 9 Oxygen ( $\text{mg L}^{-1}$ ), temperature ( $^{\circ}\text{C}$ ) and pH (NBS scale) measurements made from 1995 to 2011 (black dots). Data removed in quality control process (teal dots) and weekly spot check measurements (red dots) are also plotted. ....	34
Figure 10 Weekly spot check measurements of DO (left panel), temperature (middle panel) and pH (right panel) plotted against closest in time measurement of the	

high-resolution flow-through system. Multiple linear regressions (blue lines), 1 and 2 standard deviations around regression (blue dotted lines) and a 1:1 reference line (black dashed line) are also plotted. Multiple regression equations are written above each graph.....	35
Figure 11 High-resolution temperature plotted against difference between spot check and high resolution measurement. Mean and median difference for entire data set are plotted. ....	36
Figure 12 Deviation away from a 1:1 (red dashed line) relationship when converting between DO units using temperatures recorded at the MBA pump house and accounting for in pipe warming (blue dotted line, +1.33°C). Maximum error was just over 5 percent saturation (grey shaded area, right y-axis) at 180 percent saturation measured.....	37
Figure 13 Comparisons between the Monterey Bay Aquarium (MBA) flow-through dissolved oxygen (DO) measurements and three moored CTD (14-16m depth) deployments. Left panel depicts deployment on HMS17 mooring and middle and left panels are deployments on the more inshore HMS15. Histograms depict distribution of differences between MBA DO (with lag accounted for) and moored CTD DO.....	38
Figure 14 Time series of Monterey Bay Aquarium (MBA) flow-through dissolved oxygen (DO) measurements and three moored CTD (14-16m depth) deployments. DO over time from MBA (black dots) and moored CTD (red dots) in percent saturation.....	38
Figure 15 Dissolved oxygen (DO) water monitoring at Moss Landing Marine Laboratories (MLML). Time series of three DO sensors (October 9, 2010 to May 1, 2011): main lab aquarium (blue), shore lab scientific (black) and shore lab industrial (red).....	40
Table 2 High Resolution Water Monitoring Quality Control Limits.....	40
Figure 16 Percent of 5-minute flow-through DO (top panels, April 1, 2000 – March 25, 2011) and temperature (bottom panels, September 22, 1995 - March 25, 2011) data missing at the Monterey Bay Aquarium. Missing data percentages presented by month (left panels) and year (right panels).....	41
Figure 17 Percent of 5-minute temperature (bottom panels, December 19, 2002 - October 25, 2010) data missing at MLML. Missing data percentages presented by month (left panels) and year (right panels).....	42
Figure 18 Dissolved oxygen (top panel) and temperature (bottom panel) time series measured at the Monterey Bay Aquarium April 1, 2000 – March 28, 2011. Biologically stressful oxygen levels are indicated with the 4.6 mg L <sup>-1</sup> sublethal and 2 mg L <sup>-1</sup> lethal thresholds are indicated with red lines.....	43
Figure 20 Distribution of time at different dissolved oxygen levels in percent saturation from December 15 2003 – April 29, 2011.....	44



- Figure 21 Distribution of measurements of MBA dissolved oxygen (top panel), temperature (middle panel) and pH (bottom panel), vertical grey bars, superimposed with a fitted normal distribution (black lines). ..... 45
- Figure 22 Monthly distributions of recorded dissolved oxygen values from Monterey Bay Aquarium time series, January (1, top panel) through December (12, bottom panel). ..... 47
- Figure 23 Monterey Bay Aquarium dissolved oxygen time series April 1, 2000 to March 12, 2011 showing measurements below sublethal ( $4.6 \text{ mg L}^{-1}$ ) and lethal ( $2 \text{ mg L}^{-1}$ ) threshold (top panel). Histograms of recorded hours below sublethal (grey) and lethal (red) threshold during each year (bottom left panel) and month (bottom right panel). ..... 48
- Figure 24 Monthly distributions of durations of time spend under sublethal ( $4.6 \text{ mg L}^{-1}$ ) dissolved oxygen threshold from the Monterey Bay Aquarium time series, April 1, 2000 to March 12, 2011. Each panel is a month, January (1, top panel) through December (12, bottom panel). ..... 49
- Figure 25 Distribution of durations of time spent under sublethal ( $4.6 \text{ mg L}^{-1}$ , white bars) and lethal ( $2 \text{ mg L}^{-1}$ , grey bars) dissolved oxygen thresholds from the Monterey Bay Aquarium time series, April 1, 2000 to March 25, 2011. .... 50
- Figure 26 Dissolved oxygen time series from the Monterey Bay Aquarium flow-through system in southern Monterey Bay on several days surrounding hypoxic events reaching below the  $2 \text{ mg L}^{-1}$ . ..... 51
- Figure 26 Weekly spot check (blue asterisks) and high-resolution (black dots) measurements of pH in nearshore waters in southern Monterey Bay measured by the Monterey Bay Aquarium. Red line indicates a pH value of 7.75. .... 51
- Figure 28 Temperature plotted against dissolved oxygen from Monterey Bay Aquarium seawater intake, April 2000 to April 2011. Colors indicate month as noted in the legend. Black diagonal lines are monthly linear regressions while black horizontal lines indicate 2 and  $4.6 \text{ mg/L}$  dissolved oxygen thresholds. .... 52
- Figure 29 Monthly smoothed point densities plots of temperature plotted against dissolved oxygen from Monterey Bay Aquarium seawater intake, April 2000 to April 2011. Red diagonal lines are monthly linear regressions while black horizontal lines indicate 2 and  $4.6 \text{ mg/L}$  dissolved oxygen thresholds. .... 53
- Figure 29 Cross covariance analysis of Monterey Bay Aquarium flow-through dissolved oxygen and temperature over the entire time series, April 2000 to April 2011. .... 54
- Figure 30 Matrix of monthly correlation coefficients (color) and lags (numbers in boxes) for cross covariance analyses between Monterey Bay Aquarium (MBA) dissolved oxygen (DO) and temperature for each year, 2000-2011. White indicates insufficient data. .... 55
- Figure 31 Dissolved oxygen plotted against pH from Monterey Bay Aquarium seawater intake, September 2009 to March 2010. Colors indicate month as

	noted in the legend. Black diagonal lines are monthly linear regressions while black horizontal lines indicate 2 and 4.6 mg/L dissolved oxygen thresholds.....	56
Figure 32	Top panel, time series of normalized dissolved oxygen and pH from the Monterey Bay Aquarium September 2009 to February 2011. Bottom panel, cross covariance analysis of dissolved oxygen and pH over the entire time series. ....	56
Figure 33	Top panel, dissolved oxygen at the Monterey Bay Aquarium against day of year. All years are overlaid (colored lines) with daily mean (thick black line) and daily standard deviation (thin black line) over all years. Bottom panel, absolute value of daily standard deviation. Individual years are plotted as colored lines and mean as a thick black line. ....	58
Figure 34	Top panel, temperature at the Monterey Bay Aquarium against day of year. All years are overlaid (colored lines) with daily mean (thick black line) and daily standard deviation (thin black line) over all years. Bottom panel, absolute value of daily standard deviation. Individual years are plotted as colored lines and mean as a thick black line. ....	59
Table 3	Inter-lab comparison of carbonate chemistry. Total CO <sub>2</sub> (TCO <sub>2</sub> ) and pH samples measured at the Monterey Bay Aquarium (MBA) and by Dr. Jim Barry's lab at the Monterey Bay Aquarium Research Institution (MBARI). MBARI pH measurements measured converted from Total scale to NBS scale using CO2SYS. ....	61
Figure 35	Weekly carbonate chemistry time series conducted at the Monterey Bay Aquarium. Top panel, Total Alkalinity (TA, red), Total CO <sub>2</sub> (TCO <sub>2</sub> , black), and carbonate (CO <sub>3</sub> <sup>2-</sup> , green). Note carbonate values were increases by 2 mmol L <sup>-1</sup> to facilitate plotting on the same scale as other variables. Inter-lab comparison of TCO <sub>2</sub> by Barry lab (blue triangles). Middle panel, 5-minute pH samples from the flow-through system (green dots) and values at time of weekly 'spot check' (black circles), weekly spot check value (black line and asterisks). Inter-lab comparison of pH by Barry lab (blue triangles). Red line indicates Feely et al. 2008 7.75 threshold in pH associated with a $\Omega_{\text{arag}}$ of 1. Bottom panel, time series of $\Omega_{\text{arag}}$ estimated using TCO <sub>2</sub> and pH by CO2SYS, MBA values (black line and dots) and Barry lab (blue triangles).....	62
Figure 36	Frequency distributions of weekly discrete 'spot-check' carbonate chemistry results and associated pH values taken from flow-through time series. Red lines indicate the mean (solid) and 1 <sup>st</sup> (dashed) and 2 <sup>nd</sup> (dotted) standard deviations. ....	63
Figure 37	Saturation state of aragonite ( $\Omega$ ) plotted against pH, dissolved oxygen, temperature and date. Linear regressions are plotted as black lines Colors indicate date of sample. Black lines in lower panel show mean for upwelling (March-September) and winter (October-February) seasons.....	63
Figure 38	Box plots of carbonate chemistry samples for winter (October-February, black) and upwelling (March-September, green) seasons. ....	64

- Figure 39 Comparison between MBA oxygen time series and four CTD profiles collected within 150 m of MBA intake pipe mouth. Top panel, MBA dissolved oxygen values (black line) over several days in April 2009 and oxygen levels of four CTD casts at 17 m depth (colored asterisks). Bottom panels, four CTD profiles showing changing hydrography. Horizontal black dotted line indicated 17 m depth associated with MBA intake..... 65
- Figure 40 Running 1-day standard deviation of dissolved oxygen ( $\text{mg L}^{-1}$ ) taken by the Monterey Bay Aquarium (April 2000 – November 2010) (top panel) and NOAA upwelling index for  $36^\circ\text{N}$  ( $\text{metric tons sec}^{-1} 100 \text{ m}^{-1}$  of coastline) (middle panel) over day of year. All years are overlaid (gray lines) and day of year means are plotted in black. Bottom panel, monthly total precipitation in Monterey, CA with all years overlaid (grey lines) and monthly means across years (black line). ..... 68
- Figure 41 Autospectra of MBA dissolved oxygen (top panels) and temperature (bottom panels) using a smaller (left panels) and larger (right panels) window size used to resolve diurnal ( $K_1$ )/semidiurnal ( $M_2$ ) and seasonal frequency peaks, respectively. Peaks of interest are circled in red. Time step = 1hour. .... 69
- Figure 42 Autospectra of MBA dissolved oxygen (black) and T-Tide tidal harmonics (red) overlaid with labeled tidal constituents (green) near diurnal frequencies. Height of green tidal constituents indicates relative strength of signal. Frequency is in cycles per day (cpd) and both axes are log scale. compareMBAto2tide\_spec\_diurnal\_.png ..... 70
- Figure 43 Autospectra of MBA dissolved oxygen (black) and T-Tide tidal harmonics (red) overlaid with labeled tidal constituents (green) near semidiurnal frequencies. Height of green tidal constituents indicates relative strength of signal. Frequency is in cycles per day (cpd) and both axes are log scale..... 70
- Figure 44 Cross covariance results comparing dissolved oxygen (DO) from the Monterey Bay Aquarium (MBA) and sea surface height (SSH) from NOAA's Monterey wharf tide gauge. Colors indicate correlation coefficient and lag times are printed in hours..... 72
- Figure 45 Cross power spectra between MBA dissolved oxygen and temperature. .... 72
- Figure 46 Coherence (top panel) and phase (bottom panel) plots for MBA dissolved oxygen and temperature. Top panel, horizontal line is level of 99% significance. Bottom panel, horizontal line is at a phase of  $0^\circ$ . ..... 73
- Figure 47 Example of covariation of oxygen (solid blue record), temperature (red) and pH (dashed, black). Data are from MBA seawater intake during a series of intense hypoxic/low pH/cold episodes in April, 2010. Nighttime hours are shaded. .... 75
- Figure 48 The intrinsic mode function components (IMF) from the ensemble empirical mode decomposition (EEMD) of dissolved oxygen at the Monterey Bay Aquarium. Top panel, the original dissolved oxygen ( $\text{mg L}^{-1}$ ) time series. Bottom panels, IMF 1 through 8 in  $\text{mg O}_2 \text{ L}^{-1}$  over time. See next figure for

IMF 9-17. The EEMD was run with a ratio of the standard deviation of the added noise of 0.1 and an ensemble number of 100.....	78
Figure 49 The intrinsic mode function components (IMF) 9 through 16 ( $\text{mg O}_2 \text{ L}^{-1}$ ) from the ensemble empirical mode decomposition (EEMD) of dissolved oxygen at the Monterey Bay Aquarium. The final IMF (15) is the residual of the analysis. See pervious figure for IMF 1-8. The EEMD was run with a ratio of the standard deviation of the added noise of 0.1 and an ensemble number of 100. ....	79
Figure 50 The intrinsic mode function components (IMF) from the ensemble empirical mode decomposition (EEMD) of temperature at the Monterey Bay Aquarium. Top panel, the original temperature ( $^{\circ}\text{C}$ ) time series. Bottom panels, IMF 1 through 8 in $^{\circ}\text{C}$ over time. See next figure for IMF 9-16. The EEMD was run with a ratio of the standard deviation of the added noise of 0.1 and an ensemble number of 100.....	80
Figure 51 The intrinsic mode function components (IMF) 9 through 16 ( $^{\circ}\text{C}$ ) from the ensemble empirical mode decomposition (EEMD) of temperature at the Monterey Bay Aquarium. The final IMF (16) is the residual of the analysis. See pervious figure for IMF 1-8.....	81
Figure 52 The percent of variance and variance of each intrinsic mode function components 1 through 16 from the ensemble empirical mode decomposition (EEMD) of dissolved oxygen at the Monterey Bay Aquarium. The EEMD was run with a ratio of the standard deviation of the added noise of 0.1 and an ensemble number of 100. Estimated periods are denoted below each mode number, see Figure 54.....	82
Figure 53 The percent of variance and variance of each intrinsic mode function components 1 through 17 (units of $(^{\circ}\text{C})^2$ ) from the ensemble empirical mode decomposition (EEMD) of temperature at the Monterey Bay Aquarium. The EEMD was run with a ratio of the standard deviation of the added noise of 0.1 and an ensemble number of 100. Estimated periods are denoted below each mode number, see Figure 55.....	83
Figure 54 Distribution of differences between peaks of each intrinsic mode function components (IMF) 1 through 15 from the ensemble empirical mode decomposition (EEMD) of dissolved oxygen at the Monterey Bay Aquarium. The median ‘period’ for each IMF is displayed above each distribution plot. The EEMD was run with a ratio of the standard deviation of the added noise of 0.1 and an ensemble number of 100.....	84
Figure 55 Distribution of differences between peaks of each intrinsic mode function components (IMF) 1 through 15 from the ensemble empirical mode decomposition (EEMD) of temperature at the Monterey Bay Aquarium. The median ‘period’ for each IMF is displayed above each distribution plot. The EEMD was run with a ratio of the standard deviation of the added noise of 0.1 and an ensemble number of 100.....	85

Figure 56 MBA Temperature IMF 11+12, Oceanic Niño Index (ONI) and Northern Oscillation Index (NOI) comparison. IMF 11 + 12 over time overlaid with ONI and NOI.....	87
Figure 57 Example of event based analysis of upwelling influence on oxygen, temperature and ph at the Monterey Bay Aquarium from January 12-27 <sup>th</sup> 2011. The Bakun Upwelling Index (BUI) is plotted in blue (metric tons/sec/100m of coastline) and a vector plot of offshore wind from the NDBC buoy #46042 in black.....	88
Figure 58 Cross covariance results comparing the daily standard deviation of Monterey Bay Aquarium (MBA) dissolved oxygen (DO) to the NOAA Bakun Upwelling Index (BUI). Black dot and labels indicate lag time (days) at strongest correlation coefficient.....	90
Figure 59 Yearly cross covariance analysis results comparing the daily standard deviation of Monterey Bay Aquarium (MBA) dissolved oxygen (DO) to the NOAA Bakun Upwelling Index (BUI). Black dots and labels indicate lag time (days) at strongest correlation coefficient.....	91
Figure 60 Matrix of monthly correlation coefficients (color) and lags (numbers in boxes) for cross covariance analyses between the daily standard deviation of Monterey Bay Aquarium (MBA) dissolved oxygen (DO) and the Bakun Upwelling Index (BUI) for each year, 2000-2011. White indicates insufficient data.....	92
Figure 61 Auto-spectra of temperature measurements recorded from October 20, 2009 through October 27, 2010 at different depths along the Monterey Bay Aquarium Research Institution's M1 mooring (colored lines). Dominant tidal constituents are labeled. Plotted in log-log space, frequency in cycles per day (cpd).....	93
Figure 62 Temperature measurements recorded from October 20, 2009 through October 27, 2010 at the Monterey Bay Aquarium seawater intake (black dashed line) and at different depths along the Monterey Bay Aquarium Research Institution's M1 mooring (colored lines).....	94
Figure 63 Example Monterey Bay Aquarium (black) and Moss Landing Marine Laboratories (green) dissolved oxygen (top panel) and temperature (bottom panel) over several days in March 2011.....	96
Figure 64 Top panel, time series of Monterey Bay Aquarium (black) and Moss Landing Marine Laboratories (green) temperature. Bottom panel, A cross covariance between DO and temperature over the entire time series, December 2002 to October 2010.....	97
Figure 65 Running 1-day standard deviation of temperature at Monterey Bay Aquarium (top panel) and Moss Landing Marine Laboratories (bottom panel). All years are overlaid (colored lines) and day of year average over all years (black line).....	98

Figure 66 Monterey Bay Aquarium (black) and Moss Landing Marine Laboratories (green) dissolved oxygen and temperature time series, October 9, 2010 to May 1, 2011. Oxygen sublethal ( $4.6 \text{ mg L}^{-1}$ ) and lethal ( $2 \text{ mg L}^{-1}$ ) thresholds are shown in red. ....	98
Figure 67 Distribution of measurements of MLML temperature (vertical grey bars) superimposed with a fitted normal distribution (black lines). ....	99
Figure 68 The variance of each intrinsic mode function components (IMF) 1 through 16 (units of $(^{\circ}\text{C})^2$ ) from the ensemble empirical mode decomposition (EEMD) of temperature at the Moss Landing Marine Laboratories (MLML). The EEMD was run with a ratio of the standard deviation of the added noise of 0.7 and an ensemble number of 100. ....	100
Figure 69 Distribution of differences between peaks of each intrinsic mode function components (IMF) 1 through 16 from the ensemble empirical mode decomposition (EEMD) of temperature at the Moss Landing Marine Laboratories (MLML). The EEMD was run with a ratio of the standard deviation of the added noise of 0.7 and an ensemble number of 100. The median ‘period’ for each IMF is displayed above each distribution plot. ....	101
Figure 70 The intrinsic mode function components (IMF) from the ensemble empirical mode decomposition (EEMD) of temperature at the Moss Landing Marine Laboratories (MLML) December 2002 – October 2010. Top panel, the original temperature ( $^{\circ}\text{C}$ ) time series. Bottom panels, IMF 1 through 7 in $^{\circ}\text{C}$ over time. See next figure for IMF 9-16. The EEMD was run with a ratio of the standard deviation of the added noise of 0.7 and an ensemble number of 100. ....	102
Figure 71 The intrinsic mode function components (IMF) 8 through 14 ( $^{\circ}\text{C}$ ) from the ensemble empirical mode decomposition (EEMD) of temperature at the Moss Landing Marine Laboratories (MLML) December 2002 – October 2010. The final IMF (16) is the residual of the analysis. See pervious figure for IMF 1-7. The EEMD was run with a ratio of the standard deviation of the added noise of 0.7 and an ensemble number of 100. ....	103
Figure 72 Auto-spectra of Monterey Bay Aquarium (MBA, top panels) and Moss Landing Marine Laboratories (MLML) temperature (bottom panels) using a smaller (left panels) and larger (right panels) window size used to resolve diurnal/semidiurnal and seasonal frequency peaks, respectively. Peaks of interest are circled in red. Time step = 1hour. ....	105
Figure 73 Auto-spectra of Monterey Bay Aquarium (MBA, black) and Moss Landing Marine Laboratories (MLML, green) temperature and tidal constituents (blue). Plotted in log-log space, frequency is in cycles per day (cpd). Selected tidal constituents are labeled. ....	105
Figure 74 Cross power spectra between Monterey Bay Aquarium (MBA) and Moss Landing Marine Laboratories (MLML) temperature. ....	106

- Figure 75 Coherence (top panel) and phase (bottom panel) plots for Monterey Bay Aquarium (MBA) and Moss Landing Marine Laboratories (MLML) temperature. Top panel, horizontal line is level of 99% significance. Bottom panel, horizontal line is at a phase of  $0^\circ$ . ..... 107
- Figure 76 Schematic of average low DO/ low pH event in the nearshore of southern Monterey Bay (Monterey Bay Aquarium) over a 24 hour period at ~17 m depth. Center plot shows the DO/pH/temperature signal fluctuating with the semidiurnal internal tide. Additional axes indicated different oxygen units and the associated pH and temperature ranges. Far right labels show origin of the water sampled..... 109
- Figure 77 Schematic of cold, hypoxic and low pH water transport into nearshore. Right panel illustrates the winter, non-upwelling season when hypoxic water is deep and the mixed layer is deep. The water advected inshore by internal tidal motions is similar to surface waters. The left panel, shows upwelling conditions where deep cold, hypoxic water is shallow enough for the internal tide to transport it inshore. .... 111

## ACKNOWLEDGEMENTS

I would like to thank Erika McPhee-Shaw for being not just a knowledgeable and supportive advisor but a friend too. Her invaluable advice and direction has enriched my academic, professional and personal life. I thank William Gilly for his unwavering support and keen writing and thinking-outside-the-box contributions. Larry Breaker's enthusiasm for this project and time series analysis is contagious and I have really enjoyed our time tinkering around together. I could not have done this project without immeasurable assistance from Paul Chua and Eric Kingsley. They have been my partners in crime on the nitty-gritty parts of chemical analyses, data processing and data management. Roger Phillips has been key in coordinating this project and, without him, I would not have had access to these unique data. Craig Hunter was a tremendous asset in managing the MLML data. I would like to thank Steven Bograd, Brock Woodson, Louis Zeidberg, Mark Denny, Kenneth Coale, and Lisa Levin for valuable advice and discussions. My lab mates at both Hopkins and MLML have been true friends, Julie Stewart, Danna Staaf, Judit Pungor, Shandy Buckley, Tanya Novak, Katie Morrice, Melinda Nakagawa, and Dustin Carroll. Last but not least, I want to thank my parents, family and wonderful roommate, Kris Ingram, for their unwavering support.



## INTRODUCTION

Recent studies have reported marked decreases in midwater oxygen (Bograd et al. 2008; Stramma et al. 2008; Stramma et al. 2010) and increases in acidification from anthropogenic carbon dioxide (Caldeira and Wickett 2003; Orr et al. 2005; Feely et al. 2008) both globally and in the California Current System (CCS). It is important to understand situations where natural hypoxia and low pH occur in order to understand ecosystem variability, biological tolerances and to prevent additive or synergistic effects with anthropogenic hypoxia and acidification.

The Monterey Bay Aquarium has been monitoring the temperature of its raw seawater drawn from the adjacent kelp bed at 17 m depth since it opened in 1984. In July of 1999, the MBA experienced a hypoxia-induced fish die-off in a tank fed with raw seawater. An oxygen sensor was installed to warn of future hypoxic exposure. This incident and other hypoxic events that occurred in the last decade raise many questions. Are these events anthropogenically or naturally derived? What is the frequency of occurrence and has it changed over time? What factors in the system dictate when these events occur? Are there precursors? What is the spatial extent of the nearshore hypoxia? How is the coastal ecosystem affected by hypoxic waters?

After some preliminary analysis of these time series, a continuously sampling oxygen sensor was installed at the nearby Moss Landing Marine Laboratories (MLML) where temperature was already being recorded and monitoring of pH and carbonate chemistry was initiated at the MBA to further characterize the spatial extent and chemical composition of the hypoxic water. The research presented here is divided up to address the following questions:

- What has been the state of oxygen, pH and temperature in the nearshore environment of the southern Monterey Bay over the past decade? Do oxygen and pH levels drop to biologically stressful levels?
- What are the dominant time scales of high variability in oxygen and pH? What are the relationships between the measured variables and underlying drivers of system variability? Are there any trends in the time series?

- Are there differences between southern and central Monterey Bay? And if so, why?

## **BACKGROUND**

### **Marine Oxygen and pH**

The dissolved oxygen (DO) content of the ocean ranges from ~0-13 mg/L and is controlled by both physical and biological processes. Physical mixing aerates surface waters, increasing oxygen concentrations. Deep ocean circulation allows for ventilation of deep basin waters, and low carbon input to these depths creates a low oxygen demand keeping oxygen above hypoxic levels. In some productive upwelling regions like eastern coastal boundary currents (explained further below) and equatorial divergence zones, high surface nutrient concentrations can lead to biologically induced depletion of oxygen (Figure 1) through the following process: When nutrients are introduced to surface waters, they induce phytoplankton growth and photosynthesis, which supersaturate oxygen in the surface mixed layer. When these organisms die and sink, aerobic decomposition occurs utilizing DO and generating carbon dioxide (Wyrski 1962; Sarmiento et al. 1988; Diaz 2001). In the midwaters below productive regions off Western North America and in the Eastern Pacific equatorial divergence zone, cumulative oxygen depletion has occurred. Deeper water is not as affected as much, because most of the surface productivity is consumed before this organic material reaches these depths, thus creating an oxygen minimum at midwater depths (Figure 2). These hypoxic midwaters have been termed Oxygen Minimum Zones (OMZ) and occur between ~100 to 1500 m with oxygen levels less than 10% of surface values (Aydin et al. 2004; Helly and Levin 2004). The OMZ is defined by DO levels lower than 20  $\mu\text{mol/kg}$  (0.64 mg/L), a concentration where bacterial aerobic respiration changes to primarily anaerobic (Paulmier and Ruiz-Pino 2009; Seibel, in prep.).

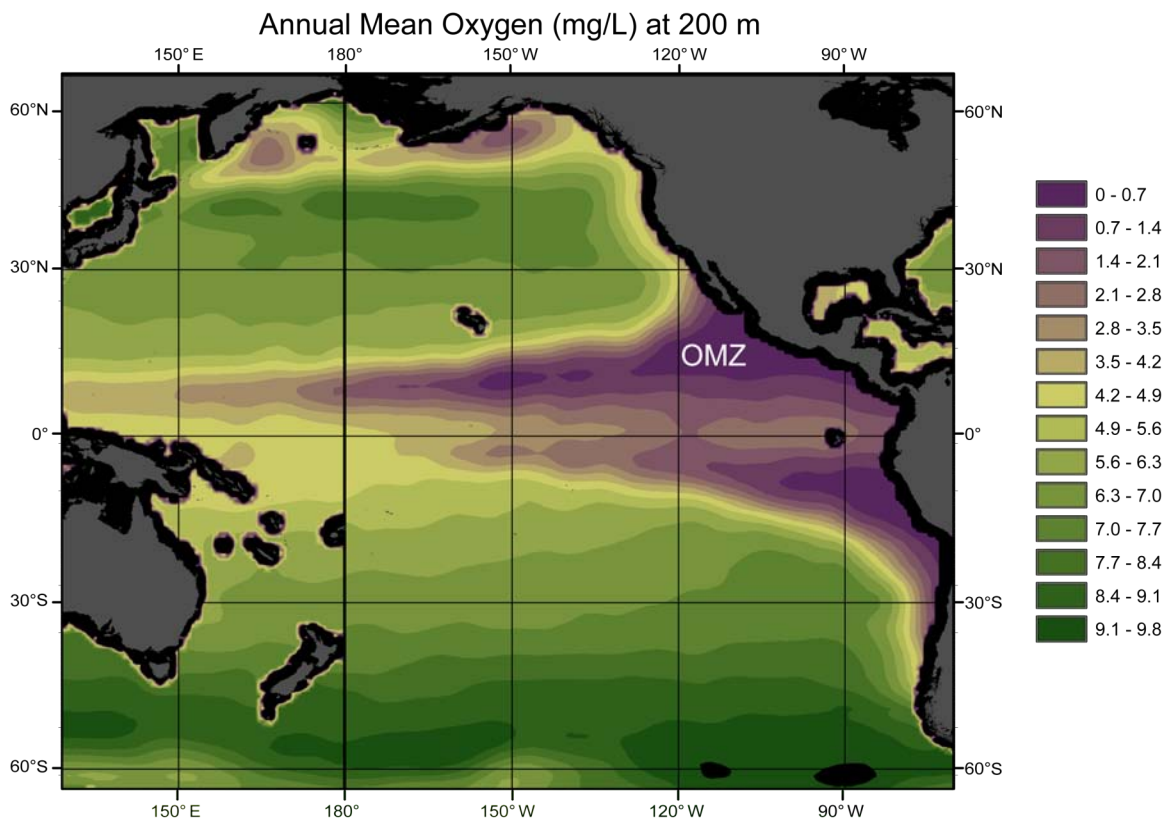


**Figure 1** Map of Pacific oxygen levels at 200 m depth. Dark purple indicates oxygen levels below 0.64 mg/L, the Oxygen Minimum Zone (OMZ). Black indicates no data. Data from World Ocean Database 2005 and map by J. A. T. Booth.

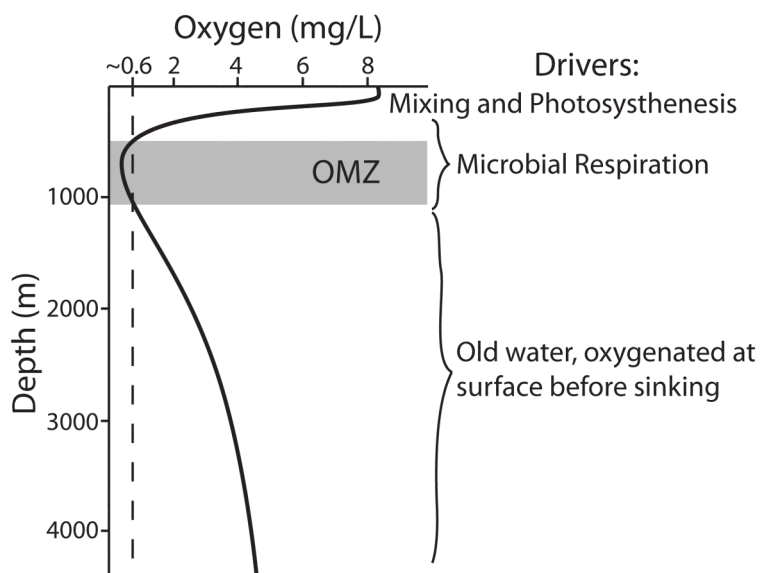


**Figure 2 Diagram of dissolved oxygen concentrations in the Northeast Pacific and biological and physical forcing mechanisms. The Oxygen Minimum Zone (OMZ) is noted between 500-1,100 m.**

Biological hypoxia is typically described as below  $2 \text{ mg O}_2 \text{ L}^{-1}$  (Diaz 2001; Vaquer-Sunyer and Duarte 2008), which is lethal to most benthic taxa (Gray et al. 2002; Vaquer-Sunyer and Duarte 2008). However, Vaquer-Sunyer & Duarte (2008) determined that to preserve 90% of community diversity, DO levels should remain above  $4.6 \text{ mg L}^{-1}$  to avoid the majority of detrimental but non-lethal effects on the more sensitive species (Figure 3). Breitburg (2002) used a threshold of  $< 50\%$  saturation (approximately  $4.4 \text{ mg L}^{-1}$  at a temperature of  $12^\circ\text{C}$ , 34 PSU) citing that at these levels fish showed avoidance behaviors, reduced growth and other signs of physiological stress. Gray et al. (2002) cite negative effects on growth below  $6 \text{ mg L}^{-1}$  and on metabolism below  $4 \text{ mg L}^{-1}$ . The introduction of hypoxic water into ecosystems not adapted to it can have drastic biological consequences (Diaz and Solow 1999; Grantham et al. 2004).

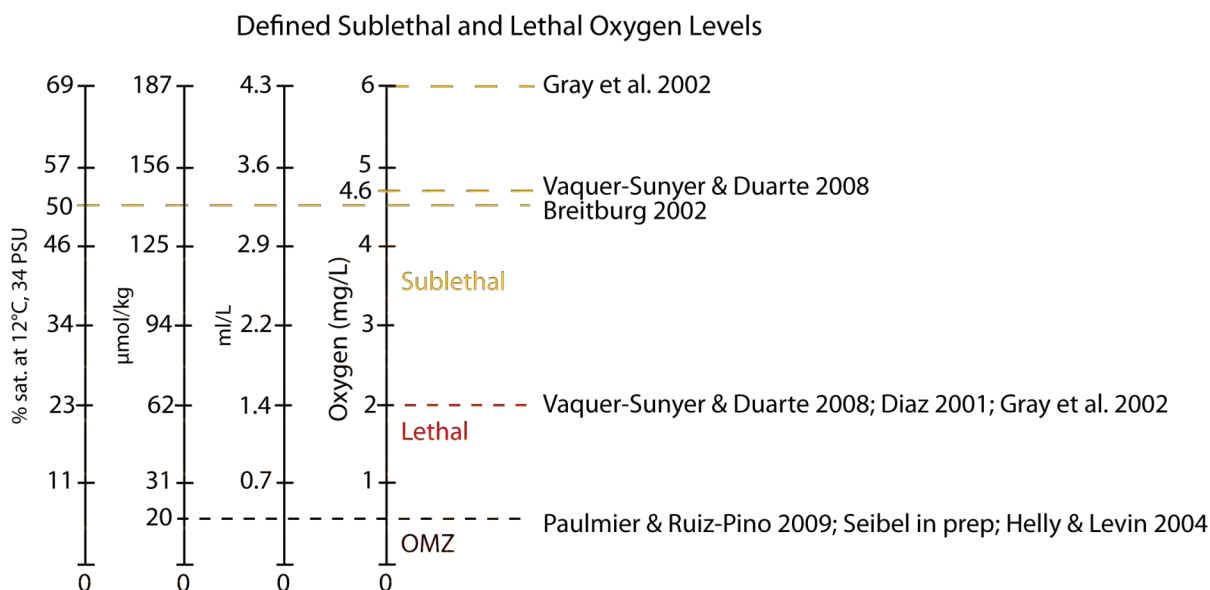


**Figure 3 Sublethal, lethal and Oxygen Minimum Zone (OMZ) oxygen levels as defined in the literature.**

The same respiration that uses oxygen in the process of breaking down organic matter, generates carbon dioxide (CO<sub>2</sub>), which hydrolyzes water releasing a hydrogen ion in the following equilibrium:



Oxygen Minimum Zones are also characterized by low pH and high CO<sub>2</sub> levels (Helly and Levin 2004; Paulmier and Ruiz-Pino 2009).

The free hydrogen ion concentration affects the availability of carbonate ions (CO<sub>3</sub><sup>2-</sup>) necessary to react with calcium ions (Ca<sup>2+</sup>) to form calcium carbonate (CaCO<sub>3</sub>). High CO<sub>2</sub>, often indicated by low pH levels, can reduce rates of calcium carbonate and magnesium calcite generation (Gazeau et al. 2007; Andersson et al. 2008) and in conjunction with hypoxia, can cause respiratory stress on organisms not adapted to those condition (Pörtner et al. 2005).

The majority of research on coastal marine hypoxia has been conducted in systems perturbed by anthropogenic eutrophication, such as coastal embayments and the Mississippi River delta (Diaz 2001; Breitburg 2002; Rabalais et al. 2002; Diaz and Rosenberg 2008). But the California Current System (CCS) is likely to not be controlled by the same processes. Terrestrial and anthropogenic nutrient input in the CCS, particularly in the Monterey Bay region, is limited and episodic, caused by winter

storms (November – March). Terrestrial nutrient delivery is weak compared to upwelling and internal waves (McPhee-Shaw et al. 2007; Carroll 2008). The CCS is a productive eastern boundary current system with strong coastal upwelling and hypoxia naturally occurs offshore where there is a well-established mid-water OMZ (Helly and Levin 2004). Only recently has coastal hypoxia been recorded in the CCS (Grantham et al. 2004; F. Chan et al. 2008; Connolly et al. 2010). On the Oregon and Washington inner continental shelf, exposure to upwelled nutrient-rich subarctic Pacific water and local DO depletion by bacteria responding to high productivity has caused hypoxia-induced mortalities of fish and invertebrates. These events have been linked to climate change via reduced ventilation of deep water (Whitney et al. 2007), as surface waters warm causing increased stratification and decreased mixing.

Shallow coastal hypoxia and low pH, as suggested by the MBA time series and previous research, is associated with coastal upwelling (Grantham et al. 2004; Escribano and Schneider 2007). Coastal upwelling along the Pacific coast of North America occurs when there are persistent southward alongshore winds, typically between February and June. Frictional shear by equatorward winds on a rotating planet leads to Ekman transport to the right of the wind direction (in northern hemisphere). This process pushes water mass offshore and establishes a west to east pressure gradient, which causes a southward flowing geostrophic current due to the same rotational field. Frictional stress between the seafloor and this geostrophic current leads to onshore (to right of direction of stress) bottom Ekman transport, and dense, cold, nutrient-rich waters are brought upward to euphotic zone along the coastal margin. Water is typically upwelled from depths of 50-100 m or more (Schwing et al. 1996). Upwelled water not only brings nutrients but may also be low in DO and pH, and this will be demonstrated by the MBA time series.

El Niño/Southern Oscillation (ENSO) events can influence coastal hypoxia by changing the depth of the OMZ (Sanchez et al. 1999). Under normal, non-ENSO conditions, trade winds along the equatorial Pacific push water westward, establishing a sea surface height difference and a pressure gradient across the Pacific. This pressure gradient causes an isopycnal tilt raising the depth of the thermocline in the eastern Pacific. This tilt brings dense, high-nutrient water masses relatively close to the surface on the eastern side of the basin, and coastal upwelling can access waters conducive to

intense productivity. ENSO conditions disrupt and even flatten the deep isopycnal east-west tilt, leaving less dense, warm and nutrient-poor water masses at the depths normally accessed by coastal upwelling. During these times upwelling thus brings onshore and upward waters that are warm and nutrient-poor relative to non-ENSO years. Thus, the foundation of a normally productive ecosystem is significantly reduced. Sanchez et al. (1999) have shown that during ENSO events, the OMZ is depressed by 100 m off Peru, and it is reasonable to suspect that a similar effect may occur in the CCS. La Niña events follow El Niños and are generally colder than normal as the system swings back to the other extreme. La Niñas are characterized by a shallower thermocline than normal and likely bring the OMZ to a shallower depth.

### **Climate Change and Increasing CO<sub>2</sub>**

In recent decades, global marine hypoxia has been increasing and the OMZ has been expanding and shoaling, which has been attributed to increased water stratification reducing ventilation (Y. Watanabe et al. 2001; Emerson et al. 2004; Whitney et al. 2007; Bograd et al. 2008; Stramma et al. 2008; Stramma et al. 2010). Global warming alone is predicted to increase global ocean hypoxia by 4 to 7% by the end of this century due to a lower oxygen saturation level in warmer waters (Bopp et al. 2002; Keeling and Garcia 2002; Matear and Hirst 2003; Shaffer et al. 2009). Additionally, changing climate may increase upwelling (Bakun 1990; Snyder et al. 2003; McGregor et al. 2007; García-Reyes and Largier 2010), but this is still under debate. If true, this mechanism could further draw up water from the OMZ. On top of deoxygenation, increasing CO<sub>2</sub> levels will stress respiration further (Brewer and Peltzer 2009).

Increasing atmospheric CO<sub>2</sub> from anthropogenic sources has resulted in a lowering of seawater pH by about 0.1 since the beginning of the industrial revolution (Caldeira and Wickett 2003; Feely, Sabine, Schlitzer, et al. 2004; Sabine et al. 2004; Orr et al. 2005; Doney 2010). As ocean acidification continues (Orr et al. 2005; Doney 2010) there will be a profound impact both chemistry (Feely, Sabine, Lee, et al. 2004) and biology (Pörtner et al. 2004; Pörtner 2008) of the oceans.

In addition to detrimental physiological effects on marine organisms, increasing hypoxia and the shoaling of the OMZ has caused habitat compression as organisms not

adapted to low oxygen levels are pushed out of their established habitats (Prince and Goodyear 2006; Stramma et al. 2010). It may also aid the spread of hypoxia-tolerant species to new areas, which can have detrimental effects on the local community (Gilly et al. 2006; Field et al. 2007).

It is important to separate the effects of natural and anthropogenic sources of hypoxia and acidification. Without an understanding of the natural fluctuation in DO and pH, efforts to predict how climate change and increasing CO<sub>2</sub> will affect the neritic ecosystem will be seriously compromised.

### **Internal tides, Internal Waves and Monterey Bay, California**

Monterey Bay is an important marine ecosystem. It is home to many fisheries and marine reserves while being close to fairly high population densities. A submarine canyon whose head is very close to shore and a narrow continental shelf expose the Bay directly to offshore deep waters.

Internal tides are a common feature of continental shelves, and on California shelves these events cause temperature fluctuations of 2-4°C during the spring and summer (Storlazzi et al. 2003; McPhee-Shaw et al. 2007; Woodson et al. 2011). Internal waves are often forced by barotropic (surface) tides, in which case they can be referred to as “internal tides.” However, diurnal baroclinic motions, which fall into the same frequency range as tides, are often caused by winds and not by the surface tide. For the purposes of this study I will be using the terms “internal tides” and “internal waves” interchangeably, and acknowledge that we do not truly know the forcing of all motions observed in the water column. Local winds add to diurnal energy in internal waves (Woodson et al. 2007; Carroll 2008; Cudaback and McPhee-Shaw 2009; Woodson et al. 2011). Internal tides have been shown to bring cold, hypoxic, deep water up to the continental shelf near the head of the Monterey Canyon (Shea and Broenkow 1982) close to shallow, nearshore environments. Mean yearly oxygen was seen to be 15% lower inshore than 0-5 km seaward and oxygen was 36% lower during the upwelling season, May through August (Shea and Broenkow 1982).

The Monterey Submarine Canyon throughout its depth as well as at its head (at Moss Landing) has energetic internal tidal energy, and some of this energy “spills up”



onto the nearby shelf (Kunze et al. 2002; Jachec et al. 2006; Carroll 2008; Carter 2010). Right at the canyon head tidal sea surface height and subsurface isopycnals often fluctuate in phase (i.e. temperature lags sea surface height by half a cycle (Shea and Broenkow 1982). But this is not always the case. The phase relationship between surface tides and internal waves, both deep in the canyon and on the shallow shelf, is complex and varies in space and time (Petruncio et al. 1998; Storlazzi et al. 2003).

While internal waves are a persistent feature in the coastal ocean, except for special cases such as the head of a submarine canyon (like at Moss Landing), it is difficult to identify which internal oscillations are forced by tides or winds, the direction of propagation, or to predict the intensity of internal oscillations. Additionally, there is considerable variability along the coast in regard to the internal wave field in Monterey Bay caused by both baroclinic and barotropic forcing (Kunze et al. 2002; Jachec et al. 2006; Carroll 2008; Carter 2010). There are differences in internal wave amplitude around Monterey Bay, with intense tidal-frequency currents closer to the head of the Monterey Submarine Canyon (Mid-Bay) and closer to Point Piños (southern tip), and weaker currents in the southern corner (Monterey) and throughout the northern Bay. The large movement of water caused by these internal motions plays a dominant role in the hydrographic time series described in this thesis.

It is important to understand both naturally and anthropogenically, because both mechanisms will affect the diversity of the local ecosystems and important fisheries (Diaz and Solow 1999). Along the California coast, nutrient inputs are primarily from upwelling and internal wave sources, whereas anthropogenic and terrestrial nutrient loading is weak (McPhee-Shaw et al. 2007; Carroll 2008). The long time series collected in the southern and central Monterey Bay presented here will be valuable to answer questions about the role of upwelling and internal waves in the variability of DO and pH in the nearshore.

## METHODS

### Oceanographic Measurements

#### WATER MONITORING AT THE MONTEREY BAY AQUARIUM AND MOSS LANDING MARINE LABORATORIES

Continuous seawater measurements were recorded at two sites in Monterey Bay (Figure 4), one on the inner shelf at the Monterey Bay Aquarium (36.621°N, 121.899°W) and the other at the head of the Monterey Canyon at the Moss Landing Marine Laboratories (36.8025°N, -121.7915°W). Both opportunistic data sets were not collected for scientific monitoring purposes, but rather were derived from water quality programs associated with animal husbandry.

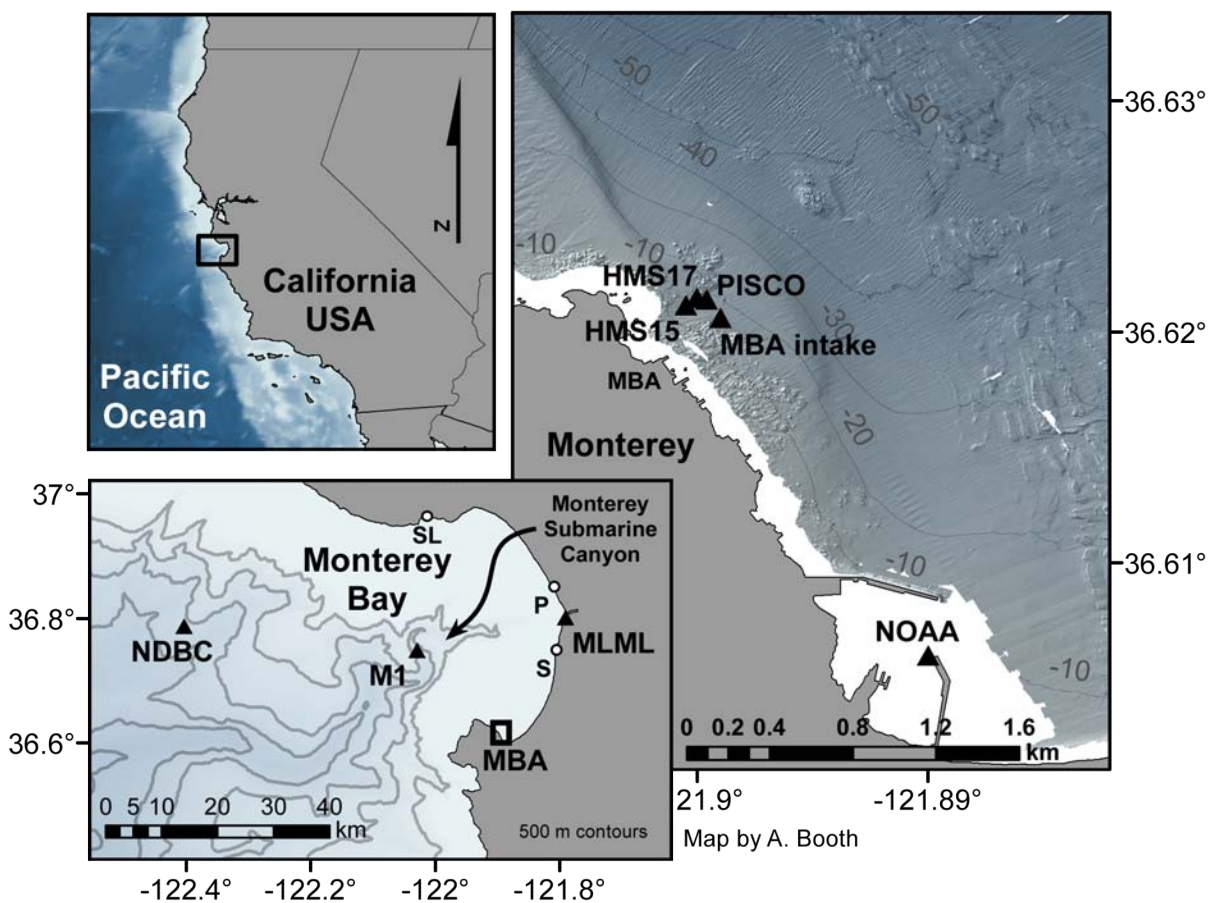


**Figure 4 Map of California, USA and study region of Monterey Bay showing locations of sampling sites at Monterey Bay Aquarium (MBA) and Moss Landing Marine Laboratories (MLML) as well as NOAA tide sensor on the Monterey municipal wharf (NOAA) and meteorological sensors on National Data Buoy Center #46042 (NDBC). Other hydrographic data were recorded at MBARI's M1 buoy (M1), Partnership for Interdisciplinary Studies of Coastal Oceans (PISCO) mooring and at two location near the Hopkins Marine Station a CTD was moored (HMS 15 and HMS17). Bathymetric data from Seafloor Mapping Lab of California State University Monterey Bay and the California Department of Fish and Game.**

At the Monterey Bay Aquarium, seawater from the adjacent kelp bed is drawn in through one of two intake pipes, the mouths of which are protected by coarse mesh screen. The intake lies at 17 meters depth, approximately 340 m offshore from the aquarium pump house and main facilities (Figure 4, Figure 5). Flow-through seawater measurements include temperature, dissolved oxygen (DO) and pH. Temperature has been recorded since September 21, 1995 by an AGM thermocouple at the pump house (Figure 5). Dissolved oxygen, conductivity, pH and carbonate chemistry were measured from the same water at a site inside the aquarium main facility (Figure 5). Dissolved oxygen has been recorded since April 1, 2000 with a Point Four OxyGuard Stationary Probe (Type 1). On September 24, 2009 a GLI Encapsulated LCP (Liquid Crystal Polymer) Differential pH Sensor with Internal Preamplifier and Glass Electrode was

installed and calibrated using Fisher Scientific NBS buffers (Table 1,

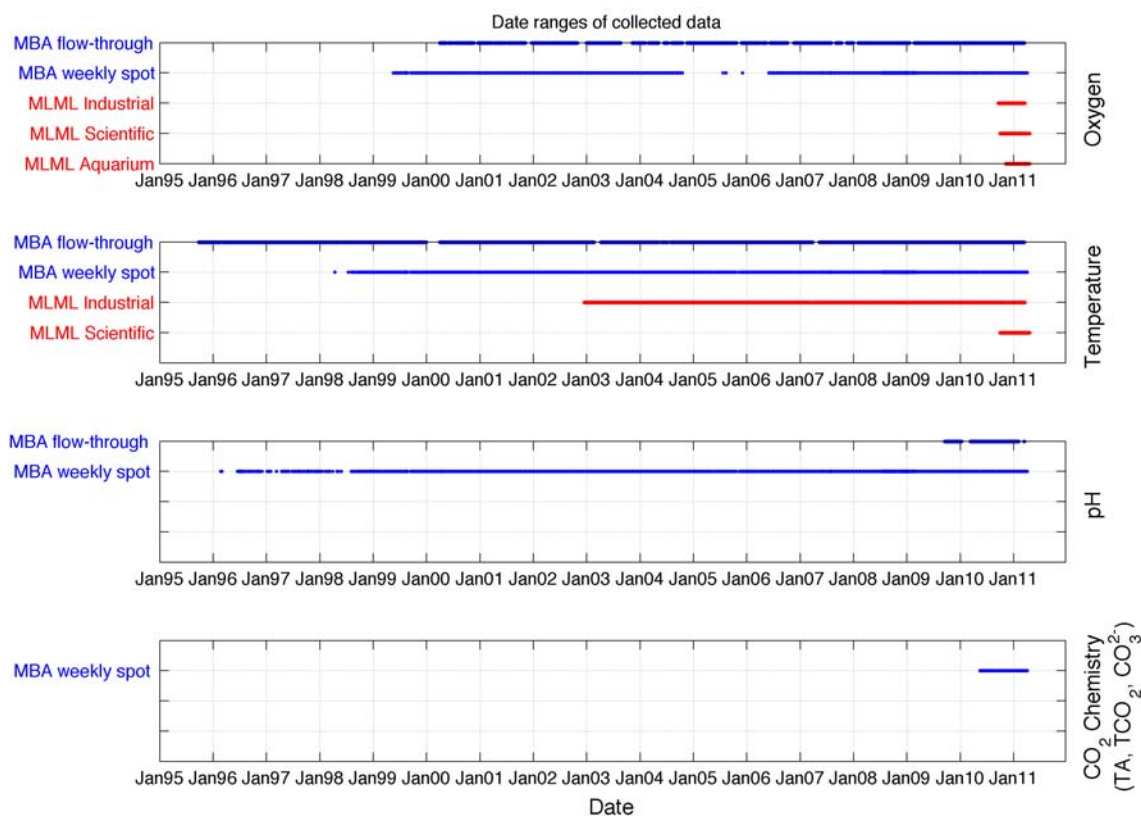
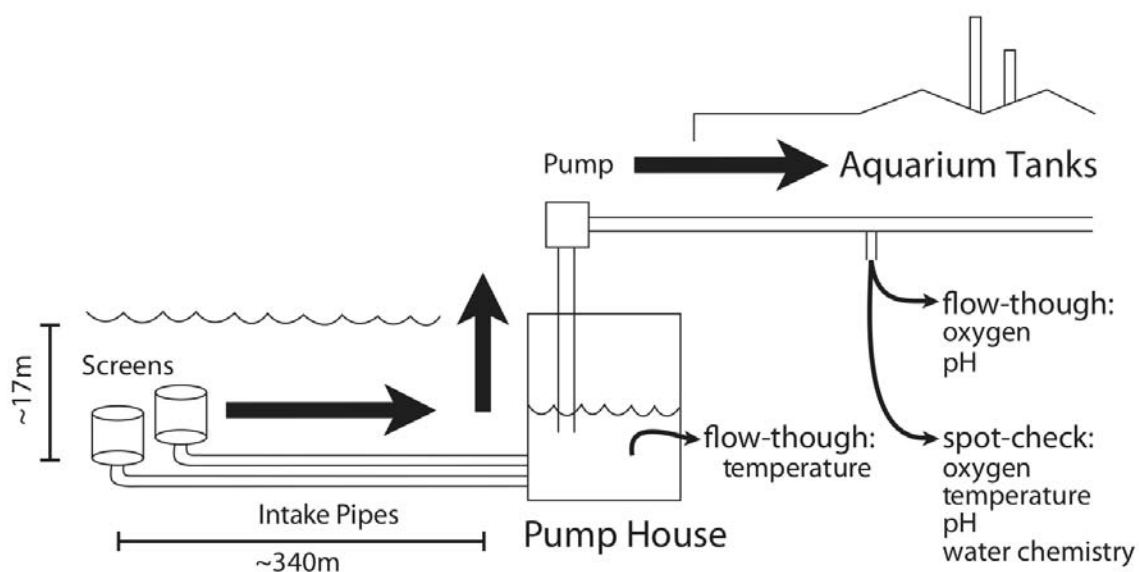


Figure 6). All flow-through monitoring was recorded every 5 min and carbonate chemistry water samples were collected approximately weekly.



**Figure 5 Schematic of seawater intake plumbing and monitoring at the Monterey Bay Aquarium in Pacific Grove, California. Flow-through measurements record every 5 minutes and spot-check measurements were conducted weekly.**

**Table 1 Seawater monitoring start dates at the Monterey Bay Aquarium (MBA) and Moss Landing Marine Laboratories (MLML).**

Variable	Start Date				
	MBA flow-through (5 minute)	MBA 'spot check' (weekly)	MLML 'industrial' (5 minute)	MLML 'scientific' (5 minute)	MLML 'aquarium' (5 minute)
Temperature (°C)	22-Sep-1995	14-Apr-1998	19-Dec-2002	9-Oct-2010	---
Oxygen (mg/L)	1-Apr-2000	21-May-1999	29-Sep-2010	9-Oct-2010	16-Nov-2010
pH (NBS scale)	24-Sep-2009	18-Jun-1996	---	---	---
Carbonate Chemistry	---	27-May-2010	---	---	---

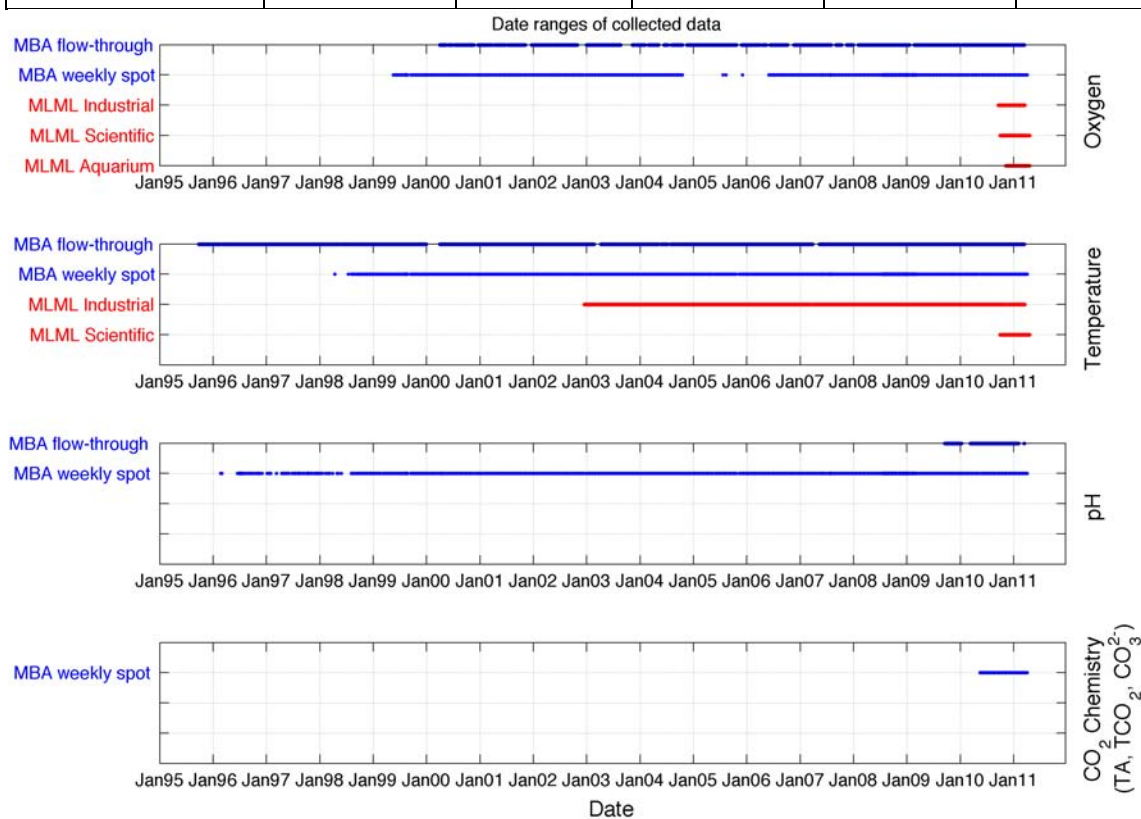


**Figure 6 Seawater monitoring dates at the Monterey Bay Aquarium (MBA) and Moss Landing Marine Laboratories (MLML).**

From April 1st, 2000 to December 15th, 2003, DO measurements were taken in units of  $\text{mg O}_2 \text{ L}^{-1}$  and in percent saturation up to the present. From April 1, 2000 to August 15, 2001, an artificial cap was put on the maximum possible DO level at  $10 \text{ mg O}_2 \text{ L}^{-1}$  after that period the range was extended to  $20 \text{ mg O}_2 \text{ L}^{-1}$ . Percent saturation

readings were converted to  $\text{mg L}^{-1}$  using the recorded temperature at the pump house and an assumed salinity value of 34 PSU (oxygen solubility equations from Colt, 1984).

The seawater system lags the environment by approximately 25 minutes. The lag time was estimated by comparing the temperature taken by MBA (2 m above bottom) and the deepest thermistor (3 m above bottom, 20 sec sampling) on a nearby Partnership for Interdisciplinary Studies of Coastal Oceans (PISCO) mooring at  $36.6214^{\circ}\text{N}$ ,  $121.8996^{\circ}\text{W}$  (Figure 4). The lag time of the MBA monitoring system may be caused by the water's travel time from the intake mouth to the pump house. Once in the system, temperature and dissolved oxygen do not lag one another by more than 5 min (the resolution of the time series). Short time scale changes ( $< 5\text{-}10$  min) in temperature are not detected by the MBA monitoring system (example shown between 17:00 and 19:00 in Figure 8). This is likely due to the mixing of the water in the pump house before its measurement.

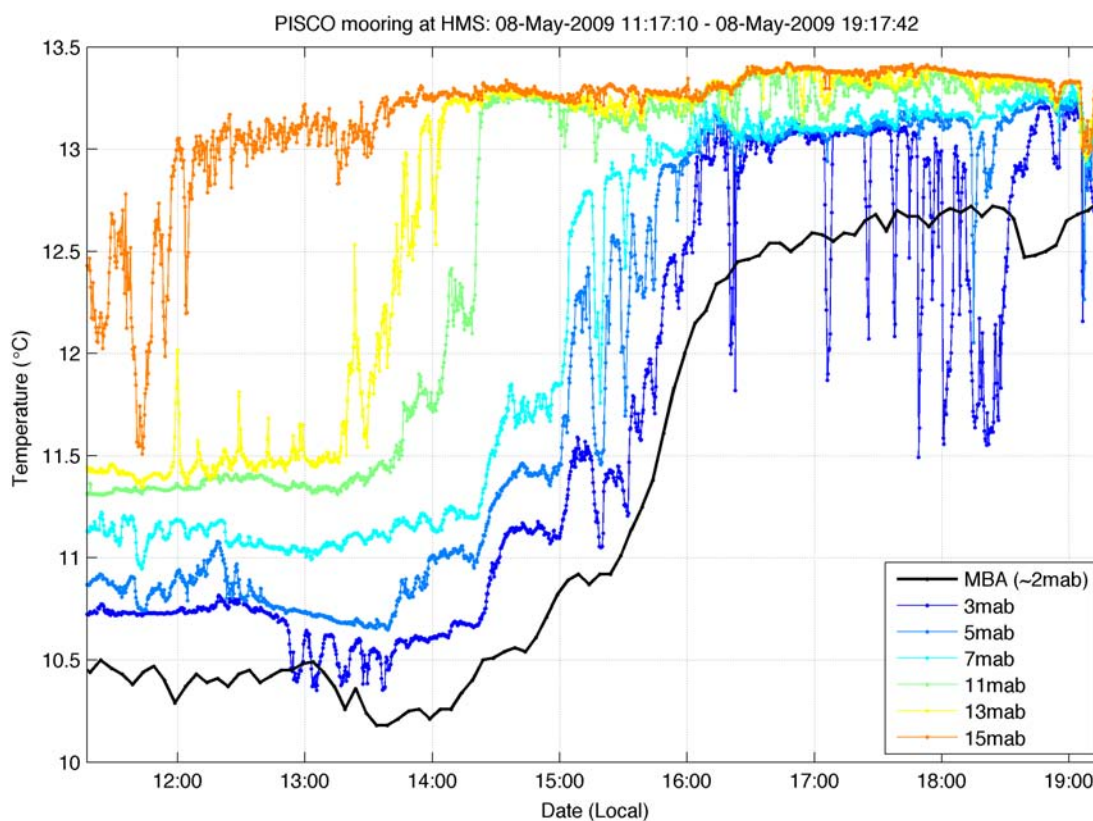


**Figure 8** Example of several hours of MBA temperature (5 min sampling) drawn from 2 meters above bottom (m.a.b.) (black line) compared to temperature taken by several thermistors (20 sec sampling) on a PISCO mooring ( $36.6214^{\circ}\text{N}$ ,  $121.8996^{\circ}\text{W}$ , Figure 4). Note high frequency temperature fluctuations between 16:00 and 18:00 are not seen in mixed MBA water.



The Moss Landing Marine Laboratories (MLML) has monitored temperature and DO from their seawater intake pipe, located at 20 m depth ~300 m offshore of the MLML shore lab (Figure 9). Since December 19, 2002, temperature (Weed Instrument 5A00A1) and DO (OxyGuard 840) were recorded as part of an ‘industrial’ monitoring system every 5-minutes (Table 1,

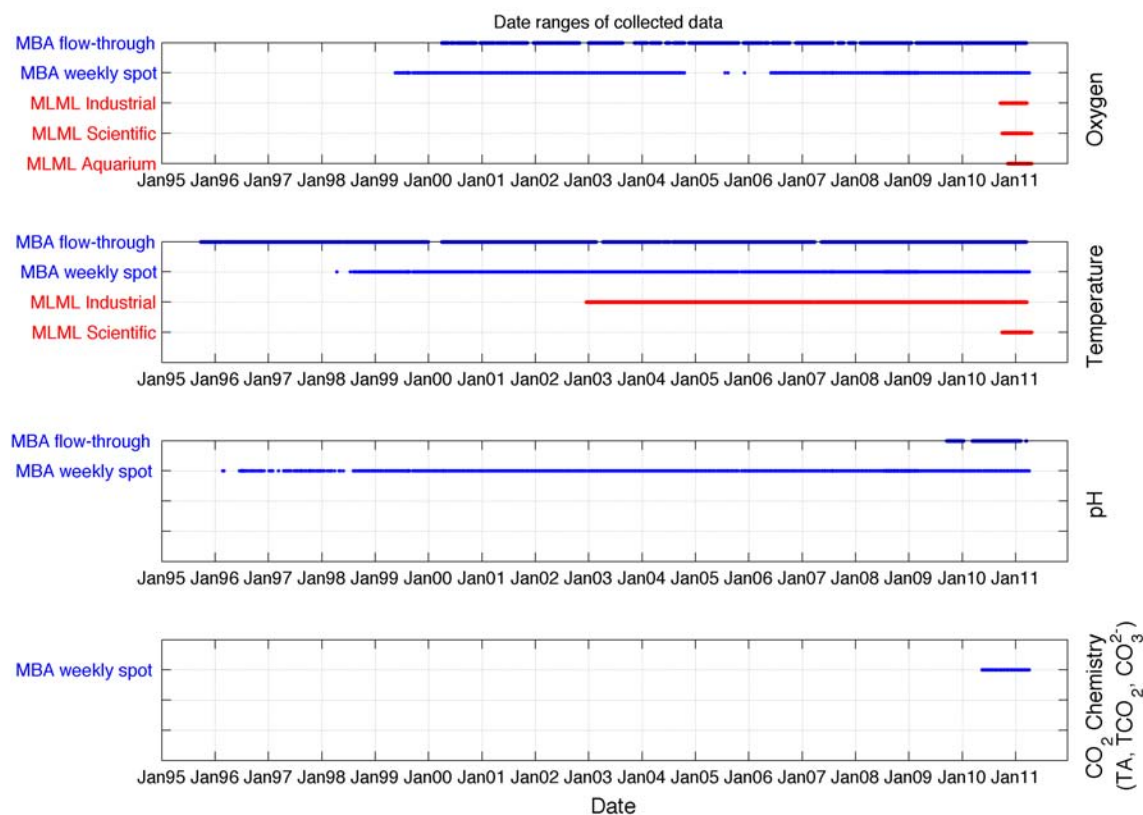


Figure 6). Dissolved oxygen measurements prior to the fall of 2010 were unreliable and proved to be unusable for analytical purposes. During the fall of 2010, a ‘scientific’ monitoring system was installed in the shore lab that was equipped with an Aanderaa AADI 3835 oxygen optode, a Wetlabs c-star transmissometer (10 cm cell), a Seabird SBE 19 CTD, and a Wetlabs Wetstar Miniature fluorometer. Another DO sensor was installed at the MLML main lab aquarium in November 2010 (OxyGuard Atlantic)

(Table 1,

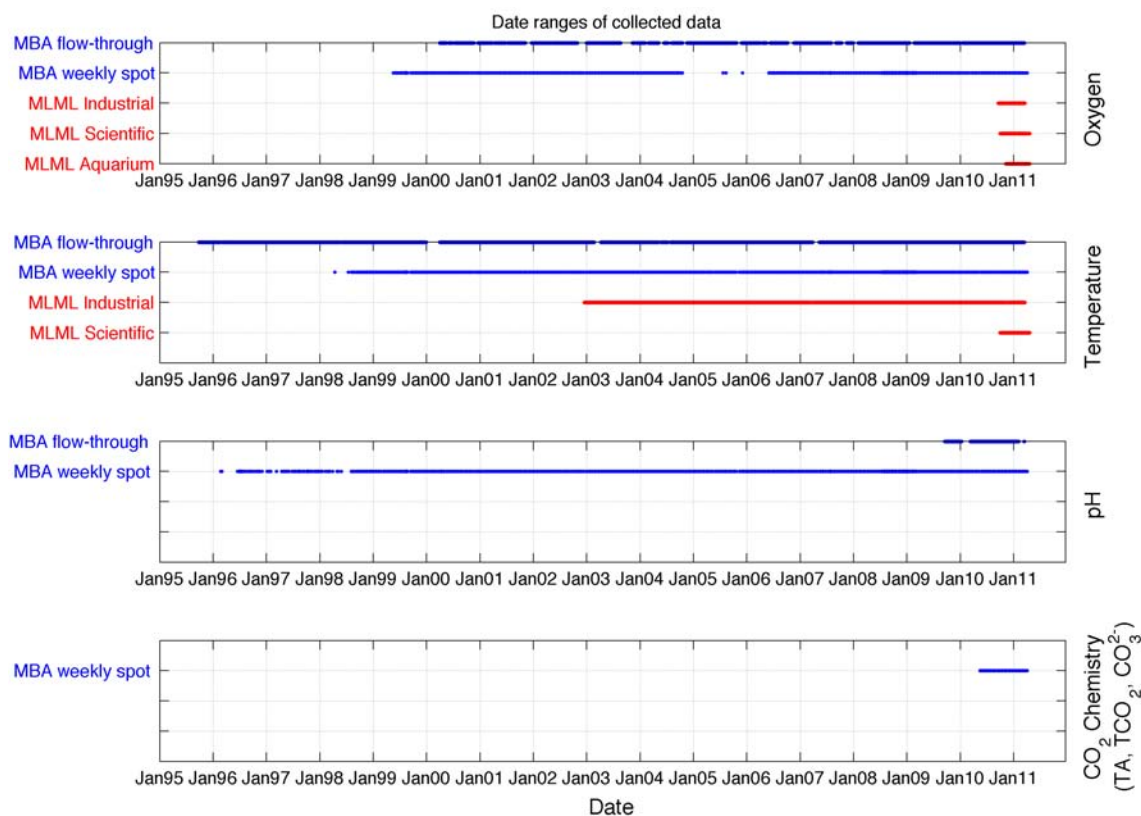
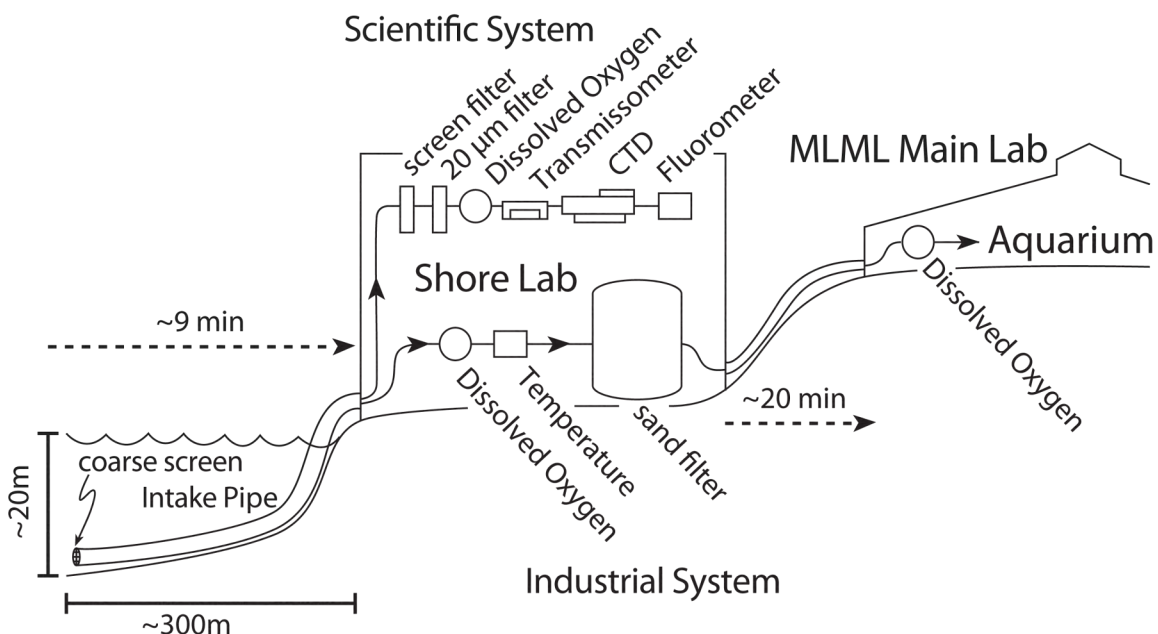


Figure 6, Figure 9). For all analyses, temperature from the industrial system and DO from the scientific system were used. Based on the flow rates and pipe diameters of the system, the MLML system was predicted to lag the environment by approximately 9 min, increasing to ~16 min when the system was in a back-pump cycle, estimated by the size of the pipe and volume of water pumped.





**Figure 9 Schematic of MLML seawater intake system and instrumentation.**

#### **MONTEREY BAY AQUARIUM WEEKLY SPOT-CHECKS**

Discrete spot-check measurements of temperature, DO, and pH were taken once or twice per week since April 14, 1998, May 21, 1999, and June 18, 1996 respectively and have continued until the present (Table 1, Figure 11). Measurements were conducted using the outflow water of the flow-through monitoring program using a Hach IntelliCAL dissolved oxygen probe (optical) and liquid filled pH electrode (Figure 5). These data were used by MBA staff to assess the accuracy of the flow-through instruments. I used these data to serve as a quality control for the flow-through time series and to look at long-term patterns in pH. Temperature spot checks were taken inside the aquarium where the DO and pH sensors were located and were on average 1.33°C higher than the values from the thermocouple in the pump house. This warming was attributed to pipe friction.

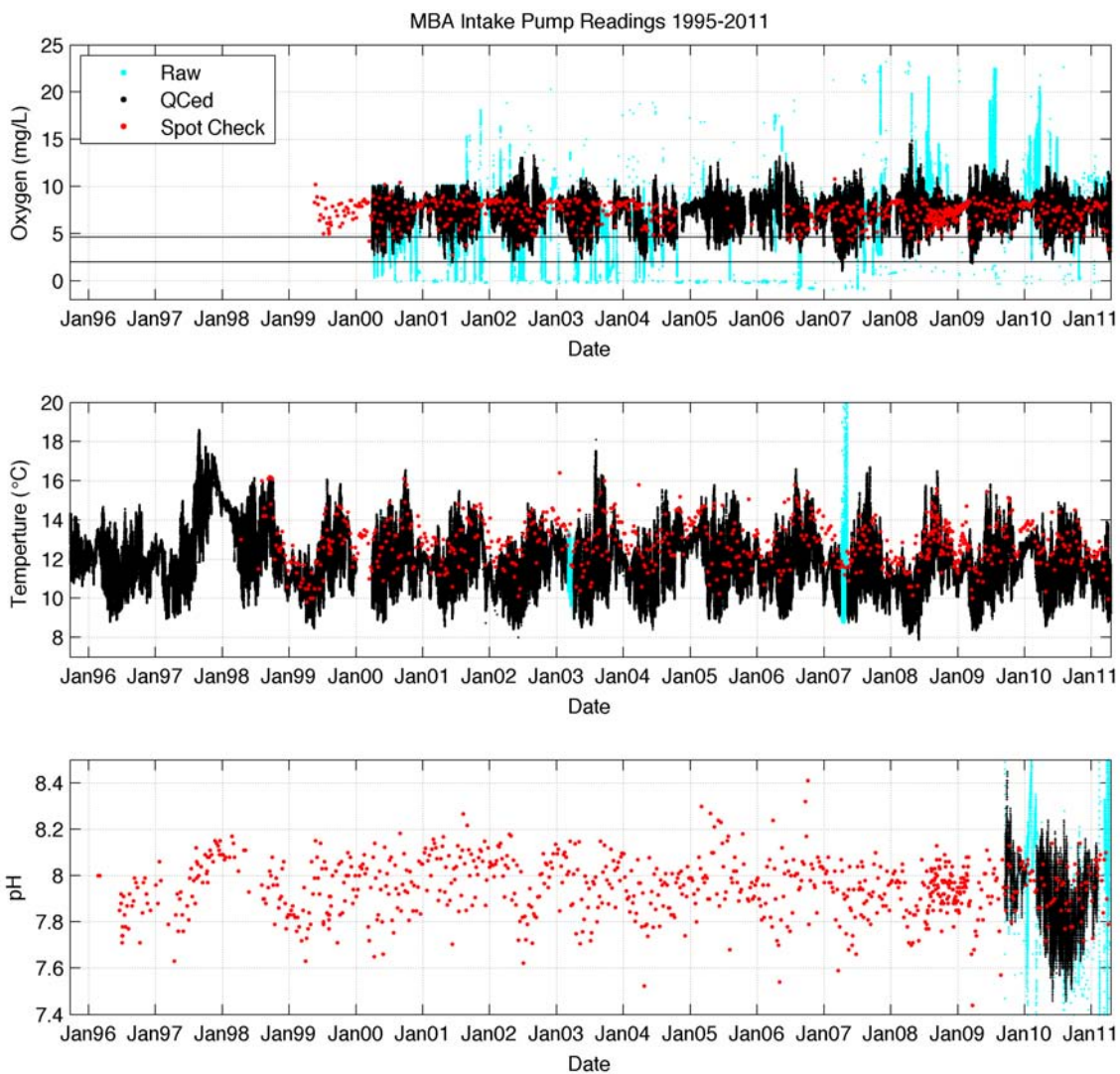


**Figure 11** Oxygen ( $\text{mg L}^{-1}$ ), temperature ( $^{\circ}\text{C}$ ) and pH (NBS scale) measurements made from 1995 to 2011 (black dots). Data removed in quality control process (teal dots) and weekly spot check measurements (red dots) are also plotted.

### *Carbonate Chemistry Monitoring*

On 27 May 2010, carbonate chemistry measurements (total carbon dioxide ( $\text{TCO}_2$ ) total alkalinity (TA), and carbonate ( $\text{CO}_3^{2-}$ )) were added to the weekly spot check at MBA. Water was collected in airtight plastic bottles inside the aquarium where the DO and pH sensors are located (Figure 5). Samples were analyzed by the Gran titration method using a Metrohm 809 Titrando using Tiamo Titration Software. The probe on the titrator was calibrated monthly.

## Assessing Error

### ERROR AT THE MONTEREY BAY AQUARIUM

In order to evaluate the accuracy of these long-term measurements, regressions between spot checks and high frequency data were conducted. The comparison did not show the expected 1:1 ratio that would indicate strict consistency between sensors (Figure 13). The spot checks themselves had high variability, and it is likely that human error accounted for some of this. Time stamp errors were ruled out as the time of the spot checks were recorded by the handheld Hach probe which is updated with the time upon data download. While spot checks occurred weekly and calibrations monthly, it was not possible to retroactively quantify the error associated with the MBA time series. A mixture of sensor drift and human error has occurred throughout both the flow-through (every 5 minutes) and weekly spot-check time series.

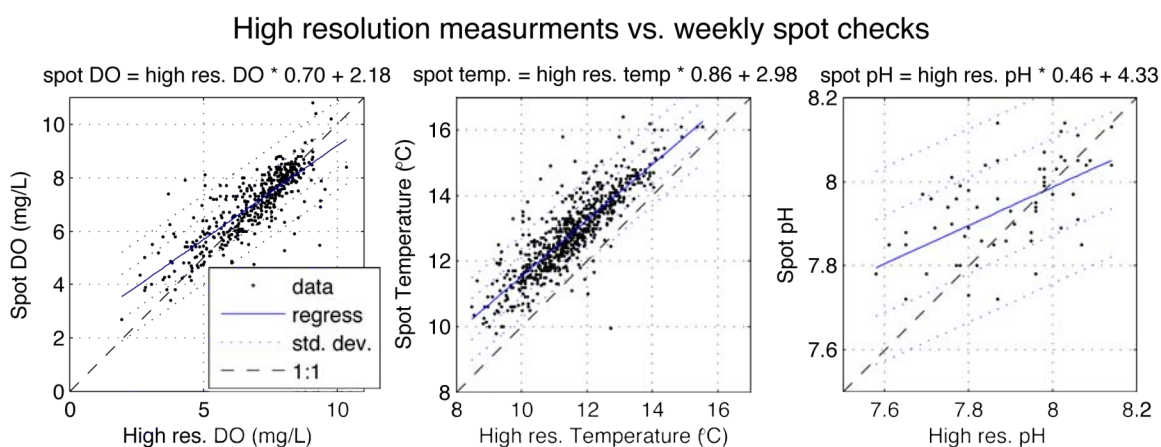


**Figure 13 Weekly spot check measurements of DO (left panel), temperature (middle panel) and pH (right panel) plotted against closest in time measurement of the high-resolution flow-through system. Multiple linear regressions (blue lines), 1 and 2 standard deviations around regression (blue dotted lines) and a 1:1 reference line (black dashed line) are also plotted. Multiple regression equations are written above each graph.**

The spot-check temperature readings were on average 1.33°C higher (Figure 14) at the sensor array inside the aquarium, where DO was measured, when compared to the flow-through temperature measurements made in the pump house (Figure 5). A warmer temperature would result in at most a difference of 5% saturation, approximately 0.44 mg L<sup>-1</sup> higher (Figure 15). This increase may account for some of the discrepancy between MBA measurements and those of a nearby mooring (see below).

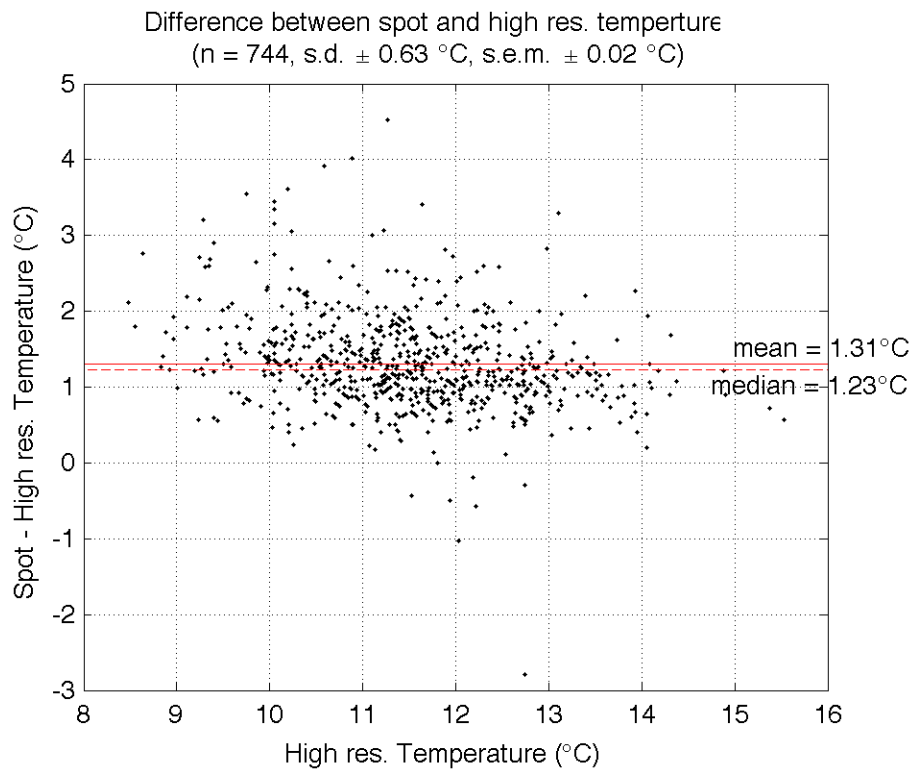


**Figure 14 High-resolution temperature plotted against difference between spot check and high resolution measurement. Mean and median difference for entire data set are plotted.**

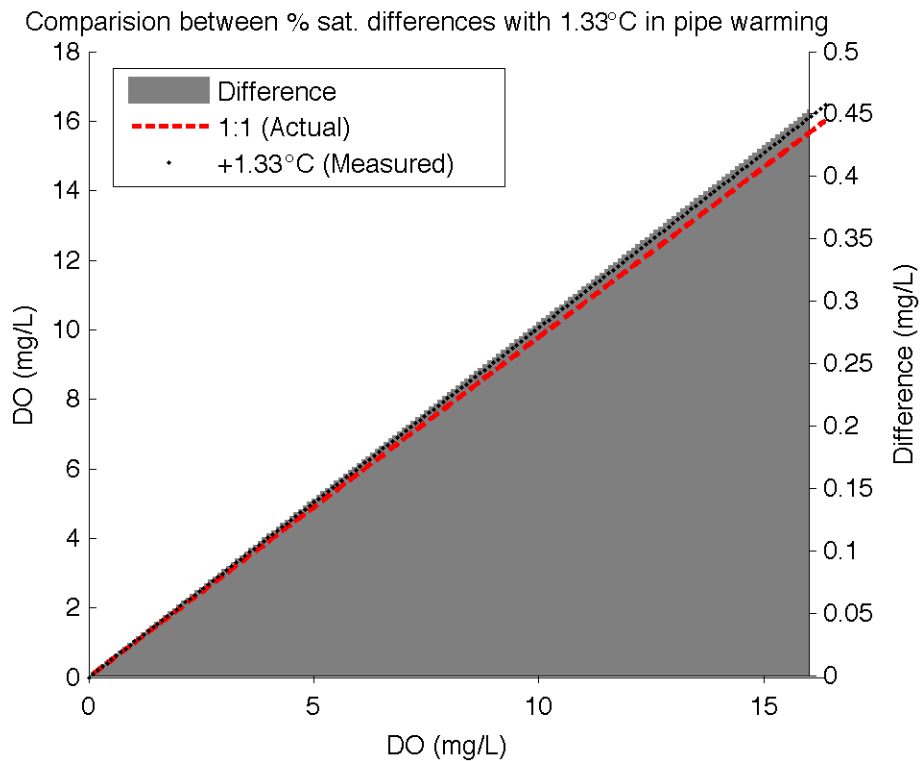


**Figure 15 Deviation away from a 1:1 (red dashed line) relationship when converting between DO units using temperatures recorded at the MBA pump house and accounting for in pipe warming (blue dotted line, +1.33°C). Maximum error was just over 5 percent saturation (grey shaded area, right y-axis) at 180 percent saturation measured.**

#### **COMPARISON BETWEEN MONTEREY BAY AQUARIUM MEASUREMENTS AND INDEPENDENT MOORING AND WATER PROFILES**

Several short time series were recorded with a Seabird SBE16plus CTD (conductivity-temperature-depth) profiler equipped with an Aanderaa oxygen optode sensor by Dr. Brock Woodson (Stanford) on two moorings, HMS17 (36.6214°N, 121.8996°W) and HMS15 (36.6212°N, 121.9005°W, Figure 4 map). These data were used to ground truth the temperature and DO measurements made by MBA. The instrument was moored between 14-16m in 17 m of water within 150 m of the MBA intake site. The first deployment, October 1- November 17, 2009, was moored at approximately the same isobath as the MBA intake mouth and the second and third deployments (July 16 – August 3, 2010; August 17 – September 30, 2010) were slightly inshore of the MBA intake. These data showed that MBA temperature measurements lagged the environment at the PISCO mooring by ~30 min and at the more inshore HMS mooring by ~10 min. The shorter lag time was attributed to the HMS mooring being closer to MBA in the presumptive direction of onshore wave travel. Temperature was strongly correlated, mean cross-covariance coefficient = 0.96 across all three deployments. DO values showed a mean cross-correlation value of 0.84 and MBA DO values were on average 0.86 mg L<sup>-1</sup> higher than the moored CTD across all three deployments when lag times were removed, which seemed to be a systematic difference between sensors and not biologically induced (Figure 16).

Estimates of error at times earlier than 2009 were not available. DO measurements recorded by both the high-resolution MBA sensor and the moored CTD often showed levels well above saturation (>8-9mg L<sup>-1</sup>, Figure 17), whereas the MBA weekly ‘spot’ checks never did (Figure 11). This suggests that the surface water indeed often became supersaturated, possibly due to high photosynthetic activity and indicated that the equipment used to take the MBA ‘spot’ checks may not have been able to measure water that was supersaturated.

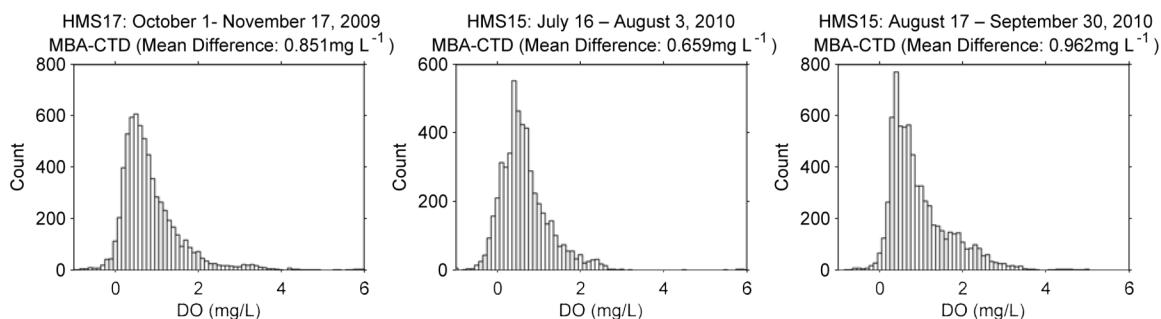


**Figure 16 Comparisons between the Monterey Bay Aquarium (MBA) flow-through dissolved oxygen (DO) measurements and three moored CTD (14-16m depth) deployments. Left panel depicts deployment on HMS17 mooring and middle and left panels are deployments on the more inshore HMS15. Histograms depict distribution of differences between MBA DO (with lag accounted for) and moored CTD DO.**

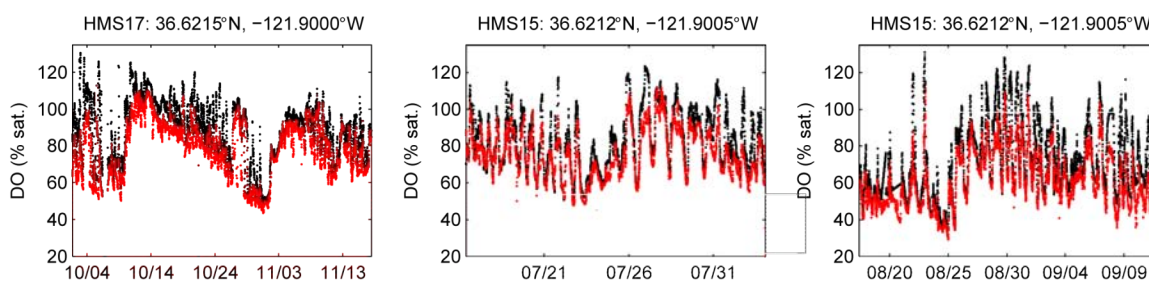


**Figure 17 Time series of Monterey Bay Aquarium (MBA) flow-through dissolved oxygen (DO) measurements and three moored CTD (14-16m depth) deployments. DO over time from MBA (black dots) and moored CTD (red dots) in percent saturation.**

Four CTD casts were also conducted at the same site in April 2009 with a Seabird SBE19plus profiler equipped with a SBE43 dissolved oxygen sensor to capture a snapshot of water column stratification under different regimes and a measure of salinity. MBA DO ranges corresponded strongly to those measured by the casts; however, direct comparisons in time were not possible due to the lag introduced by the intake system and uncertainty of the exact depth of the intake pipe. The error involved in comparing the CTD profiles to the MBA measurements is likely greater than the instrument error that is of interest. In situ salinity varied from 33.5 to 34.0 PSU, which predicts a maximum error of 0.01% for converted DO units using an assumed salinity value of 34.

## **ERROR AT THE MOSS LANDING MARINE LABORATORIES**

The accuracy of the industrial temperature measurements made at MLML could not be assessed retroactively, but over the eight years of monitoring the time series predictably followed similar patterns as the MBA time series and correlated strongly (see MBA and MLML comparison in results section). Temperature as part of the scientific system that started in Fall 2010 was  $> 1$  °C warmer than both the MLML industrial and MBA temperature, so it was not used. While DO was monitored as part of the industrial system starting in December of 2002 when temperature monitoring began, measurements were unreliable. This conclusion was reached based on the fact that DO did not correlate to temperature, as one would have expected from the pattern at MBA (see MBA results section), and did not correlate to DO at MBA as expected from the strong temperature correlation across both locations. In the fall of 2010, the DO monitoring at MLML was overhauled with three redundant systems, industrial and scientific in the shore lab and an aquarium system at the main lab aquarium (Figure 9). The DO optode sensor as part of the scientific system was considered the most accurate because it was a scientific quality instrument; the other two sensors were calibrated to it. The scientific system DO sensor correlated strongly to the aquarium sensor at a correlation coefficient of 0.82 at a lag of 85 minutes and to the industrial sensor (0.88) at no lag. Accounting for lag times, the scientific measurements were on average  $0.185 \pm 1.271$  (S.D.)  $\text{mg O}^2 \text{ L}^{-1}$  higher than the aquarium and  $0.699 \pm 0.713$  (S.D.)  $\text{mg O}^2 \text{ L}^{-1}$  lower (Figure 19). All sensors tracked each other well and patterns were consistent. This redundancy provided reassurance when DO levels got unexpectedly very low.



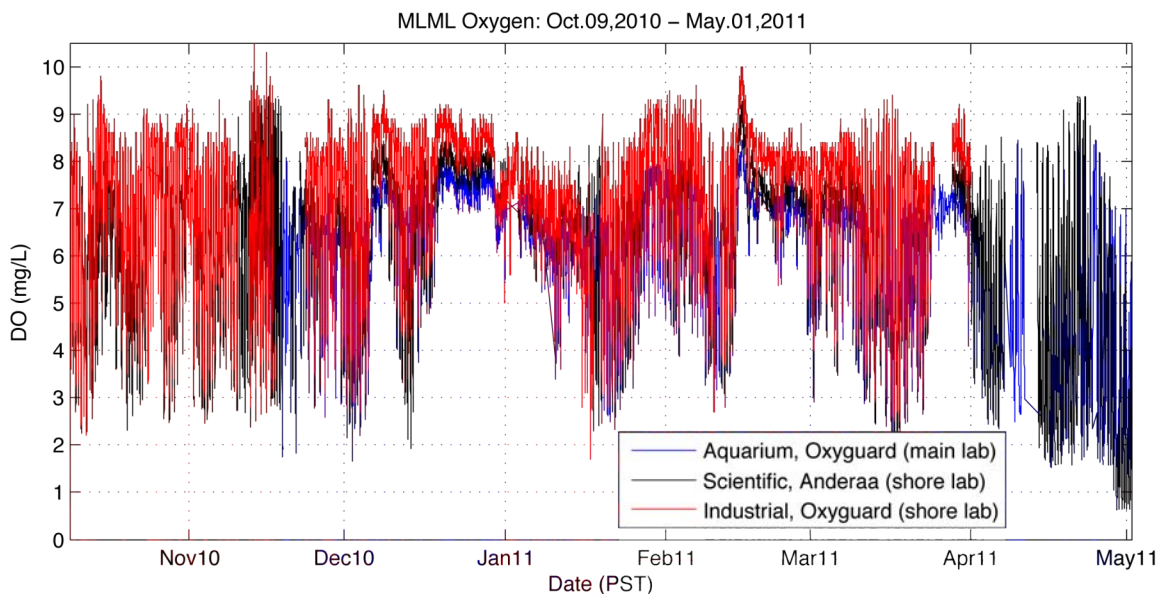


**Figure 19 Dissolved oxygen (DO) water monitoring at Moss Landing Marine Laboratories (MLML). Time series of three DO sensors (October 9, 2010 to May 1, 2011): main lab aquarium (blue), shore lab scientific (black) and shore lab industrial (red).**

### Quality Control

High temporal resolution measurements of DO, temperature, and pH data from the MBA, and temperature and DO from MLML were filtered for outliers and sensor malfunctions using the following methods. First, any measurements outside of the ranges given in Table 3 were removed as outliers based on the established range of the entire time series.

**Table 3 High Resolution Water Monitoring Quality Control Limits**

Variable	Minimum	Maximum
Temperature (°C)	7	20
Dissolved Oxygen (mg/L)	1	15
pH (NBS scale)	7.2	8.6

When the sensor was unreliable or clogged (when levels rapidly dropped to 0 mg/L), measurements were removed by hand. Temperature was a reliable measurement and when DO variations did not correlate with temperature, DO was presumed to be unreliable. Over the study period of September 22, 1995 to March 25, 2011, 2.2% of the



MBA flow-through system temperature readings were unusable or missing. For the DO study period of April 1, 2000 to March 25, 2011, the number of unusable readings was 18.7% (Figure 20). The missing data were distributed randomly throughout years and months. The MLML flow-through temperature time series from December 19, 2002 to October 25, 2010 was missing 1.5% of the data points (Figure 21).

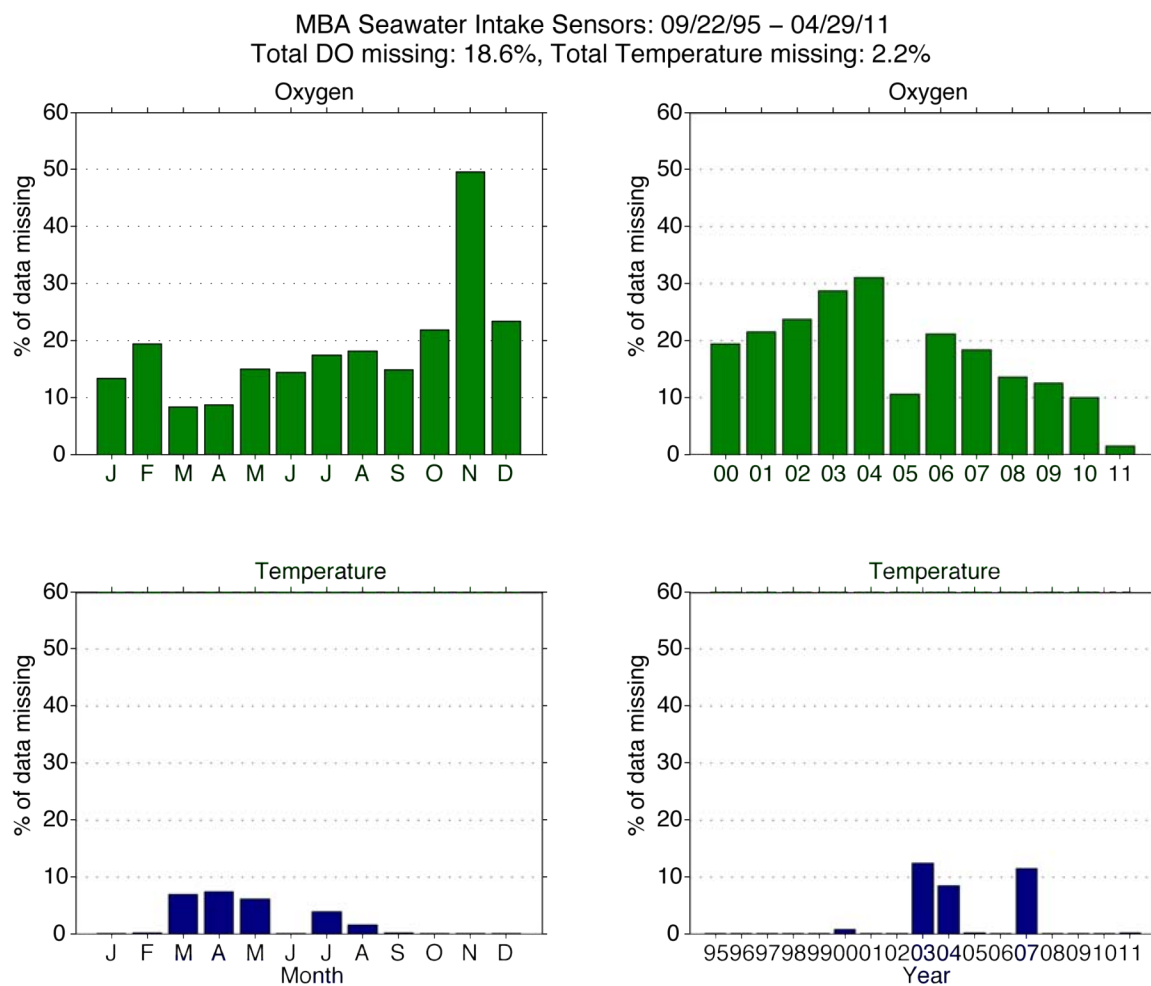


**Figure 20 Percent of 5-minute flow-through DO (top panels, April 1, 2000 – March 25, 2011) and temperature (bottom panels, September 22, 1995 - March 25, 2011) data missing at the Monterey Bay Aquarium. Missing data percentages presented by month (left panels) and year (right panels).**

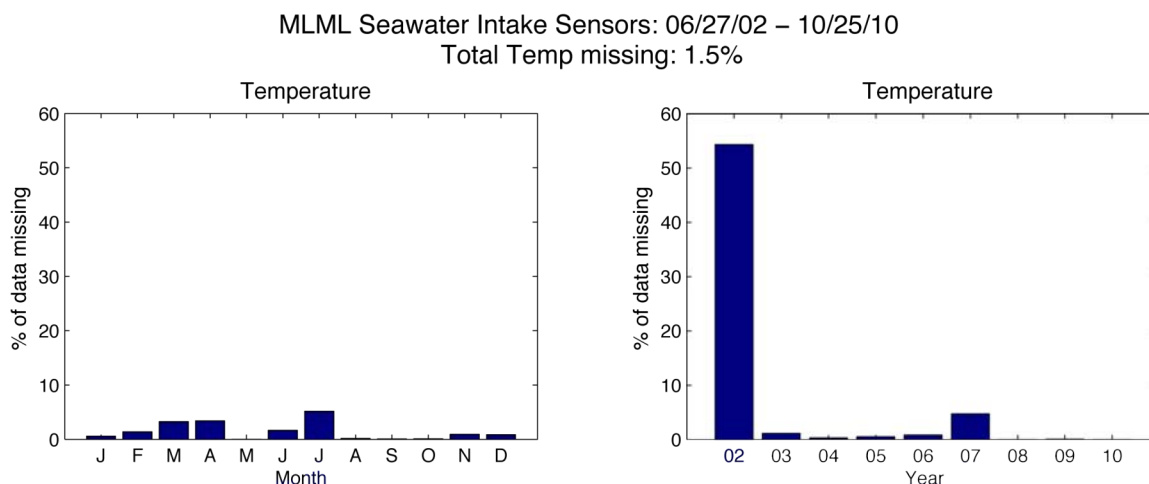


**Figure 21** Percent of 5-minute temperature (bottom panels, December 19, 2002 - October 25, 2010) data missing at MLML. Missing data percentages presented by month (left panels) and year (right panels).

**WHAT HAS BEEN THE STATE OF OXYGEN, pH AND TEMPERATURE IN THE NEARSHORE ENVIRONMENT OF THE SOUTHERN MONTEREY BAY OVER THE PAST DECADE? DO OXYGEN AND pH LEVELS DROP TO BIOLOGICALLY STRESSFUL LEVELS?**

## Results

### A DECADE AND A HALF OF SEAWATER MONITORING IN THE NEARSHORE HABITAT OF SOUTHERN MONTEREY BAY

All measurements of dissolved oxygen (DO), temperature and pH showed high variability and seasonal differences in southern Monterey Bay in the flow-through monitoring system at the Monterey Bay Aquarium (MBA) (Figure 22). Oxygen levels ranged from 1 to 15 mg L<sup>-1</sup> when outliers were removed and the peak of the distribution between 8 and 8.5 mg L<sup>-1</sup> (Figure 23), equivalent to approximately 95 percent saturation (Figure 24). Levels often fell into ranges considered stressful (<4.6 mg L<sup>-1</sup>) or lethal (<2 mg L<sup>-1</sup>) for many taxa (Vaquer-Sunyer and Duarte 2008). There were also many times when DO became supersaturated (>~8.7 mg L<sup>-1</sup>, >100 percent saturation).

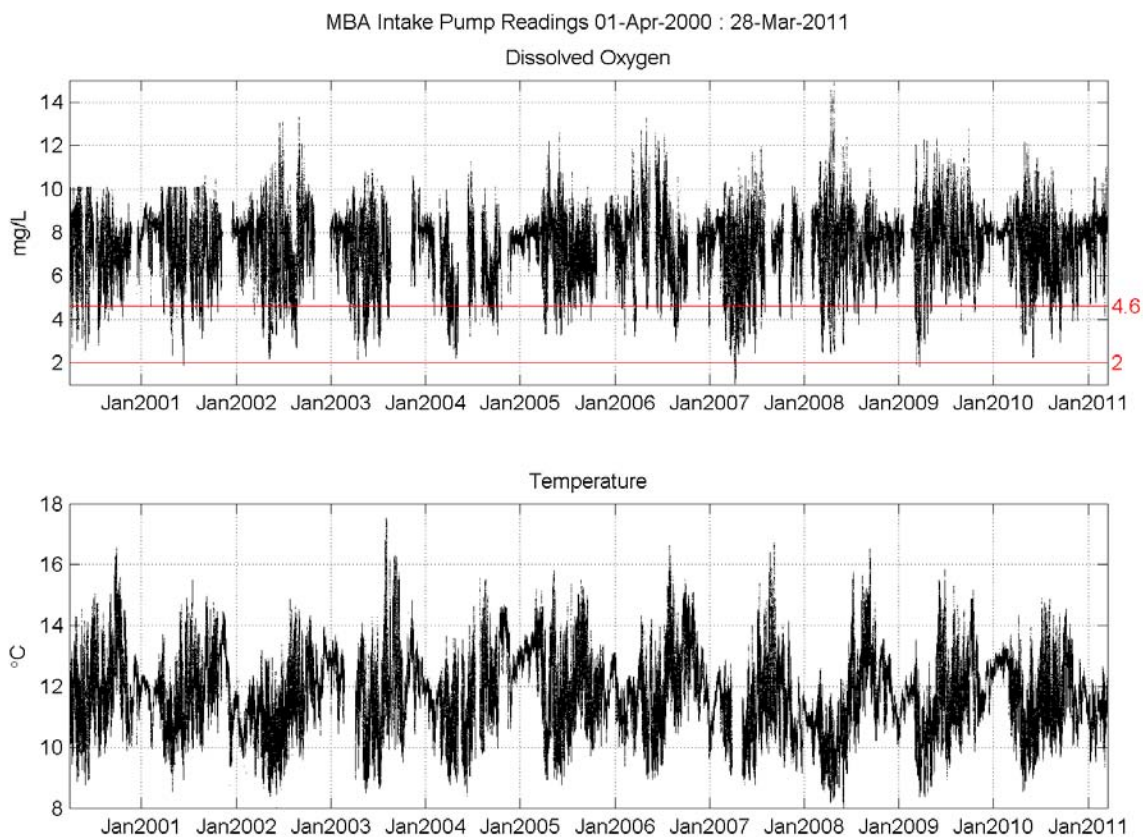


**Figure 22 Dissolved oxygen (top panel) and temperature (bottom panel) time series measured at the Monterey Bay Aquarium April 1, 2000 – March 28, 2011. Biologically stressful oxygen levels are indicated with the  $4.6 \text{ mg L}^{-1}$  sublethal and  $2 \text{ mg L}^{-1}$  lethal thresholds are indicated with red lines.**

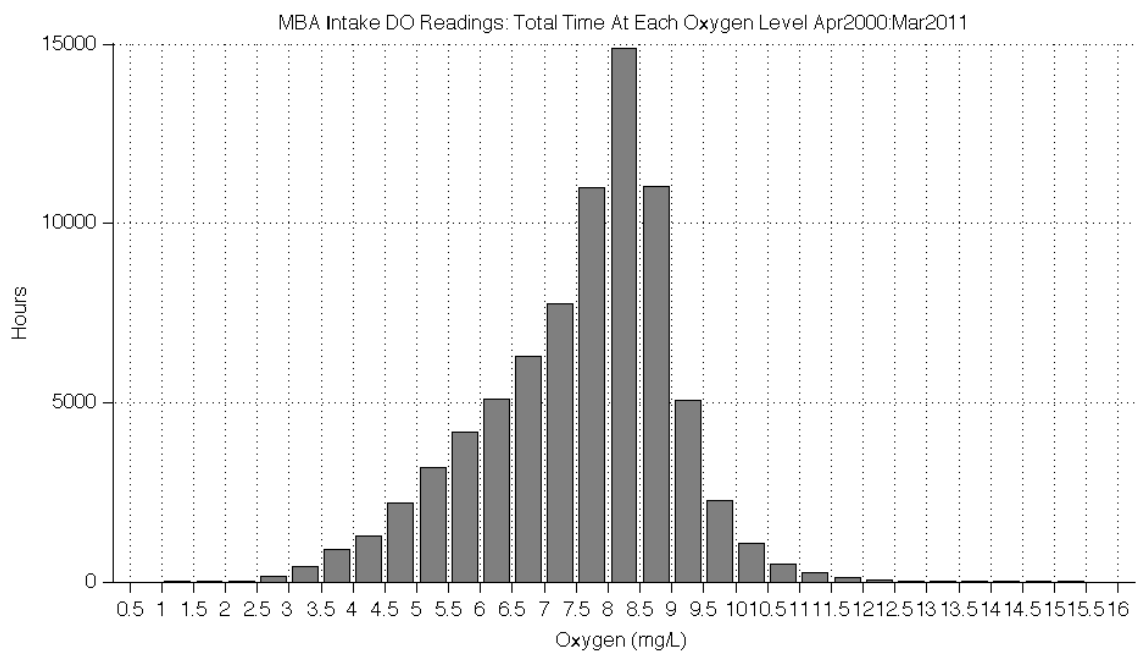


Figure 23 Distribution of time at different dissolved oxygen levels in  $\text{mg L}^{-1}$  over entire Monterey Bay Aquarium time series, April 2000 – March 2011.

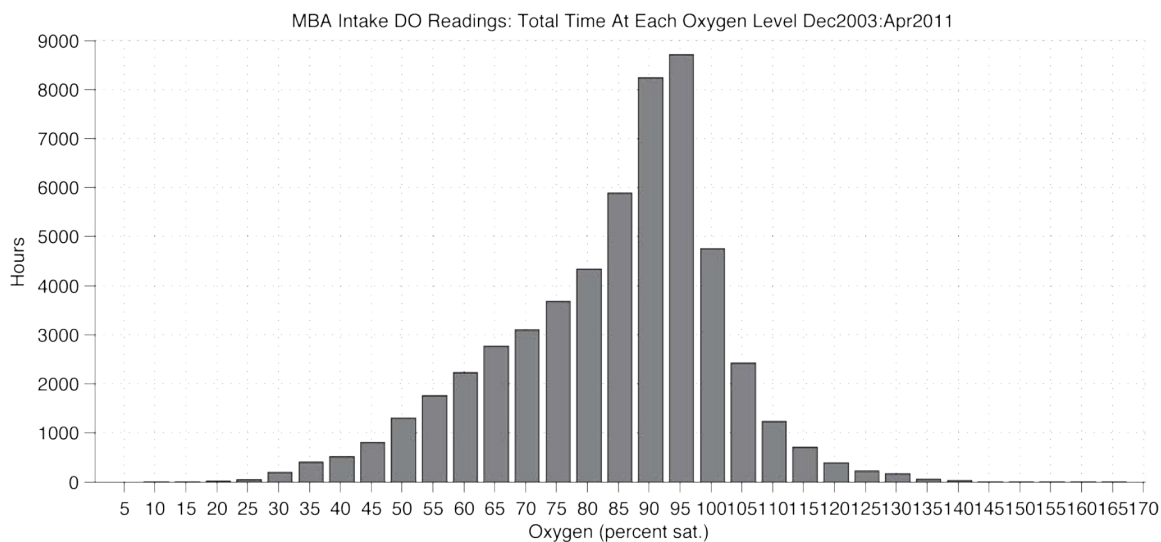
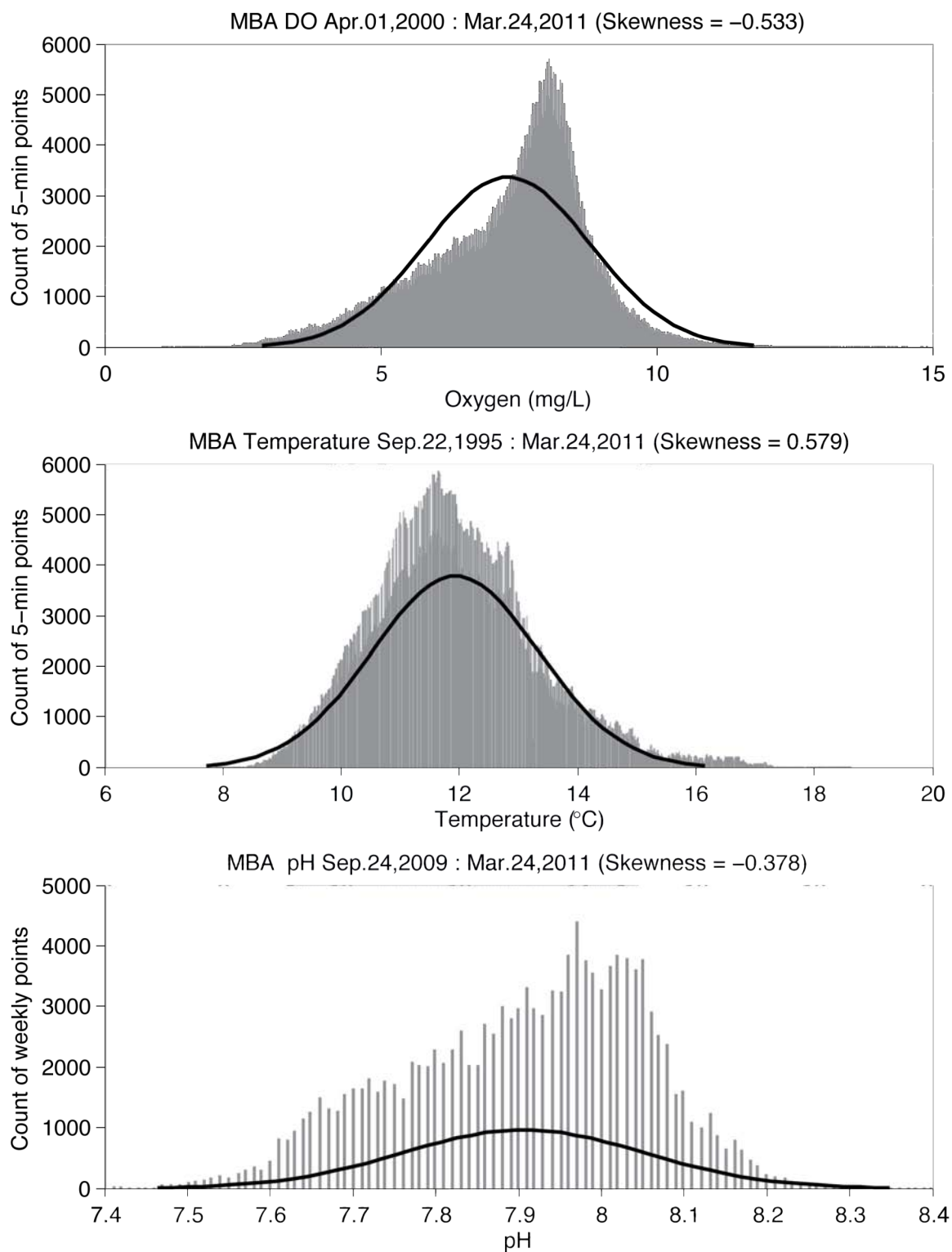


Figure 24 Distribution of time at different dissolved oxygen levels in percent saturation from December 15 2003 – April 29, 2011.

I tested the normality and skewness of the MBA flow-through DO, temperature and pH time series to determine if the time series were nonlinear (Breaker and Ruzmaikin 2010). Non-normal data and data skewed away from 0 indicate that the fluctuations of the signal are more peaked, less like a sine wave and thus nonlinear. A Lilliefors' composite goodness-of-fit test found that the DO ( $p = 0.001$ ), temperature ( $p = 0.001$ ) and pH ( $p = 0.001$ ) time series were not normally distributed at the 5% significance level. Dissolved oxygen and pH were negatively skewed (-0.53 and -0.38 respectively) while temperature showed a positive skew (0.58) (Figure 25). The skewness of DO was tested only for the period of time after the maximum recordable measurement was changed from  $10 \text{ mg L}^{-1}$  to  $20 \text{ mg L}^{-1}$ , in order to represent the true range of values. The peak in DO values at near saturation levels, at approximately  $8 \text{ mg L}^{-1}$ , is clear in the top panel of Figure 25. Both the skewness and Lilliefors' composite goodness-of-fit tests indicate that all three time series were nonlinear, which was an incentive to look at a time series analysis technique, Empirical Mode Decomposition, specifically designed to handle data like this (see next section).



**Figure 25** Distribution of measurements of MBA dissolved oxygen (top panel), temperature (middle panel) and pH (bottom panel), vertical grey bars, superimposed with a fitted normal distribution (black lines).

**NEARSHORE OXYGEN IN SOUTHERN MONTEREY BAY**

Dissolved oxygen distributions changed seasonally (Figure 26). In the winter months (November- February), the distributions were normal with a small negative skewness. From May through October, the distribution of DO became platykurtic and the peak shifted lower away from saturation. The lowest values and highest ranges were seen in April, but the peak of the distribution was lowest in August.

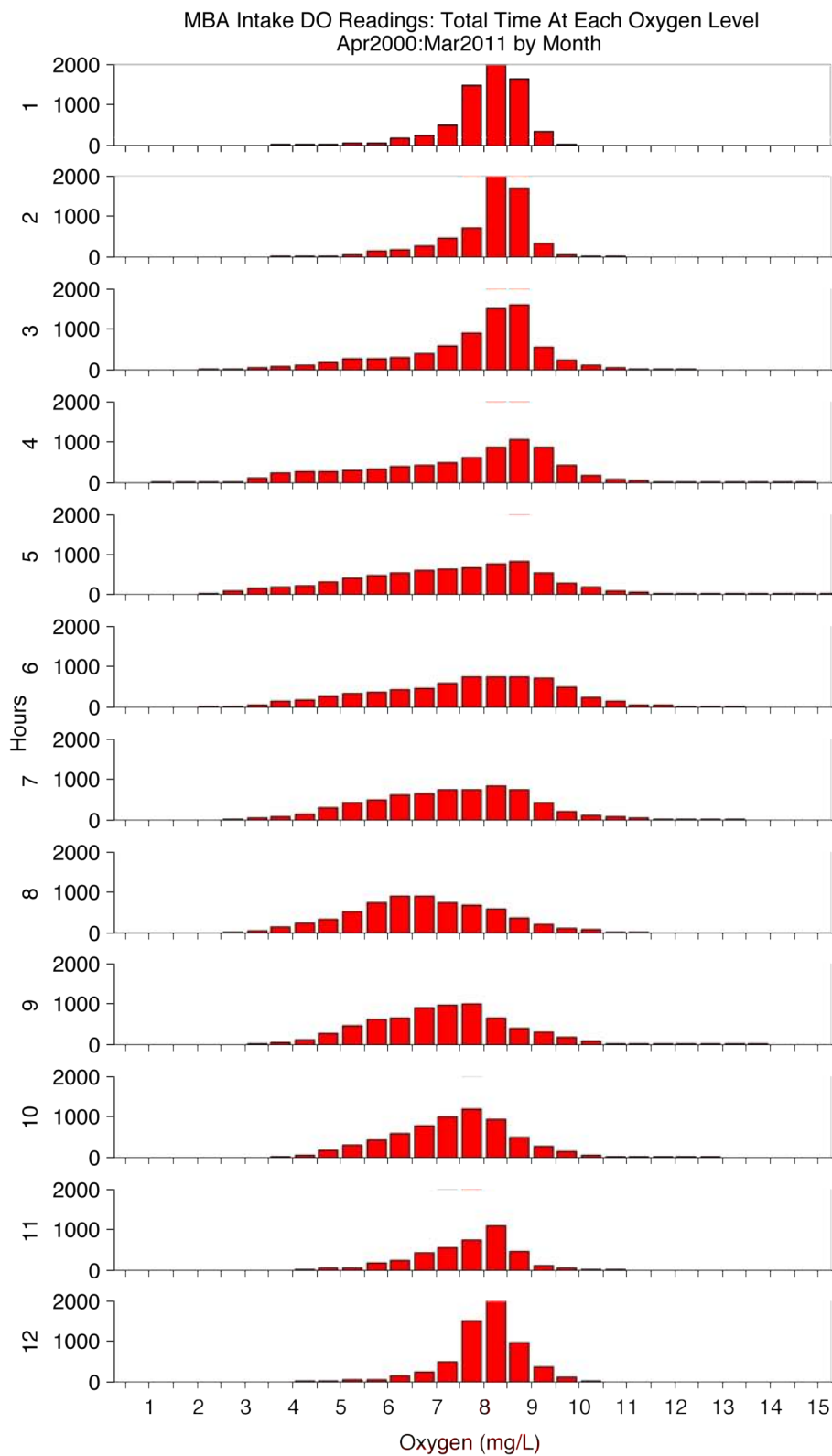


**Figure 26 Monthly distributions of recorded dissolved oxygen values from Monterey Bay Aquarium time series, January (1, top panel) through December (12, bottom panel).**

The MBA flow-through system recorded DO levels below the sublethal ( $4.6 \text{ mg L}^{-1}$ ) and lethal ( $2 \text{ mg L}^{-1}$ ) thresholds multiple times during the record (Figure 27, top panel). There were no obvious interannual trends in the cumulative time under each threshold for each year (Figure 27, bottom left panel). The MBA seawater system was exposed to more than 350 hours of sublethal hypoxic water in 2001-2004 and 2007. There was a strong seasonal pattern in the cumulative time spent under both thresholds when seen by month (Figure 27, bottom right panel). The number of hypoxic hours rose dramatically in March with a peak in April ( $>850$  hours over 10 years) and gradually decreased until October when the amount of time fell below 100 hours again.

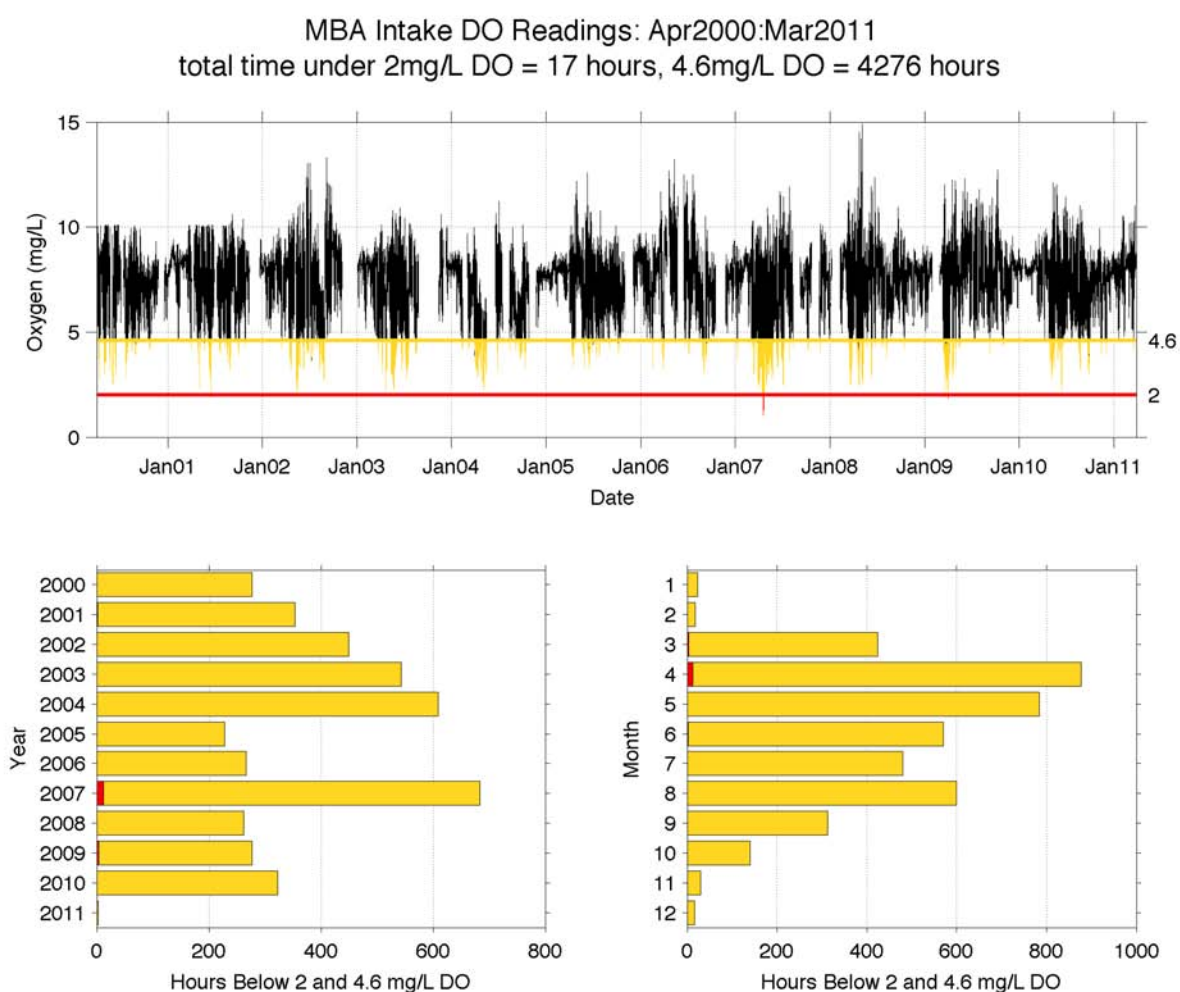


**Figure 27** Monterey Bay Aquarium dissolved oxygen time series April 1, 2000 to March 12, 2011 showing measurements below sublethal ( $4.6 \text{ mg L}^{-1}$ ) and lethal ( $2 \text{ mg L}^{-1}$ ) threshold (top panel). Histograms of recorded hours below sublethal (grey) and lethal (red) threshold during each year (bottom left panel) and month (bottom right panel).



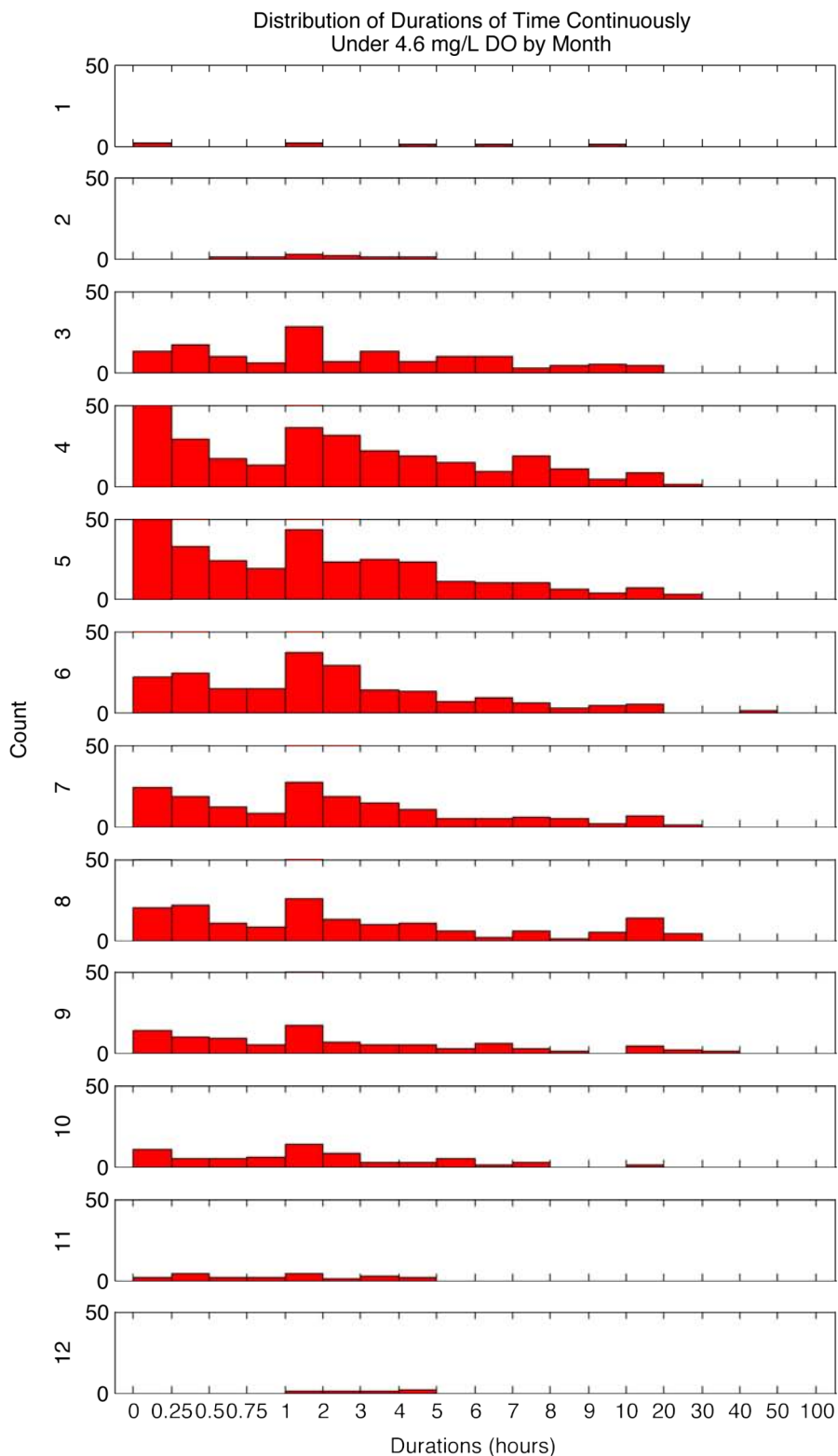


**Figure 28 Monthly distributions of durations of time spend under sublethal ( $4.6 \text{ mg L}^{-1}$ ) dissolved oxygen threshold from the Monterey Bay Aquarium time series, April 1, 2000 to March 12, 2011. Each panel is a month, January (1, top panel) through December (12, bottom panel).**

The duration of sublethal hypoxic events (DO levels below  $4.6 \text{ mg L}^{-1}$ ) was greatest from March through September (Figure 28). Durations were mostly under an hour but on one or two occasions lasted over 24 hours (Figure 28, Figure 29). The distributions of durations followed a gamma distribution. The longest sublethal hypoxic event was 40 hours long in June 2001.

There were very few lethal hypoxic events (DO levels below  $2 \text{ mg L}^{-1}$ ). They occurred only between April 19-22, 2007 (Figure 30) and the longest lethal hypoxic event was 3 hours in duration.

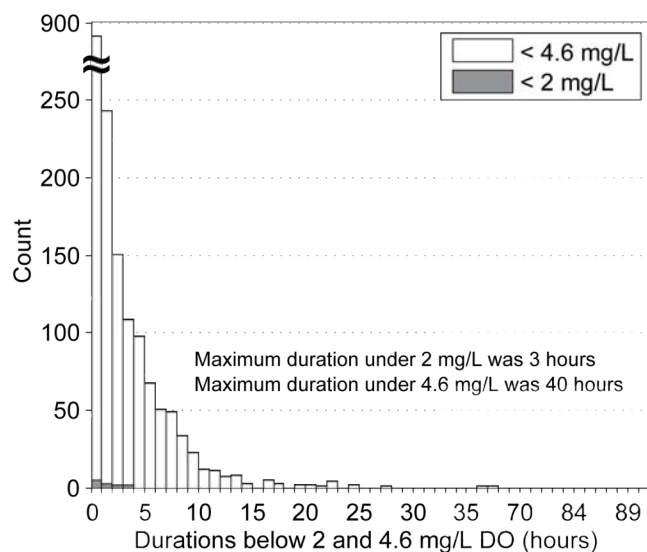


**Figure 29 Distribution of durations of time spent under sublethal ( $4.6 \text{ mg L}^{-1}$ , white bars) and lethal ( $2 \text{ mg L}^{-1}$ , grey bars) dissolved oxygen thresholds from the Monterey Bay Aquarium time series, April 1, 2000 to March 25, 2011.**

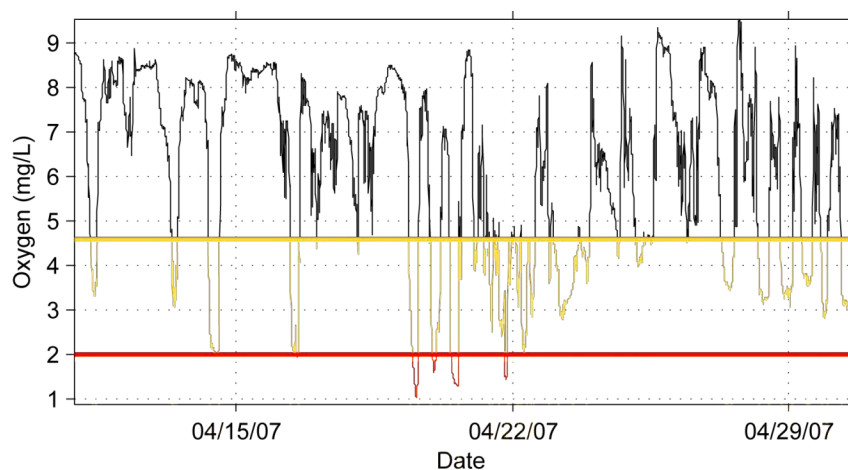


**Figure 30 Dissolved oxygen time series from the Monterey Bay Aquarium flow-through system in southern Monterey Bay on several days surrounding hypoxic events reaching below the  $2 \text{ mg L}^{-1}$ .**

### NEARSHORE pH IN SOUTHERN MONTEREY BAY

The Monterey Bay Aquarium monitored pH on a weekly basis starting in 1996, then in September 2009 an instrument was added to the flow-through system with measurements taken every 5-minutes (Figure 31). High resolution monitoring revealed rapid fluctuations from pH 8.1 to 7.7, a 2.5-fold increase in hydrogen ion concentration in under a day. Weekly ‘spot-check’ data since March 1996 have revealed 43 values below pH 7.75 (min = 7.44, n = 811), a limit that is associated with the dissolution of calcium carbonate (Feely et al. 2008). More low pH (<7.75) measurements were recorded in the later part of the weekly resolution time series.

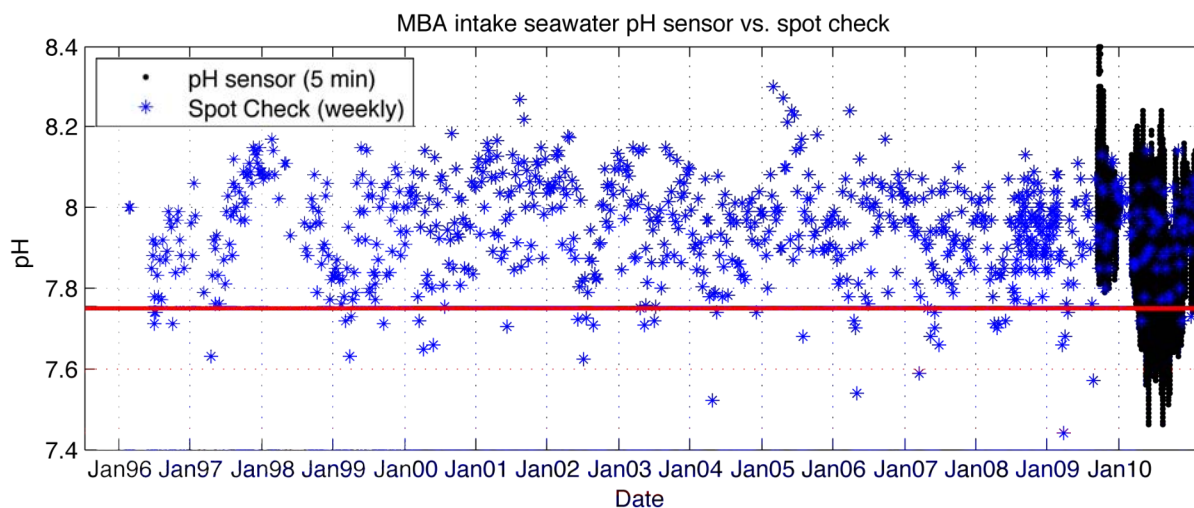


**Figure 31 Weekly spot check (blue asterisks) and high-resolution (black dots) measurements of pH in nearshore waters in southern Monterey Bay measured by the Monterey Bay Aquarium. Red line indicates a pH value of 7.75.**

### COMPARING DISSOLVED OXYGEN, TEMPERATURE AND pH IN SOUTHERN MONTEREY BAY

A comparison between the 5 minute DO and temperature from the Monterey Bay Aquarium (MBA) flow-through system showed a positive relationship that varied seasonally (Figure 32, Figure 33). Multiple linear regression slopes and  $R^2$  values are shown in Figure 33. Slopes ranged from 0.32 to 1.13. Larger slopes in the upwelling

season indicate that there was a wider DO range experienced during the upwelling season than during the winter, as mentioned above.

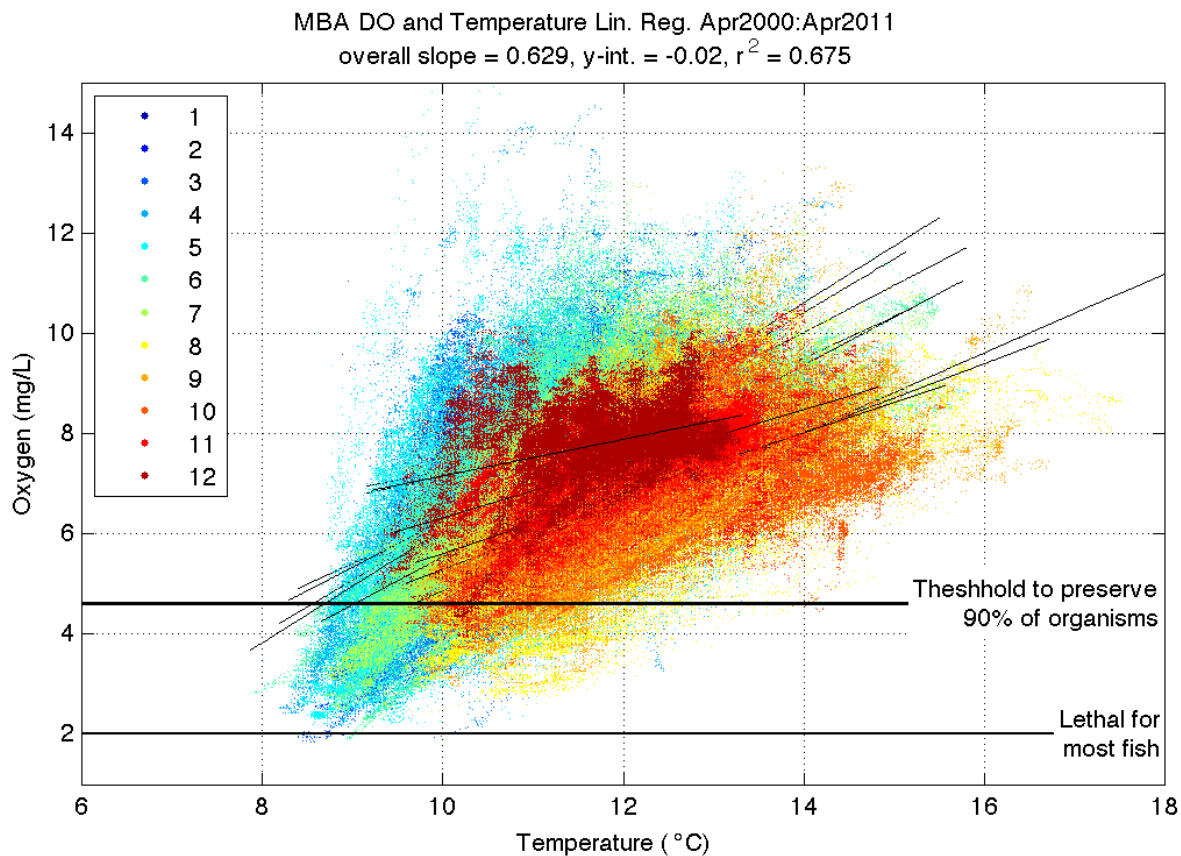


**Figure 32 Temperature plotted against dissolved oxygen from Monterey Bay Aquarium seawater intake, April 2000 to April 2011. Colors indicate month as noted in the legend. Black diagonal lines are monthly linear regressions while black horizontal lines indicate 2 and 4.6 mg/L dissolved oxygen thresholds.**

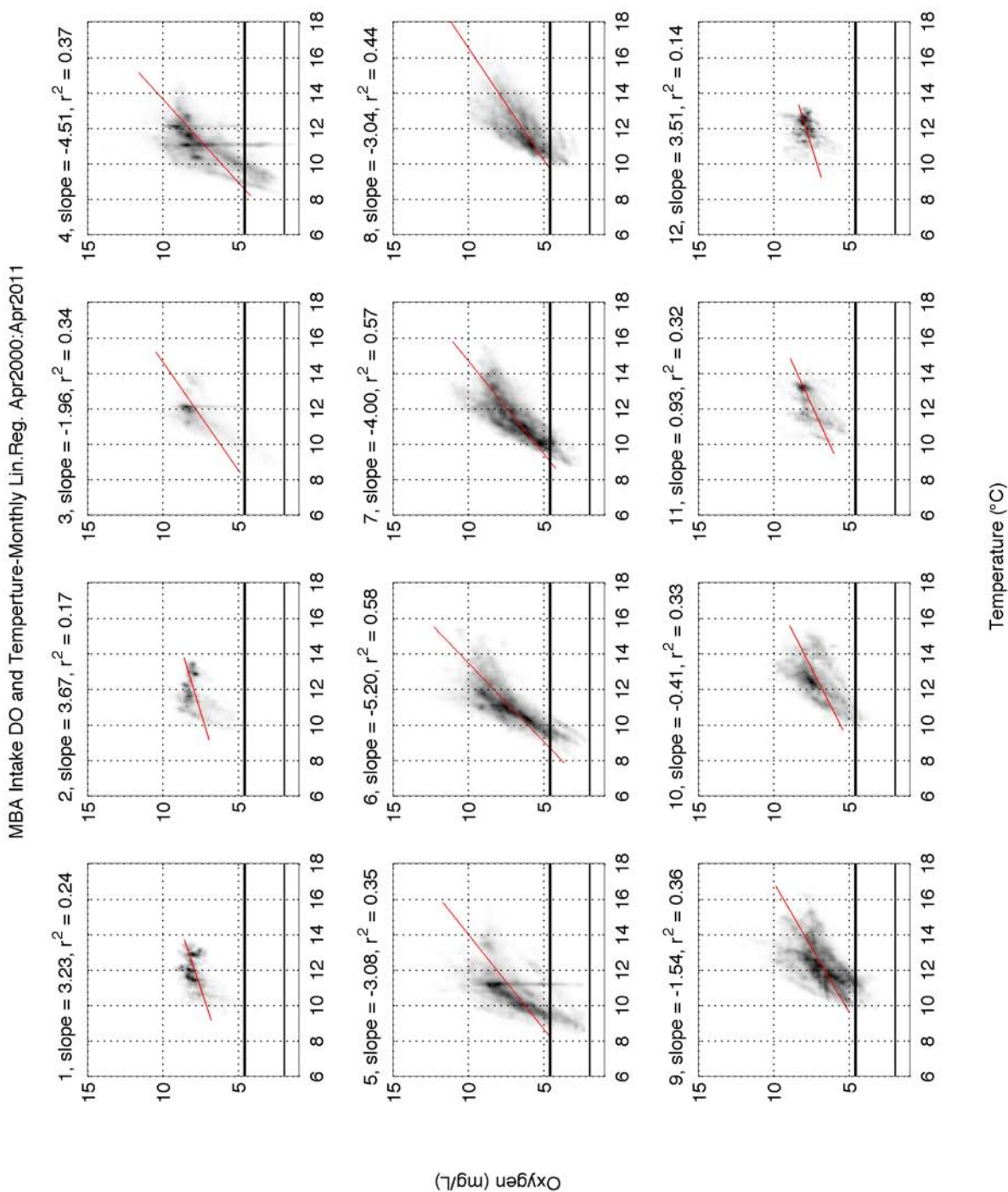


**Figure 33 Monthly smoothed point densities plots of temperature plotted against dissolved oxygen from Monterey Bay Aquarium seawater intake, April 2000 to April 2011. Red diagonal lines are monthly linear regressions while black horizontal lines indicate 2 and 4.6 mg/L dissolved oxygen thresholds.**

A cross covariance between 10-minute averaged DO and temperature over the entire time series, April 2000 to April 2011, lagging up to one day (1440 min) gave a

maximum correlation coefficient of 0.521 with no lag (Figure 34). Minor correlation coefficient peaks were seen approximately 12.4 hours before and after, indicative of the semidiurnal tidal signal in both temperature and DO. Gaps in either time series were removed from both time series and replaced with zeros. For short comparisons between temperature and DO over a few days to weeks, cross covariance analyses showed correlation coefficients as strong as 0.99. Monthly cross covariance analyses gave a range of correlation coefficients with mean of 0.73 (not normalized for missing data). Generally, higher correlation coefficients were seen during the upwelling season, April-August (Figure 35). DO acted like a conservative tracer in this system, indicating that the primary driver of variability is advection and not biological.

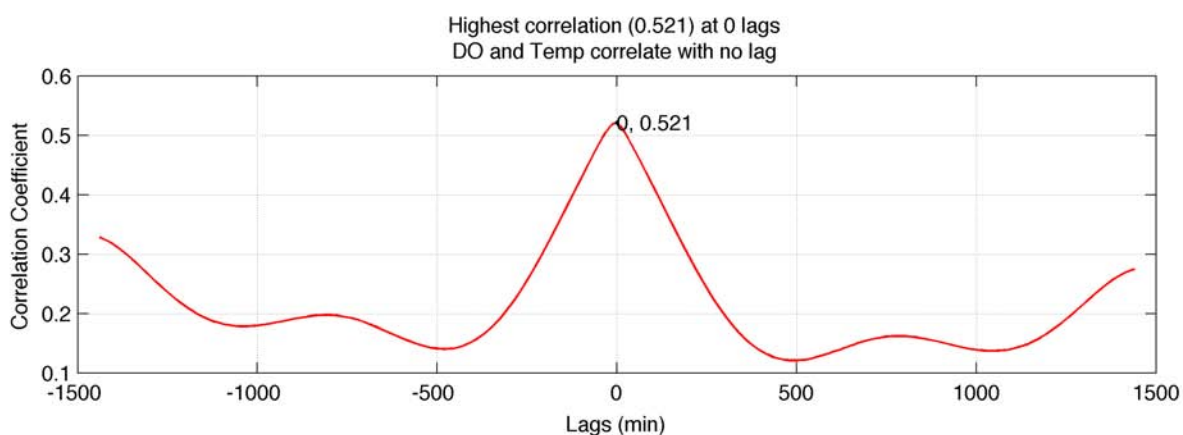


**Figure 34 Cross covariance analysis of Monterey Bay Aquarium flow-through dissolved oxygen and temperature over the entire time series, April 2000 to April 2011.**



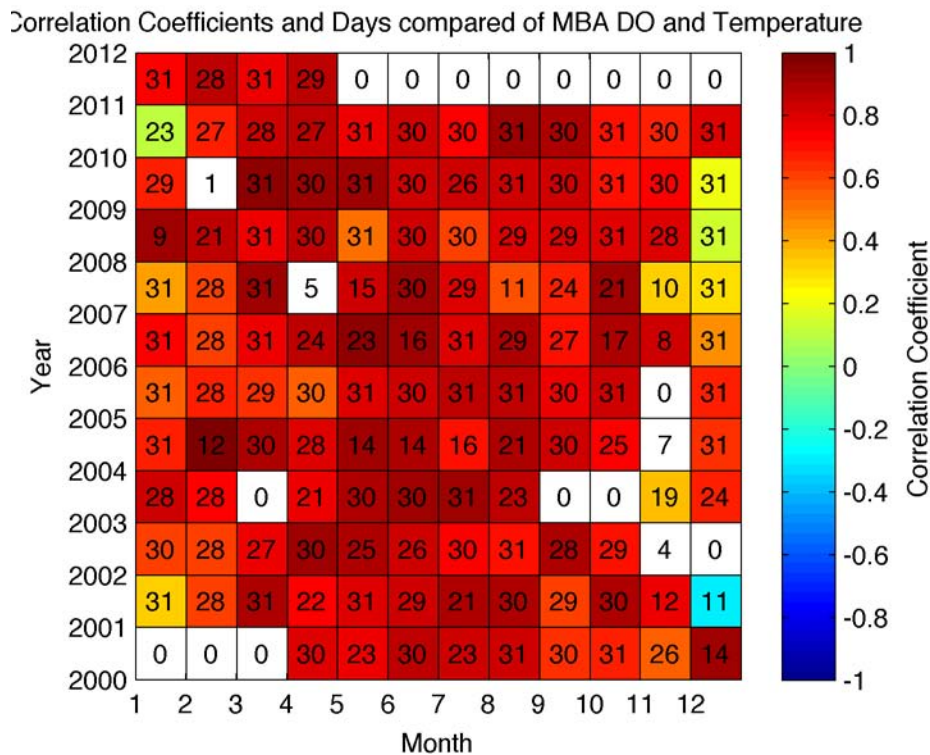


**Figure 35 Matrix of monthly correlation coefficients (color) and lags (numbers in boxes) for cross covariance analyses between Monterey Bay Aquarium (MBA) dissolved oxygen (DO) and temperature for each year, 2000-2011. White indicates insufficient data.**

Dissolved oxygen and pH from the MBA flow-through system were positively correlated (cross covariance correlation coefficient = 0.822) with no lag (Figure 36). Monthly linear regressions between DO and pH showed a higher slope during the upwelling season, indicating that for low DO values, pH was lower.

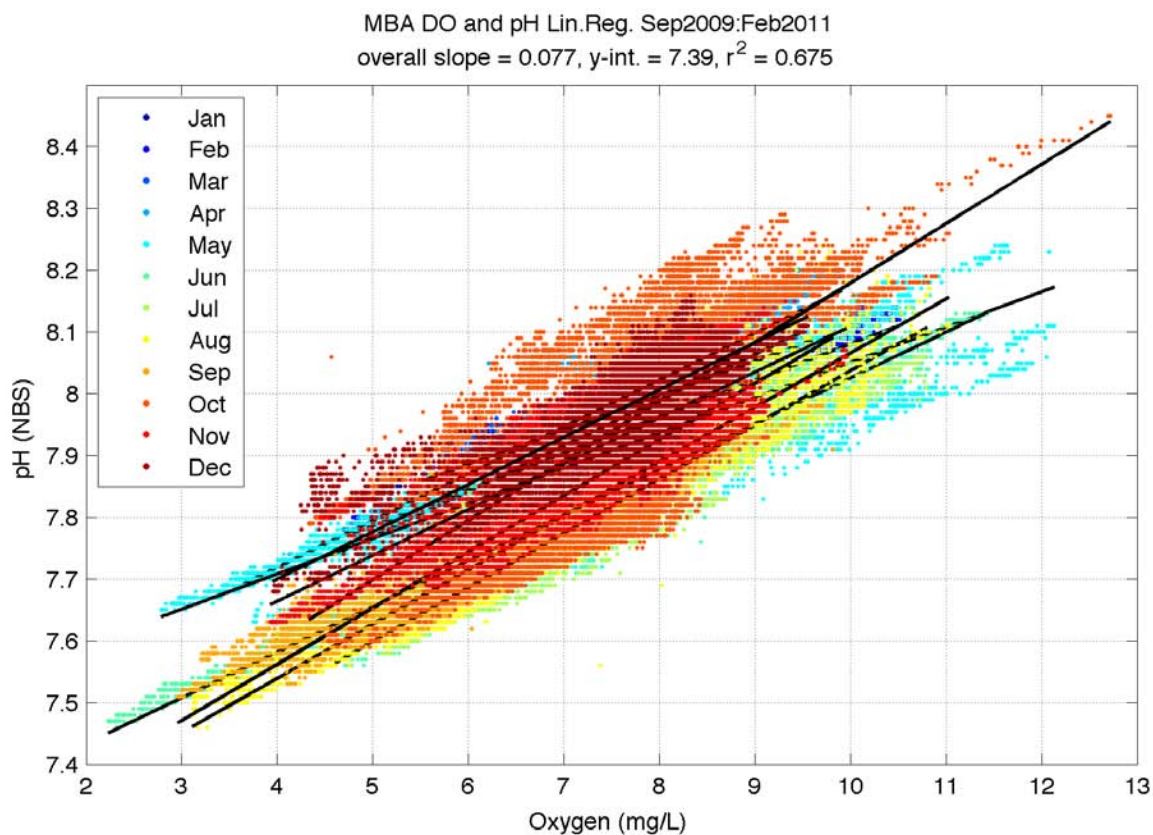


**Figure 36** Dissolved oxygen plotted against pH from Monterey Bay Aquarium seawater intake, September 2009 to March 2010. Colors indicate month as noted in the legend. Black diagonal lines are monthly linear regressions while black horizontal lines indicate 2 and 4.6 mg/L dissolved oxygen thresholds.

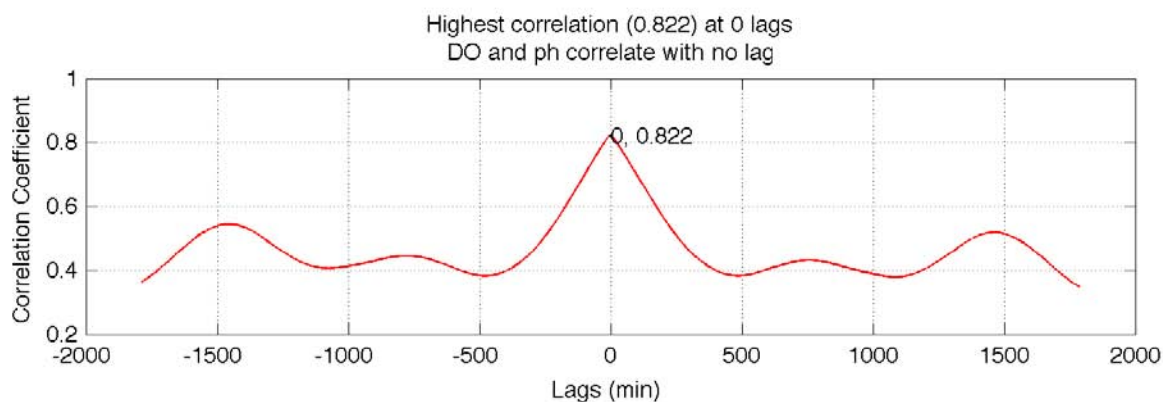


**Figure 37** Top panel, time series of normalized dissolved oxygen and pH from the Monterey Bay Aquarium September 2009 to February 2011. Bottom panel, cross covariance analysis of dissolved oxygen and pH over the entire time series.



### SEASONAL PATTERNS OF VARIABILITY

There was a consistent pattern in variability across the ten years of the Monterey Bay Aquarium time series in both dissolved oxygen (DO) and temperature. Daily variability was low during the winter (October through February), then increased dramatically around mid-March (Figure 38, Figure 39). Daily temperature variability stayed consistently high from March through October, whereas DO daily variance peaked in June-July and then gradually decreased to winter levels. When variability was high, hypoxic events were more likely to occur. Not only did DO get lower during the summer, but there were also peaks above 100 percent saturation (Figure 38). As DO variability decreased, so did the frequency of hypoxic and super-saturation events. Temperature saw its lowest levels between March and July. Unlike DO, daily maximal temperature during this time decreased as well. In late summer/early fall (July through October), daily maximums increased above the overall mean of 11.9°C (Figure 39). The pH measurements at MBA followed the same seasonal pattern as DO during the year that they were recorded (Figure 31).

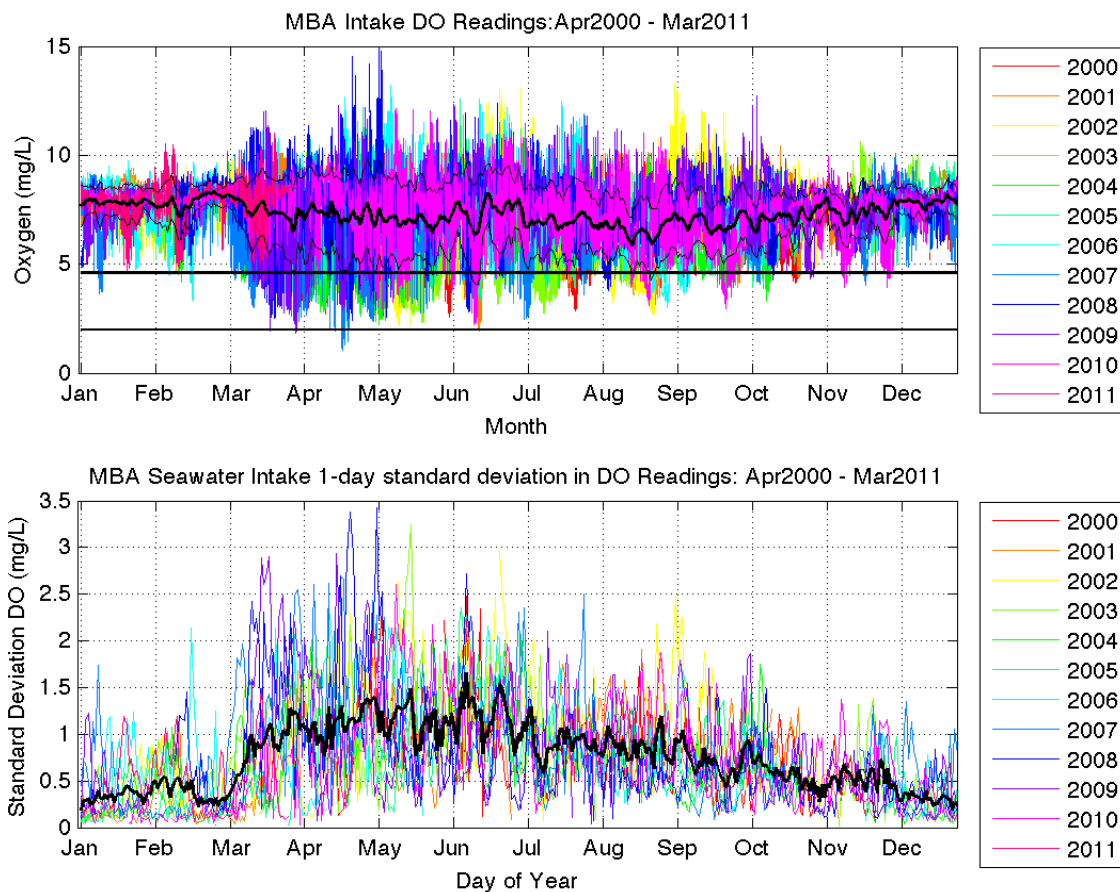


**Figure 38** Top panel, dissolved oxygen at the Monterey Bay Aquarium against day of year. All years are overlaid (colored lines) with daily mean (thick black line) and daily standard deviation (thin black line) over all years. Bottom panel, absolute value of daily standard deviation. Individual years are plotted as colored lines and mean as a thick black line.

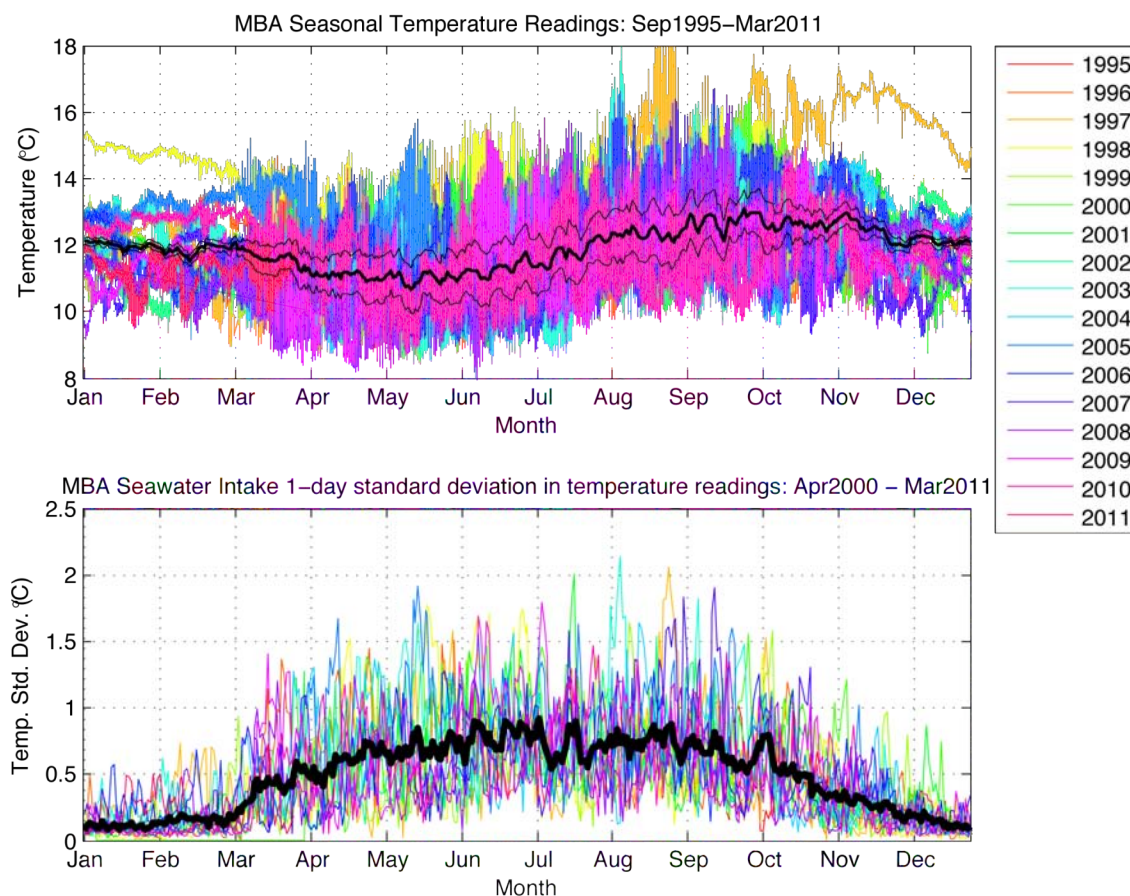


**Figure 39** Top panel, temperature at the Monterey Bay Aquarium against day of year. All years are overlaid (colored lines) with daily mean (thick black line) and daily standard deviation (thin black line) over all years. Bottom panel, absolute value of daily standard deviation. Individual years are plotted as colored lines and mean as a thick black line.

The dominant patterns in the DO, temperature and pH time series at MBA were a strong positive correlation between all variables with no lag. During the winter months, daily variability was low. In early to mid-March, it increased dramatically and stayed high until the fall. Dissolved oxygen and pH measurements often fell to levels considered physiologically stressful, less than 4.6 and 2 mg O<sub>2</sub> L<sup>-1</sup> and less than 7.75 pH.

### CARBONATE CHEMISTRY

Increasing interest in ocean acidification and the low pH values measured in both the weekly and 5-minute flow-through time series raise the question: Is the low pH water corrosive to calcium carbonate? The amount of free hydrogen ions affects the availability of carbonate ions (CO<sub>3</sub><sup>2-</sup>) necessary to react with calcium ions (Ca<sup>2+</sup>) to form calcium

carbonate ( $\text{CaCO}_3$ ). Calcium carbonate has two forms, aragonite and calcite, the former being more soluble. Both forms are used by marine organisms to build structural tests and shells. A measure of the favorability of seawater to the formation of calcium carbonate is the saturation state ( $\Omega_{\text{arag}}$ ). The saturation state is given by the equation:

$$\Omega_{\text{arag}} = \frac{[\text{Ca}^{2+}][\text{CO}_3^{2-}]}{K'_{\text{sp}}}$$

where  $K'_{\text{sp}}$  is the apparent stoichiometric solubility product of either aragonite or calcite. The concentration of calcium ions is estimated from the salinity, and the carbonate ion concentration is calculated from any two of the four measurable parameters of the  $\text{CO}_2$  system [total alkalinity (TA), total inorganic  $\text{CO}_2$  ( $\text{TCO}_2$  or DIC), pH, and partial pressure of  $\text{CO}_2$  ( $\text{pCO}_2$ )] (Lewis and Wallace 1998).

Feely et al. (2008) found that the offshore waters of the California Current System, pH values lower than 7.75 were associated with waters unfavorable to the formation of aragonite ( $\Omega_{\text{arag}} < 1$ ), which is an additional stressor to the ecosystem (Fabry et al. 2008). Measurements of total alkalinity (TA), total carbon dioxide ( $\text{TCO}_2$ ) and  $\text{CO}_3^{2-}$  were added to the weekly water chemistry monitoring program in May 2010. All variables were derived using a Gran titration method on a Metrohm 809 Titrando using Tiamo Titration Software. The saturation state of aragonite was calculated using a program developed by (Lewis and Wallace 1998) using  $\text{TCO}_2$  and flow-through pH along with salinity, temperature and  $\text{PO}_4$ . Dissolution constants by (Mehrbach et al. 1973) refit by (Dickson and F.J. Millero 1987) were applied (Lewis and Wallace 1998). Silicate was not measured and was estimated at  $50 \mu\text{mol kg}^{-1}$  (Lewis and Wallace 1998). The combination of  $\text{TCO}_2$  and pH were used because it allowed for an inter-lab comparison (see next paragraph) and showed similar results.

An inter-lab comparison of pH and  $\text{TCO}_2$  values was conducted. Five water samples were taken at MBA and analyzed by personnel in Dr. Jim Barry's lab at the Monterey Bay Aquarium Research Institution (MBARI) using the methods described in Friederich et al. (2002). Discrete measurements of pH taken by MBA staff using the same water with the Hach probe were within 0.09 pH units of estimates by the Barry lab and within 0.14 of the flow-through measurement at the time of the sampling (Table 4). The high standard deviation in the redundant MBA pH spot checks may have been due to the Hach probe

not being left in the sample long enough to stabilize. While the spot check measurements were closer to the Barry lab estimates, over all the pH from the flow-through system was trusted more because it avoided the introduced human error stated above. Unfortunately, the analytical variability was almost the same as the environmental variability.

**Table 4 Inter-lab comparison of carbonate chemistry. Total CO<sub>2</sub> (TCO<sub>2</sub>) and pH samples measured at the Monterey Bay Aquarium (MBA) and by Dr. Jim Barry's lab at the Monterey Bay Aquarium Research Institution (MBARI). MBARI pH measurements measured converted from Total scale to NBS scale using CO2SYS.**

	MBA TCO <sub>2</sub> (mmol/L)	MBARI TCO <sub>2</sub> (mmol/L)	MBA 'spot' pH (NBS scale)	MBA flow- through pH (NBS scale)	MBARI pH (Total scale)	MBARI pH (NBS scale)
	1.97	2.1299	7.80	7.78	7.824	7.901
	2.10	2.0877	7.96		7.827	7.933
	2.00	2.1019	7.80		7.812	7.936
	1.99		7.80		7.823	7.921
	2.04		7.80			
mean	2.02	2.1065	7.83	7.78	7.822	7.923
range	0.13	0.0422	0.16	-	0.015	0.035
std. dev.	0.05	0.0215	0.07	-	0.007	0.016

Total Alkalinity values estimated by MBA were relatively stable throughout the time series, only varying by 0.09 meq L<sup>-1</sup> with a mean of 2.27 meq L<sup>-1</sup> while both TCO<sub>2</sub> and CO<sub>3</sub><sup>2-</sup> varied by about 0.2 mmol L<sup>-1</sup> (Figure 41). The saturation state of aragonite, calculated from TCO<sub>2</sub> and pH, often fell below saturation ( $\Omega_{\text{arag}} = 1$ ) with a mean of 1.27 and standard deviation of 0.33. When  $\Omega_{\text{arag}}$  was estimated using different parameters results varied. Using TA and pH the mean of  $\Omega_{\text{arag}}$  was 1.33±0.32 and with TA and TCO<sub>2</sub> the mean was 2.23±0.57. Estimates using TA and TCO<sub>2</sub> were much higher and never fell below 1; these results were far from the Barry lab estimate, which may be due to the fact that TA and TCO<sub>2</sub> were not independently estimated.

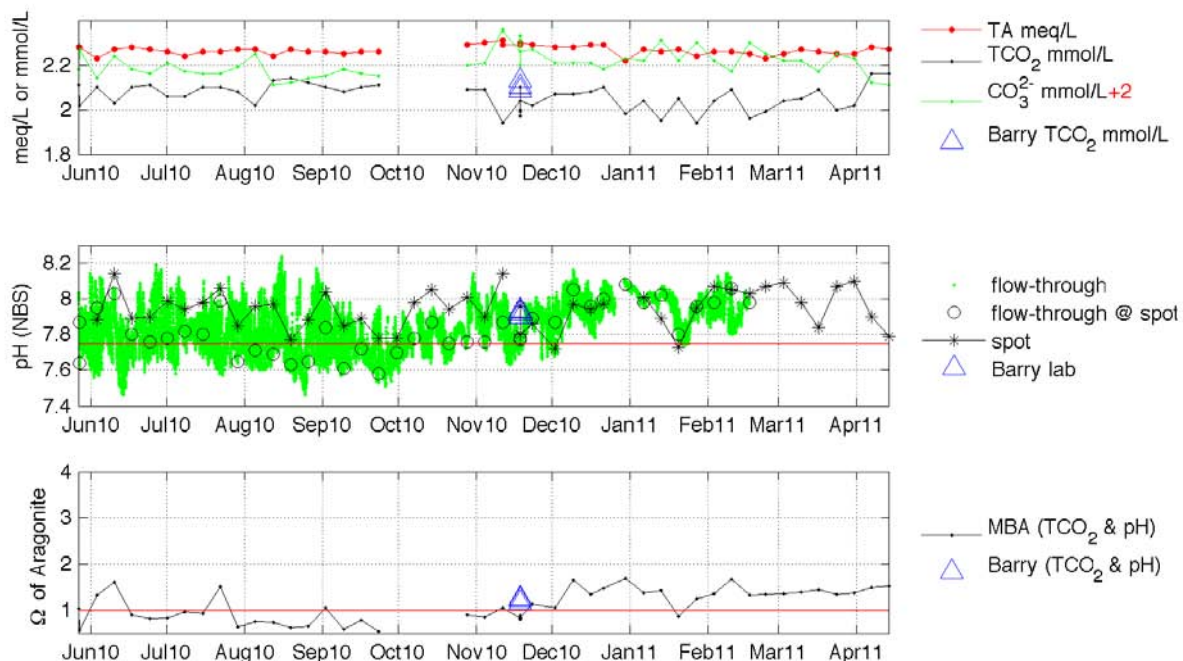


**Figure 36** Weekly carbonate chemistry time series conducted at the Monterey Bay Aquarium. Top panel, Total Alkalinity (TA, red), Total CO<sub>2</sub> (TCO<sub>2</sub>, black), and carbonate (CO<sub>3</sub><sup>2-</sup>, green). Note carbonate values were increases by 2 mmol L<sup>-1</sup> to facilitate plotting on the same scale as other variables. Inter-lab comparison of TCO<sub>2</sub> by Barry lab (blue triangles). Middle panel, 5-minute pH samples from the flow-through system (green dots) and values at time of weekly ‘spot check’ (black circles), weekly spot check value (black line and asterisks). Inter-lab comparison of pH by Barry lab (blue triangles). Red line indicates Feely et al. 2008 7.75 threshold in pH associated with a Ω<sub>arag</sub> of 1. Bottom panel, time series of Ω<sub>arag</sub> estimated using TCO<sub>2</sub> and pH by CO<sub>2</sub>SYS, MBA values (black line and dots) and Barry lab (blue triangles).

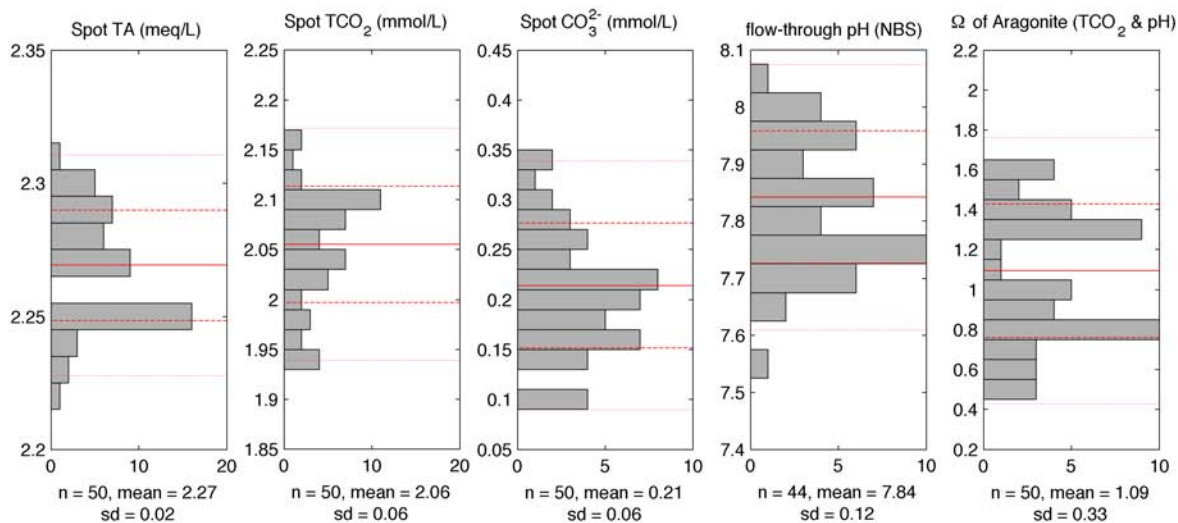


**Figure 41** Frequency distributions of weekly discrete ‘spot-check’ carbonate chemistry results and associated pH values taken from flow-through time series. Red lines indicate the mean (solid) and 1<sup>st</sup> (dashed) and 2<sup>nd</sup> (dotted) standard deviations.

The saturation state of aragonite had a positive correlation with pH, DO and temperature (Figure 38). The mean of the saturation state of aragonite was lower (higher solubility) ( $\Omega_{\text{arag}} = 1.03 \pm 0.36$ ) during the upwelling season (March-September) than in the winter (October-February) ( $\Omega_{\text{arag}} = 1.16 \pm 0.23$ ) (Figure 38, Figure 39). A seasonal difference was seen in all carbonate chemistry variables (Figure 39).

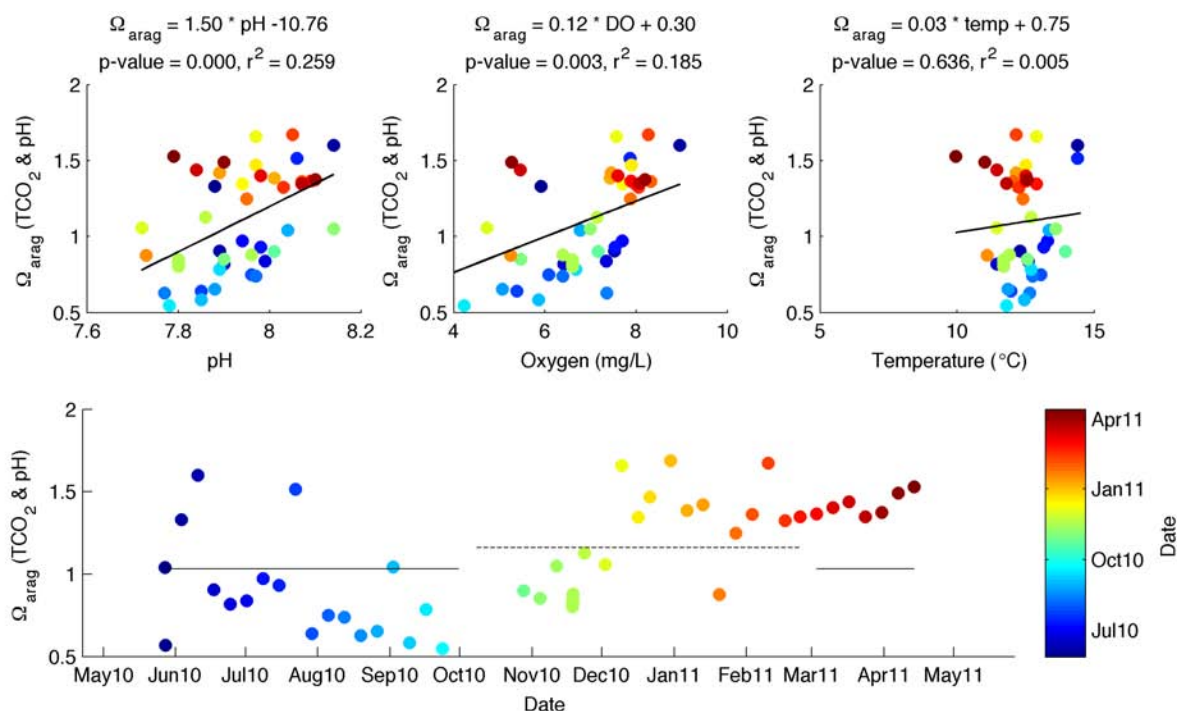


**Figure 38** Saturation state of aragonite ( $\Omega$ ) plotted against pH, dissolved oxygen, temperature and date. Linear regressions are plotted as black lines Colors indicate date of sample. Black lines in lower panel show mean for upwelling (March-September) and winter (October-February) seasons.



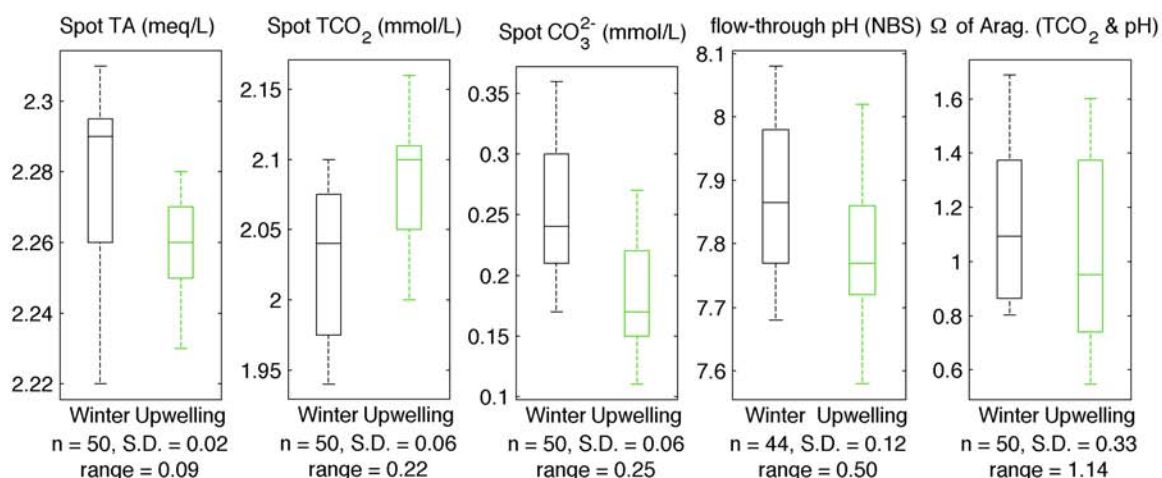


**Figure 39** Box plots of carbonate chemistry samples for winter (October-February, black) and upwelling (March-September, green) seasons.

### WATER PROFILES

In order to better understand the entire water column with respect to DO, CTD water profiling was used to compare with the high resolution DO from the MBA. Four CTD casts were conducted by members Dr. William Gilly's lab of the Hopkins Marine Station within 150 m of the MBA intake mouth. Deployments were made in April 2009 with a Seabird SBE19plus profiler equipped with a SBE43 DO sensor to capture a snapshot of water-column stratification under different regimes and a measure of salinity (Figure 40). MBA DO ranges corresponded strongly to those measured by the casts; however, direct comparisons in time were not possible due to the lag introduced by the intake system.



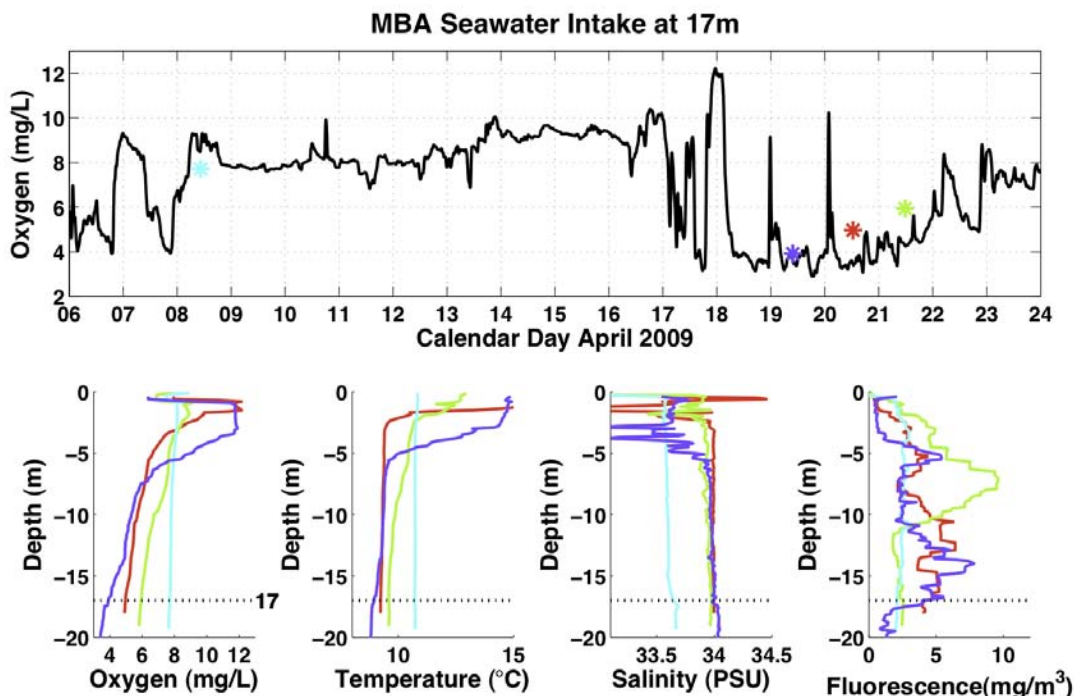


**Figure 40 Comparison between MBA oxygen time series and four CTD profiles collected within 150 m of MBA intake pipe mouth. Top panel, MBA dissolved oxygen values (black line) over several days in April 2009 and oxygen levels of four CTD casts at 17 m depth (colored asterisks). Bottom panels, four CTD profiles showing changing hydrography. Horizontal black dotted line indicated 17 m depth associated with MBA intake.**

The water profile on April 8<sup>th</sup> showed a mixed water column and from the MBA time series it appears to have stayed mixed until April 17<sup>th</sup>, when cold water appeared at depth and the mixed layer was confined to the upper 4 m. By April 20<sup>th</sup>, the mixed layer was compressed to the upper 1-2 m. The water column began to mix again by the 21<sup>st</sup> when the upper and lower layers became more similar. In the DO time series, both the upper mixed layer (Figure 40, spikes seen in MBA time series on April 18-20<sup>th</sup>) and cold bottom water were sampled. The DO levels as low as 5.5 mg L<sup>-1</sup> as shallow as 7 m was unexpected.

**WHAT ARE THE DOMINANT TIME SCALES OF HIGH VARIABILITY IN OXYGEN AND PH? WHAT ARE THE RELATIONSHIPS BETWEEN THE MEASURED VARIABLES AND UNDERLYING DRIVERS OF SYSTEM VARIABILITY? ARE THERE ANY TRENDS IN THE TIME SERIES?**

**Analysis and Results**

Several different methods were employed to understand the underlying drivers of variability in dissolved oxygen (DO), temperature and pH at the Monterey Bay Aquarium (MBA). The time scales with the most variability were detected and comparisons were made to identify possible drivers.

**SEASONAL PATTERNS**

A dramatic seasonal difference in the variance of DO, temperature and pH coincided occurred in March (Figure 41). There is no evidence that oxygen depletion is caused by nutrient enrichment from terrestrial runoff into Monterey Bay. Precipitation and elevated runoff from local rivers (Salinas, Pajaro and San Lorenzo, Figure 4 map) are typically limited in this area to the period between November and April (Western Regional Climate Center 2011) and are thus out of phase with the season for hypoxic events (Figure 41). There is likely no lagged response to terrestrial input since the seasons are completely out of phase, biological time scales are relatively short, and in eastern boundary current ecosystems, upwelling is by far the largest introduction of nutrients to the system (McPhee-Shaw et al. 2007). The dramatic onset of high variance perfectly coincides with the spring upwelling transition, typically in March-April (Bograd et al. 2009).

MBA Seawater Intake 1-day standard deviation in DO Readings: Apr2000 - Nov2010

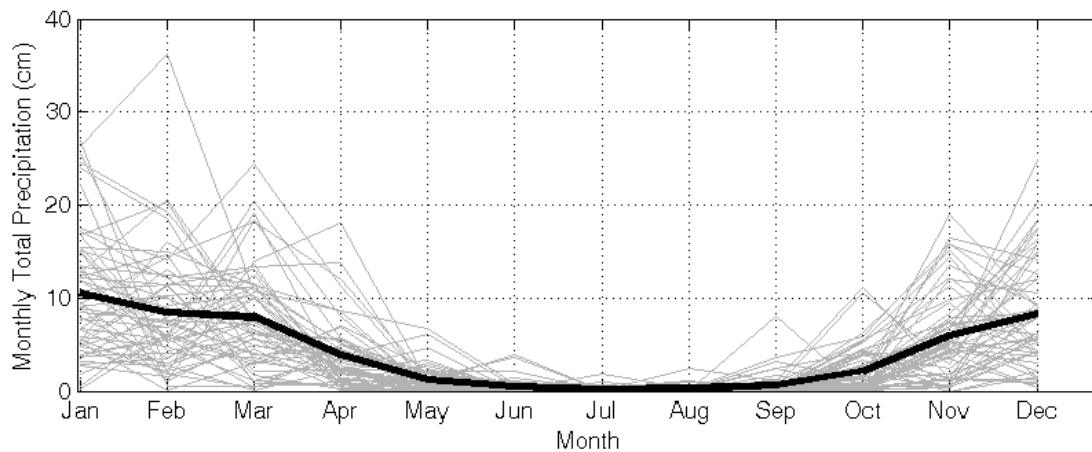
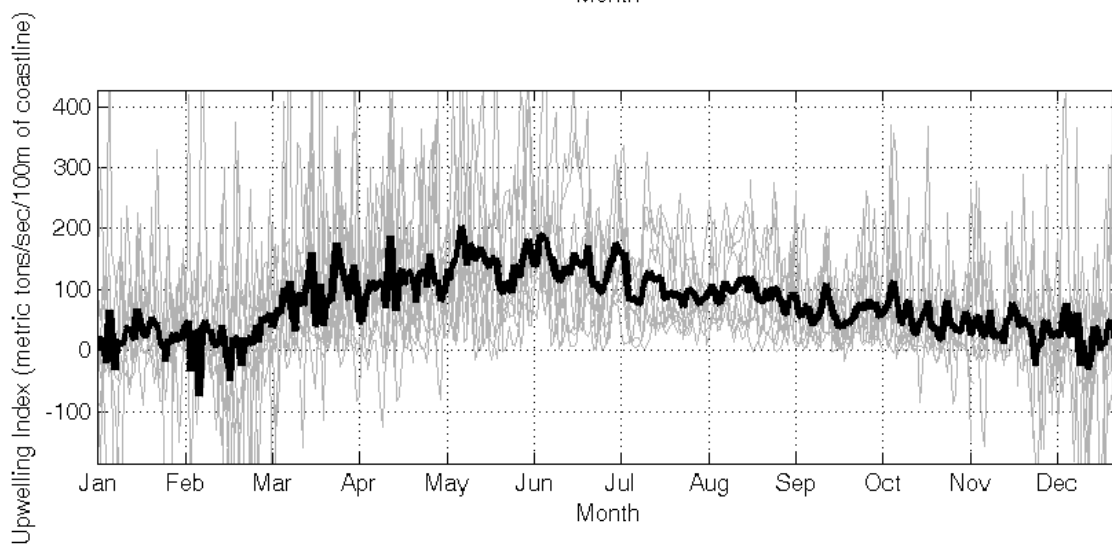
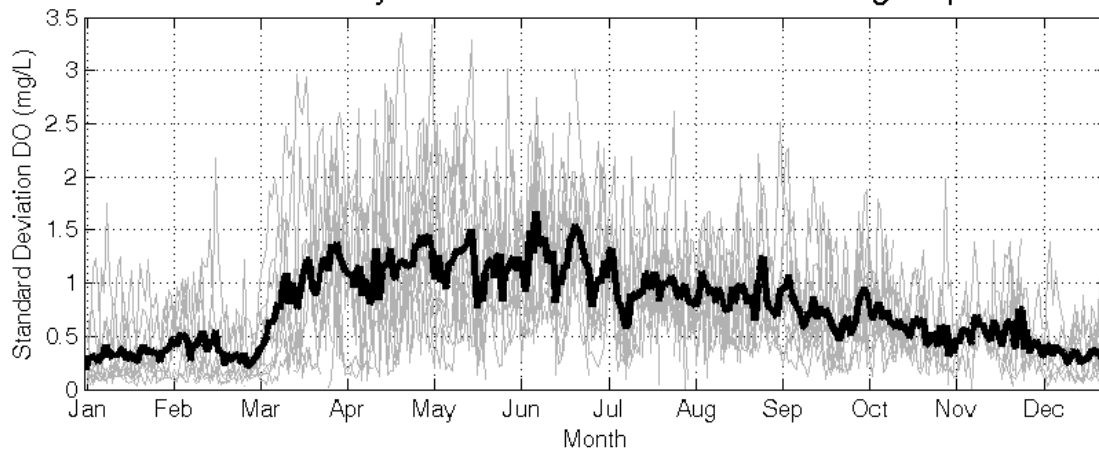


**Figure 41 Running 1-day standard deviation of dissolved oxygen ( $\text{mg L}^{-1}$ ) taken by the Monterey Bay Aquarium (April 2000 – November 2010) (top panel) and NOAA upwelling index for  $36^\circ\text{N}$  ( $\text{metric tons sec}^{-1} 100 \text{ m}^{-1}$  of coastline) (middle panel) over day of year. All years are overlaid (gray lines) and day of year means are plotted in black. Bottom panel, monthly total precipitation in Monterey, CA with all years overlaid (grey lines) and monthly means across years (black line).**

### SPECTRAL ANALYSIS

Spectral analysis was used to identify which frequencies contained the highest variance (energy) in the MBA time series, which would aid in identifying possible system drivers by matching up time scales of fluctuations. Spectral analyses of the DO and temperature time series were performed using both a short and long window length in order to resolve peaks at high and low frequencies. A smoothed power spectrum was produced by Welch's method of averaging replicate spectra calculated on a series of 50% overlapping 85-day sections of the data to look at tidal band frequencies and 7.5-year for seasonal peaks. The time series resolution was averaged to 1 hour, resulting in a maximum resolvable period of 2 hours (Nyquist frequency =  $(2 \cdot \Delta t)^{-1}$ ). Both short and long windowing methods produced dominant peaks at 1.00 and 1.93 cycles per day, the diurnal and semidiurnal tidal frequencies ( $K_1$  and  $M_2$ ), corresponding to periods of 24.0 and 12.4 hours in both DO and temperature (Figure 42, left panels, red circles). The spectral amplitudes of the diurnal peaks are much larger than lower frequency amplitudes for low-frequency fluctuations and at more than twice that of the semidiurnal peaks. A higher amplitude of  $K_1$  relative to  $M_2$  may be indicative of a diurnal wind signal (Woodson et al. 2007), but (Crabbe 2007) found no correlation between local winds and currents associated with internal waves. Smaller peaks seen at the 3 and 4 cycles per day are harmonics of the semidiurnal and diurnal tides, indicating nonlinearity in the signal and an asymmetric response of the fundamentals (McPhee-Shaw et al. 2004). The asymmetric nature of the internal tide has been documented by Storlazzi et al. (2003). Longer window length revealed a strong peak at the annual frequency (Figure 42, right panels, red circles). Peaks at the weather band, periods around 10 days, were not persistent across different window lengths.

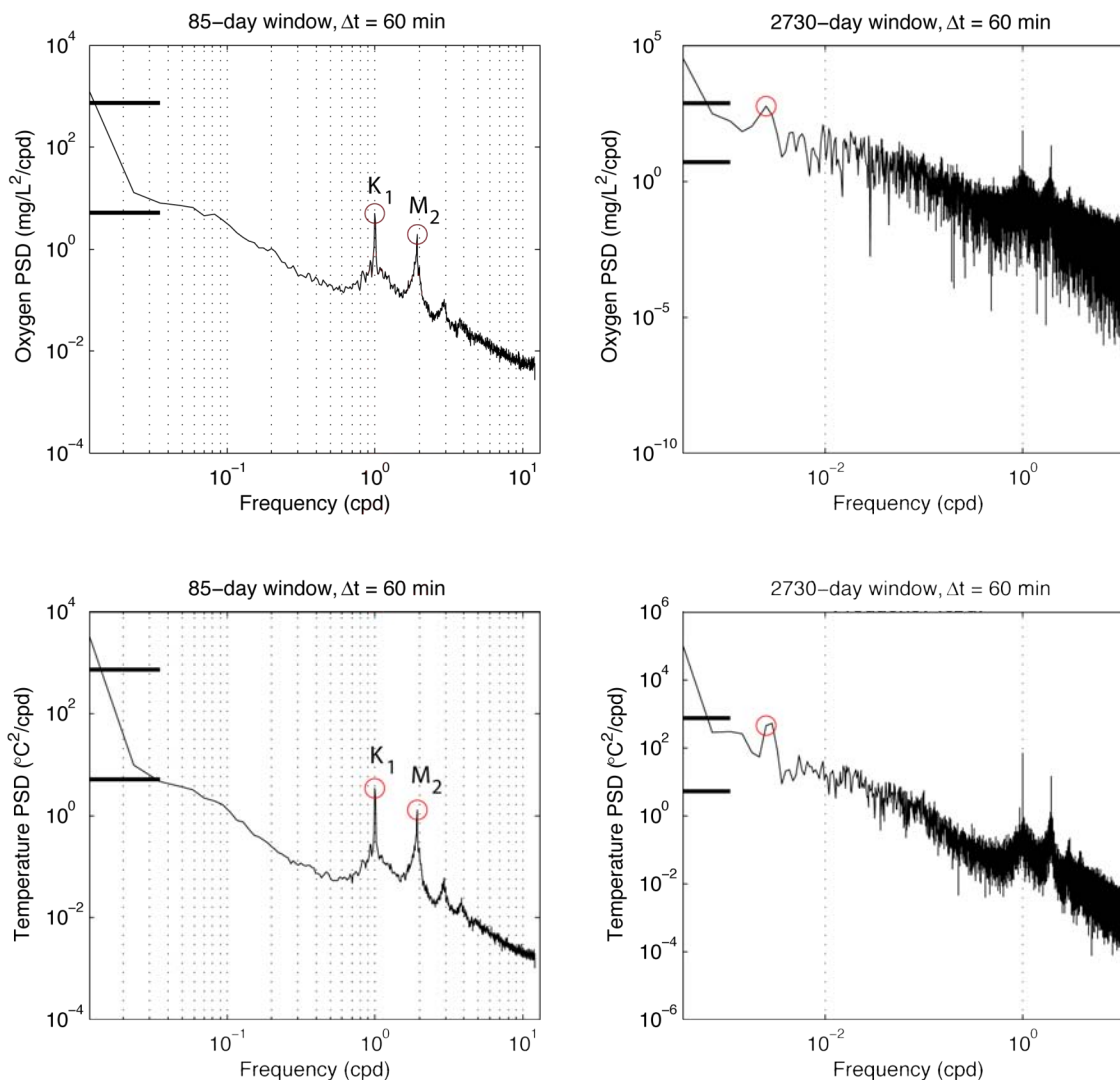


**Figure 42 Autospectra of MBA dissolved oxygen (top panels) and temperature (bottom panels) using a smaller (left panels) and larger (right panels) window size used to resolve diurnal ( $K_1$ )/semidiurnal ( $M_2$ ) and seasonal frequency peaks, respectively. Peaks of interest are circled in red. Time step = 1hour.**

DO and temperature spectra showed discernable peaks at many of the less energetic tidal constituents. Tidal constituents were taken from the t-tide Tidal Analysis Toolbox for MATLAB (Pawlowicz et al. 2002). Near the diurnal frequency, there was energy (high to low) at the  $S_1$ ,  $K_1$ ,  $P_1$ ,  $PI_1$ ,  $\phi_1$ ,  $O_1$  and  $\tau_1$  tidal constituents (Figure 43), while near the semidiurnal frequency there was energy at the  $M_2$ ,  $H_1$ ,  $H_2$ ,  $S_2$ ,  $T_2$  and  $K_2$  (Figure 44). There was no energy at fortnightly ( $M_f$ ) or monthly ( $M_m$ ) frequencies. The peak at one cycle per day likely also has energy from summer onshore diurnal winds that occur when the land heats up in the afternoon, creating an inland atmospheric low. When

a time series of the tides was generated by harmonic analysis and removed from both the MBA temperature and DO time series, there was still substantial energy leakage around the diurnal, semidiurnal and their harmonics. This leakage and the presence of harmonics are indicators that the tidal energy is non-linear.

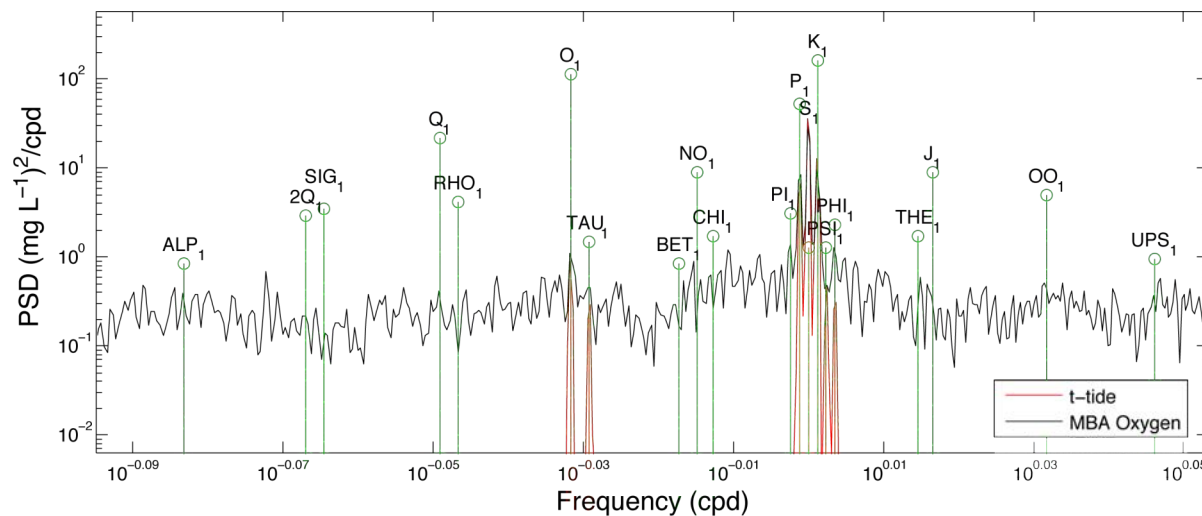


**Figure 43 Autospectra of MBA dissolved oxygen (black) and T-Tide tidal harmonics (red) overlaid with labeled tidal constituents (green) near diurnal frequencies. Height of green tidal constituents indicates relative strength of signal. Frequency is in cycles per day (cpd) and both axes are log scale.**  
compareMBAto2ttide\_spec\_diurnal\_.png

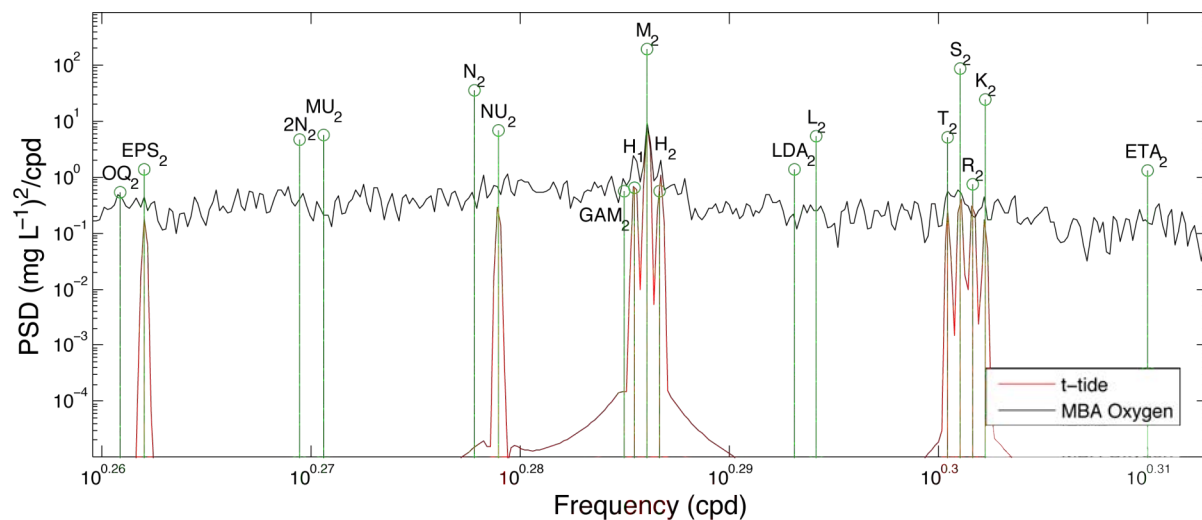


**Figure 44 Autospectra of MBA dissolved oxygen (black) and T-Tide tidal harmonics (red) overlaid with labeled tidal constituents (green) near semidiurnal frequencies. Height of green tidal constituents indicates relative strength of signal. Frequency is in cycles per day (cpd) and both axes are log scale.**



**Figure 45 Cross covariance results comparing dissolved oxygen (DO) from the Monterey Bay Aquarium (MBA) and sea surface height (SSH) from NOAA's Monterey wharf tide gauge. Colors indicate correlation coefficient and lag times are printed in hours.**

A cross-spectral analysis was performed on DO and temperature from MBA. Both DO and temperature data were divided into three 85-day sub-windows with a 50% overlap, and multiplied by a Hanning window to compute cross power spectra using a time step of one hour. The cross-spectral results looked almost identical to the autospectra supporting the strong linear relationship between DO and temperature at all frequencies (Figure 46).

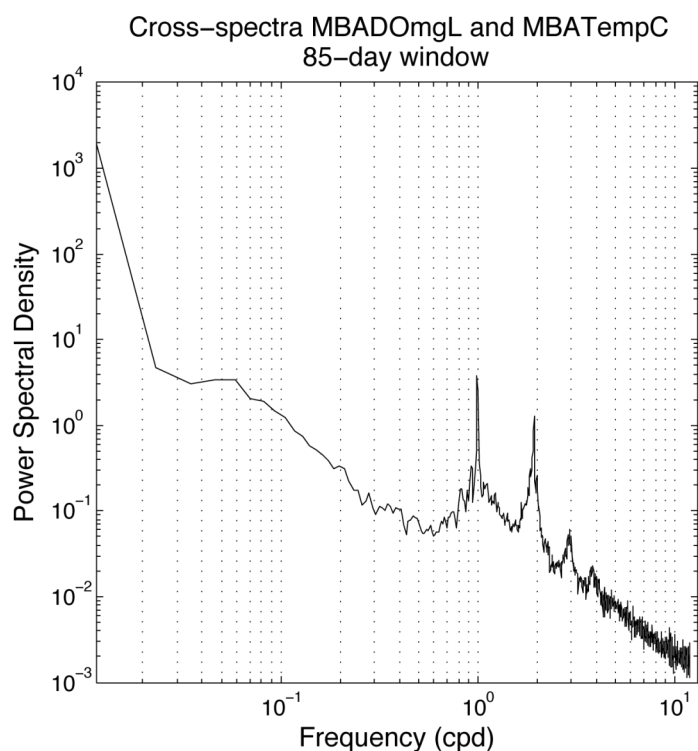


**Figure 46 Cross power spectra between MBA dissolved oxygen and temperature.**

Coherence and phase were calculated between MBA DO and temperature again using an 85-day window. There was higher coherence at the diurnal signal than the semidiurnal (Figure 47, top panel) and the phase at the diurnal frequency was approximately 0 degrees, as expected. However, phase at the semidiurnal was -5.5 degrees, translating to a lag of 12 minutes (Figure 47, bottom panel). This lag is much lower than the Nyquist period of 2 hours and would not be a discernable lag for our instruments.



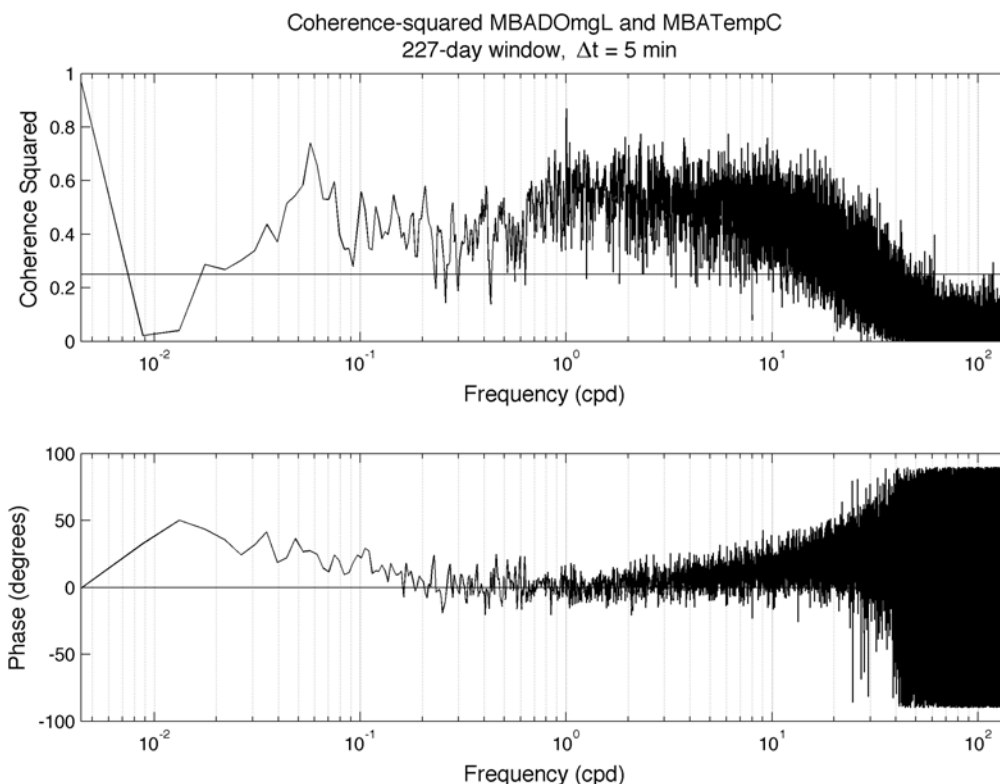


**Figure 47 Coherence (top panel) and phase (bottom panel) plots for MBA dissolved oxygen and temperature. Top panel, horizontal line is level of 99% significance. Bottom panel, horizontal line is at a phase of  $0^\circ$ .**

#### SHORT-TERM VARIABILITY

While short-term variability in the DO time series seemed to be dominated by tidal frequency energy, other possible environmental drivers were investigated that may act on a less than 24 hour scale. Short-term (diel) DO fluctuations near the ocean surface have been found to be associated with plankton respiration (K.S. Johnson 2010); however, this appears to be an unlikely forcing mechanism for the observed low-DO events for several reasons. First, respiration causes a daily maximum in subsurface DO near sunset, but our records show no clear correlation with photoperiod (Figure 48). A cross-covariance analysis between hourly Photosynthetically Active Radiation (PAR) measurements taken at the Moss Landing Marine Laboratories and DO resulted in a correlation coefficient of -0.188 when DO lead PAR by one hour (December 2000 to March 2011). The strength of the correlation did not improve with comparisons over shorter time periods; monthly correlation coefficients generally were weaker than 0.3 or -

0.3 with no consistent lag. Secondly, respiration-driven DO perturbations are of amplitude  $\sim 1 \text{ mg L}^{-1}$ , whereas the fluctuations we describe can exceed  $4 \text{ mg L}^{-1}$ . Additionally, any respiration-driven oxygen depletion would be expected to show a measurable lag between the appearance of cold, nutrient-rich water and significant oxygen depletion (or  $\text{CO}_2$  elevation). We, however, find strong positive correlations between temperature and DO at no detectable lag (cross-covariance correlation coefficient of 0.47 for the entire time series and 0.88 for the period depicted in Figure 48).

In order to assess whether temperature-driven changes in oxygen solubility could have driven the DO variance, the oxygen anomaly was calculated (DO concentration measured minus the oxygen solubility). Oxygen solubility was calculated using flow-through temperature from the MBA pump house and an assumed salinity of 33.8 (Woodson et al. 2007). The changes in salinity seen in southern Monterey Bay would not change the DO solubility by more than  $0.03 \text{ mg O}_2 \text{ L}^{-1}$  consequently it was accepted that using an assumed salinity value would not cause substantial error. Oxygen solubility had low variance ( $0.07 \text{ mg}^2 \text{ L}^{-2}$ ) while the overall variance in the oxygen anomaly was high ( $2.58 \text{ mg}^2 \text{ L}^{-2}$  as compared to  $2.20 \text{ mg}^2 \text{ L}^{-2}$  in the measured DO) indicating that DO changes due to oxygen solubility were very small.

Short-term variations of pH have been linked to solar irradiance with the lowest pH values seen around sunrise and amplitudes on the order of 0.24 (Wootton et al. 2008). The MBA pH time series showed changes of up to  $\sim 0.4$  pH units in  $\sim 12$  hours and like DO was not correlated to photoperiod (Figure 48).

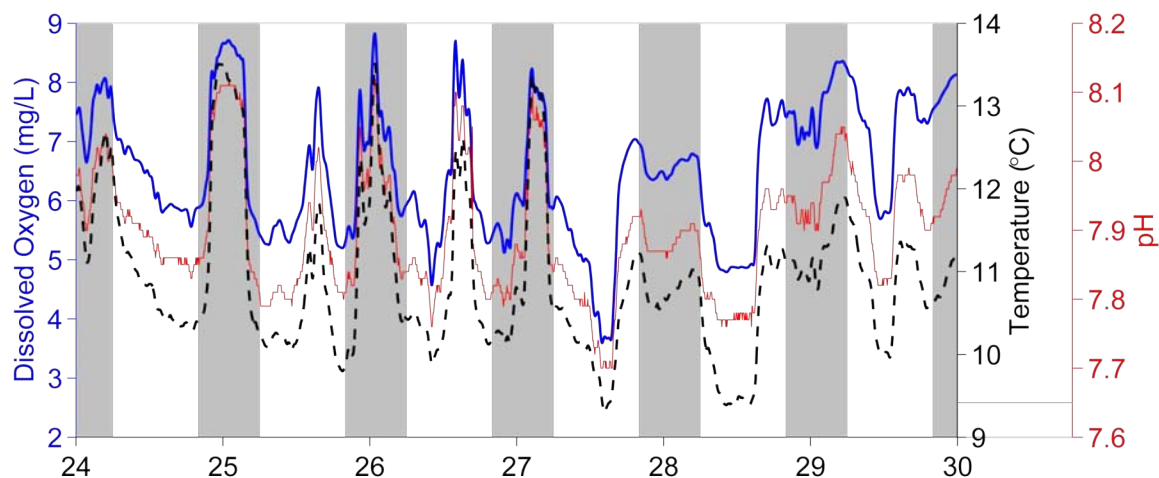


**Figure 48 Example of covariation of oxygen (solid blue record), temperature (red) and pH (dashed, black). Data are from MBA seawater intake during a series of intense hypoxic/low pH/cold episodes in April, 2010. Nighttime hours are shaded.**

#### **EMPIRICAL MODE DECOMPOSITION OF MBA TIME SERIES**

Empirical mode decomposition (EMD) was performed on both the MBA temperature and dissolved oxygen time series from the flow-through system. EMD is an analysis technique that decomposes a time series into a sequence of empirically orthogonal intrinsic mode function (IMF) components and a residual. This technique was used to look periods and characteristics of subtle forcings that could have been hidden in spectral analysis. Additionally, long term trends or large period oscillation can be seen in the residual which would have taken considerable work to uncover due to autocorrelation of the time series. When all IMFs and the residual are added together, the original time series is the result (N. Huang et al. 1998; Rao and Hsu 2008; Z. Wu and N.E. Huang 2009; Breaker and Ruzmaikin 2010). Each IMF characterizes a mode of variability with time-dependent amplitudes and frequencies that lie within a narrow band, where the center of the distribution defines the mean period of the mode. The number of modes is determined mathematically, not by the user, as in singular spectrum analysis (Golyandina et al. 2001). This technique was developed to perform time series analysis on nonstationary and nonlinear data.

I chose to apply the EMD technique to the MBA time series because the results of the skewness and Lilliefors' composite goodness-of-fit tests indicated that all three time series were nonlinear (see previous results section). Another indicator that the time series were not linear was presence of the strong tidal harmonics seen in the spectral analysis results (Figure 42). Another strength of the EMD analysis is that subtle drivers (i.e., forcing mechanisms), which do not have a lot of energy, can be identified that may be difficult to detect in other types of analyses. I used an "ensemble EMD" (EEMD) which is a noise-assisted technique run a number of times. The true IMF is defined as the mean of an ensemble of IMFs (Z. Wu and N.E. Huang 2009; Breaker and Ruzmaikin 2010). This technique narrows the frequency band of each IMF, reducing mixing, and eliminates problems with gap amplification. I conducted the EEMD analyses using MATLAB programs developed by Z. Wu ([http://rcada.ncu.edu.tw/research1\\_clip\\_program.htm](http://rcada.ncu.edu.tw/research1_clip_program.htm)).

Both the MBA temperature and DO times series were averaged to a one-hour-time step and analyzed using the EEMD technique with a ratio of the standard deviation of the added noise (Nstd) of 0.1 and an ensemble number (NE) of 100 (Figure 49-Figure 52). The DO time series decomposed into sixteen IMFs while the temperature was broken into seventeen, the last mode of both being the residuals of the analysis. Changing the Nstd (0.05, 0.1, 0.2) and/or NE (10, 20, 100) did not change the number of modes for either temperature or DO. When all modes were added and then subtracted from the original 1-hour interpolated time series there was almost no difference (DO = -0.3 and Temp = 6.3). The variance for each IMF was calculated as an indicator of the contribution of each mode to the total variance in the original signal (Figure 53, Figure 54). An estimate of the period of each IMF was derived by identifying the peaks and troughs in the entire time series and then calculating the approximate “period” (Figure 55, Figure 56). The median of the distribution of periods was chosen as the most representative period for a given IMF.

The similar number of IMFs and associated periods for both DO and temperature suggests that the relevant forcing mechanisms are closely related; however, the differing variance within each IMF indicates that the influence of each driver is different. IMF 1 and 2, with median periods of 3 and 7 hours, could not be associated with known drivers. The high variance in IMF 2 may be due to its proximity to the energetic semidiurnal tide contained within IMF 3. The nonlinearity of the semidiurnal tidal signal may have been characterized by this shorter period mode (IMF 2) and caused the bimodal distribution (mode mixing) seen in IMF 3 (Figure 56). In both data sets, IMF 3 and 4 contained periods indicative of the semidiurnal (IMF 3) and diurnal tides (IMF 4). The semidiurnal tide was more energetic than the diurnal (Figure 53, Figure 54), consistent with spectral analysis results (Figure 42). The sixth IMF of DO had high variance (Figure 53), and median period of 5 days, which would contain any energy within in the synoptic weather band. IMF 7 may be energetic because it has a median period of ~14 days, which is associated with the spring/neap tidal cycles. The following IMF (8), at a median period of 26 days, encompasses energy at the lunar tidal period.

IMF 8, 9 and 10 of both DO and temperature show agreement between amplitude bursts, suggesting that they can be combined. The period distributions for these three

modes and the associated intermittent amplitude bursts are consistent with the Madden-Julian Oscillation (Madden and Julian 1994; Zhang 2005), between ~30-90 days (Figure 55). The Madden-Julian Oscillation was first identified in the zonal winds of the lower atmosphere (Madden and Julian 1994), and are sometimes called the “intra-seasonal oscillations” or “40 to 50-day” oscillations. The waves originate in the western tropical Pacific and Indian oceans. The ocean expression of this atmospheric phenomenon is the generation of internal waves that propagate eastward along the Equator, forced by equatorial Kelvin waves. When they interact with the coasts of the Americas, they take the form of poleward-propagating, coastal-trapped waves with phase speeds of 150–200 km/day (Spillane et al. 1987). These oscillations have been seen in sea level data along the North American coast at least as far north as central California (Breaker et al. 2001; Breaker 2005). The eleventh DO IMF contains periods associated with the annual cycle. The final DO IMF corresponds to the residuals of the EEMD analysis.

The temperature EEMD showed the most variance at the seasonal cycle, which showed up in IMF 10 (Figure 54). The temperature annual signal is stronger than that of DO; this is due to the strong cooling in the spring and warming through the summer (Figure 39). DO does not show such a strong seasonal pattern because mean DO does not change markedly through the year, only the variance (Figure 38). The large peaks in IMF 11 and 12 around 1997/8 corresponded to the strong ‘97/98 El Niño event, which indicated that these modes may contain energy from the ENSO cycle. IMF 11 appears to be a combination of the annual and ENSO signals. The temperature did not show as strong variance in the weather band as the DO EEMD results did. Again, the influence of the Madden-Julian Oscillation was apparent in IMF7 and 8.

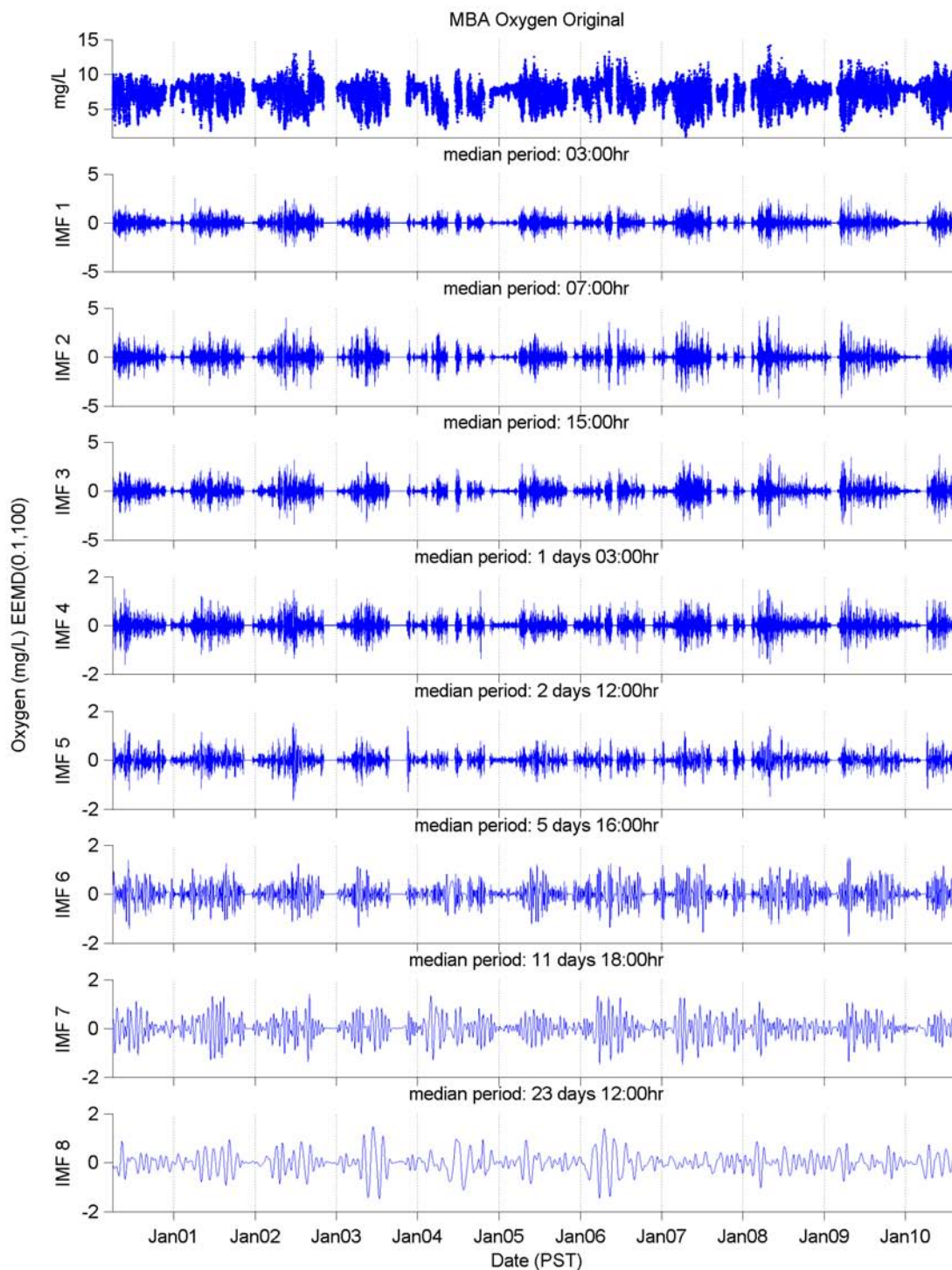


**Figure 49** The intrinsic mode function components (IMF) from the ensemble empirical mode decomposition (EEMD) of dissolved oxygen at the Monterey Bay Aquarium. Top panel, the original dissolved oxygen ( $\text{mg L}^{-1}$ ) time series. Bottom panels, IMF 1 through 8 in  $\text{mg O}_2 \text{ L}^{-1}$  over time. See next figure for IMF 9-17. The EEMD was run with a ratio of the standard deviation of the added noise of 0.1 and an ensemble number of 100.

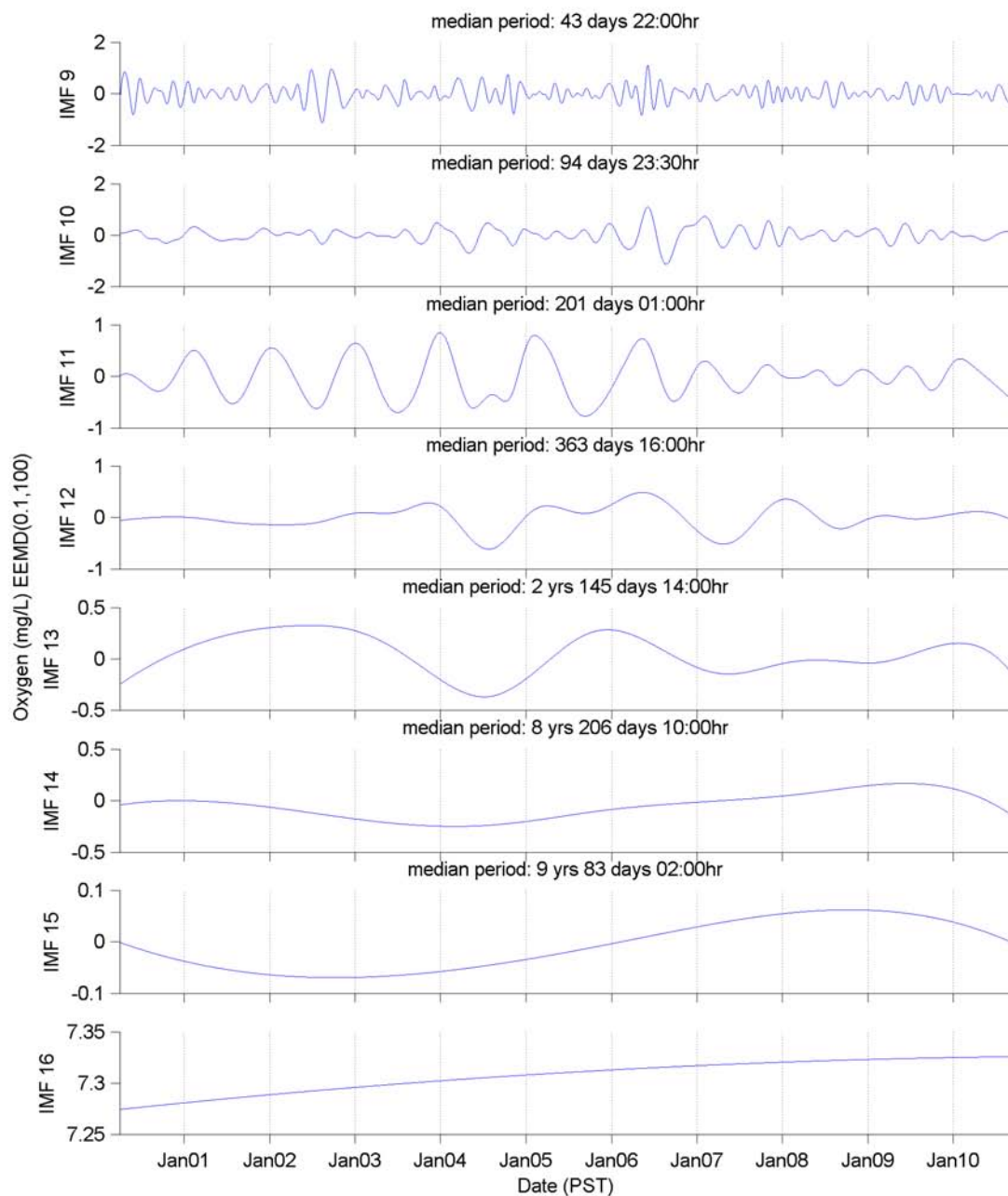


**Figure 50** The intrinsic mode function components (IMF) 9 through 16 ( $\text{mg O}_2 \text{ L}^{-1}$ ) from the ensemble empirical mode decomposition (EEMD) of dissolved oxygen at the Monterey Bay Aquarium. The final IMF (15) is the residual of the analysis. See previous figure for IMF 1-8. The EEMD was run with a ratio of the standard deviation of the added noise of 0.1 and an ensemble number of 100.



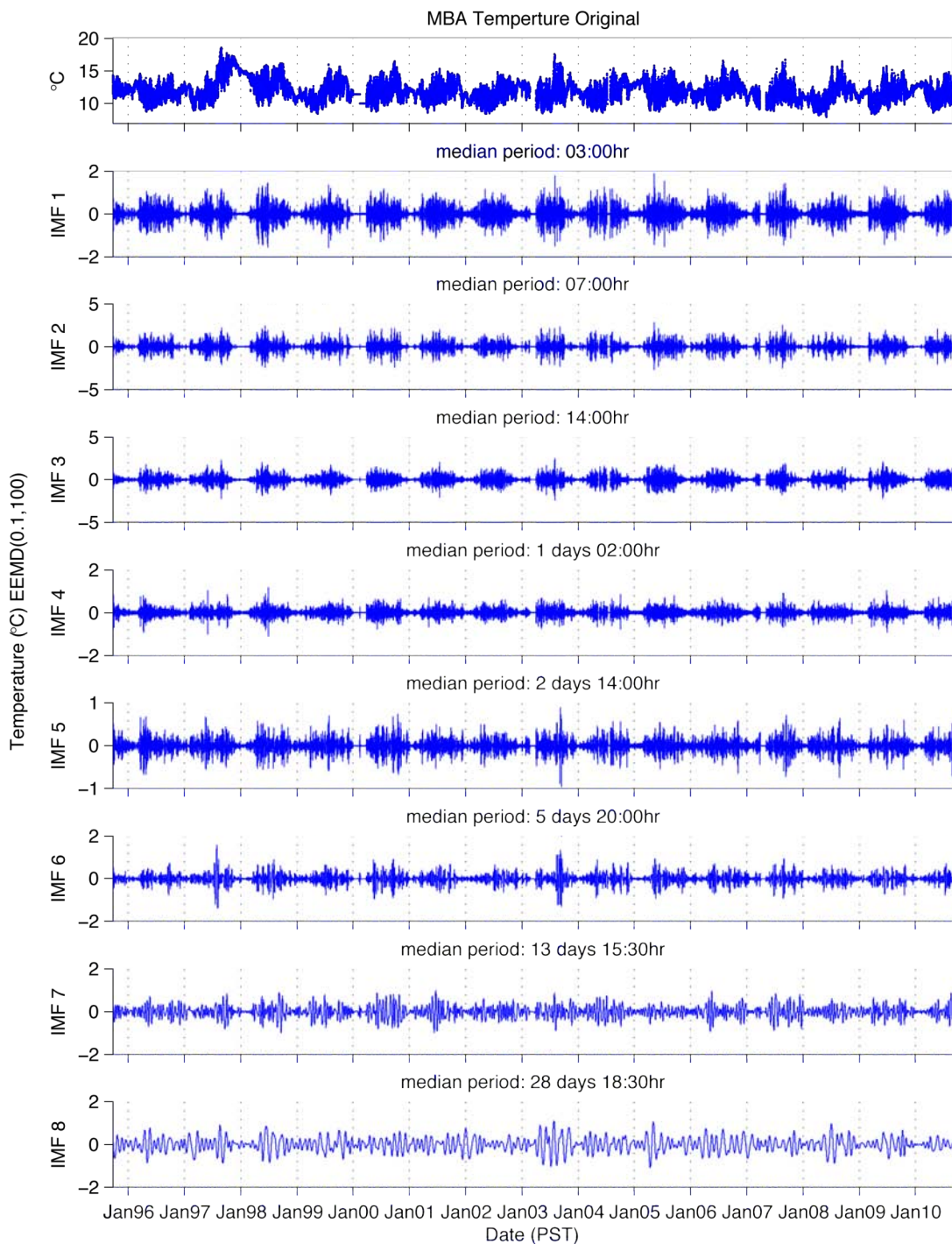


**Figure 51** The intrinsic mode function components (IMF) from the ensemble empirical mode decomposition (EEMD) of temperature at the Monterey Bay Aquarium. Top panel, the original temperature ( $^{\circ}\text{C}$ ) time series. Bottom panels, IMF 1 through 8 in  $^{\circ}\text{C}$  over time. See next figure for IMF 9-16. The EEMD was run with a ratio of the standard deviation of the added noise of 0.1 and an ensemble number of 100.



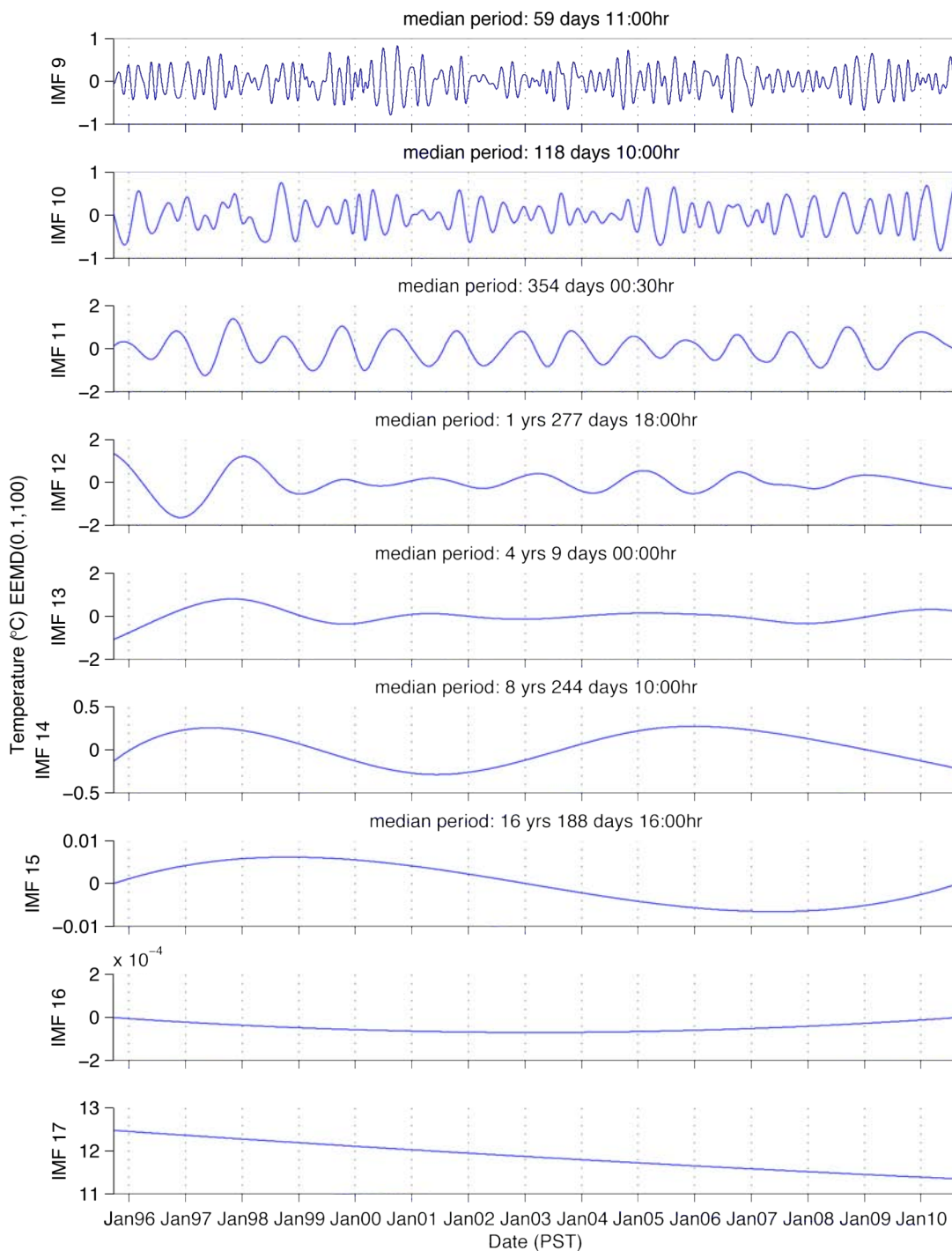


**Figure 52** The intrinsic mode function components (IMF) 9 through 16 (°C) from the ensemble empirical mode decomposition (EEMD) of temperature at the Monterey Bay Aquarium. The final IMF (16) is the residual of the analysis. See pervious figure for IMF 1-8.

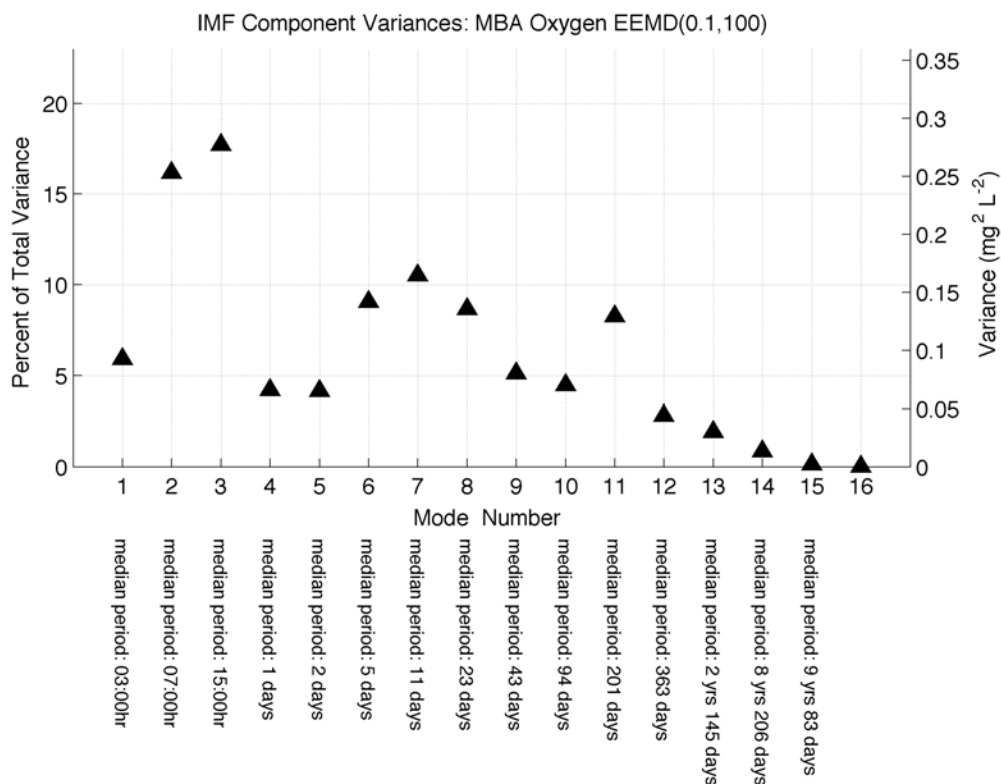


**Figure 53** The percent of variance and variance of each intrinsic mode function components 1 through 16 from the ensemble empirical mode decomposition (EEMD) of dissolved oxygen at the Monterey Bay Aquarium. The EEMD was run with a ratio of the standard deviation of the added noise of 0.1 and an ensemble number of 100. Estimated periods are denoted below each mode number, see Figure 55.

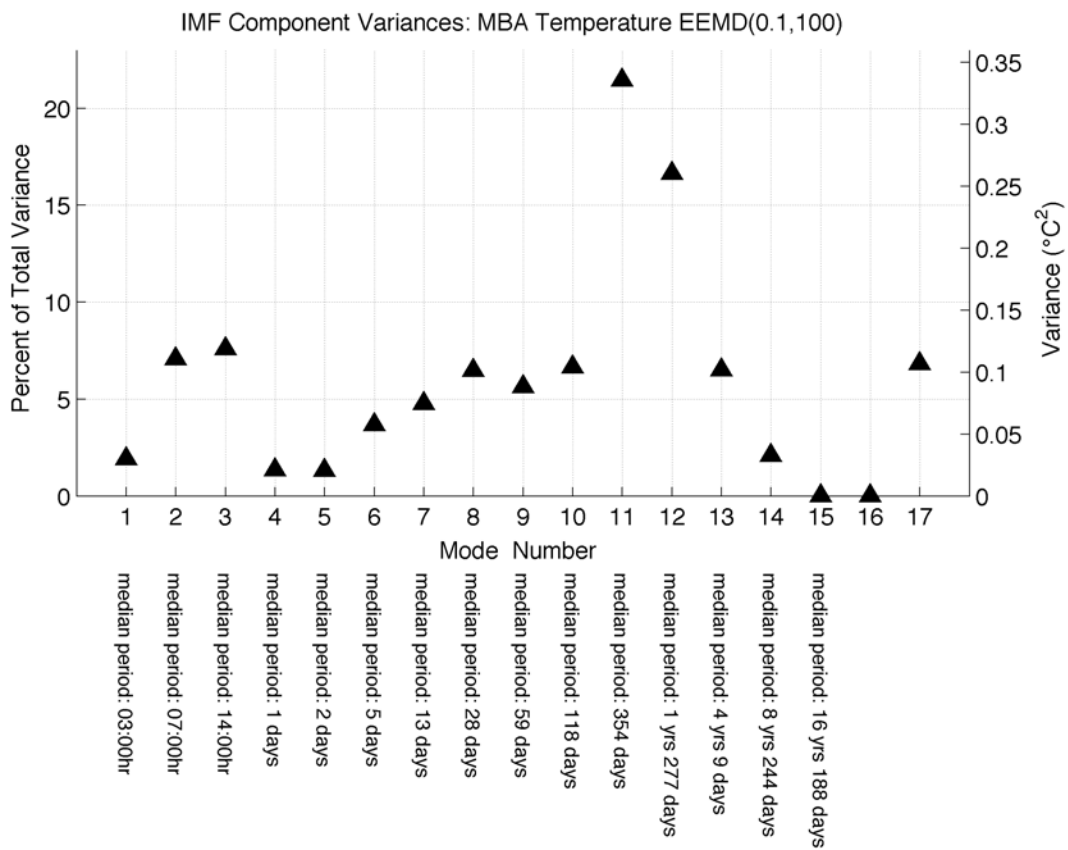


**Figure 54** The percent of variance and variance of each intrinsic mode function components 1 through 17 (units of  $(^{\circ}\text{C})^2$ ) from the ensemble empirical mode decomposition (EEMD) of temperature at the Monterey Bay Aquarium. The EEMD was run with a ratio of the standard deviation of the added noise of 0.1 and an ensemble number of 100. Estimated periods are denoted below each mode number, see Figure 56.

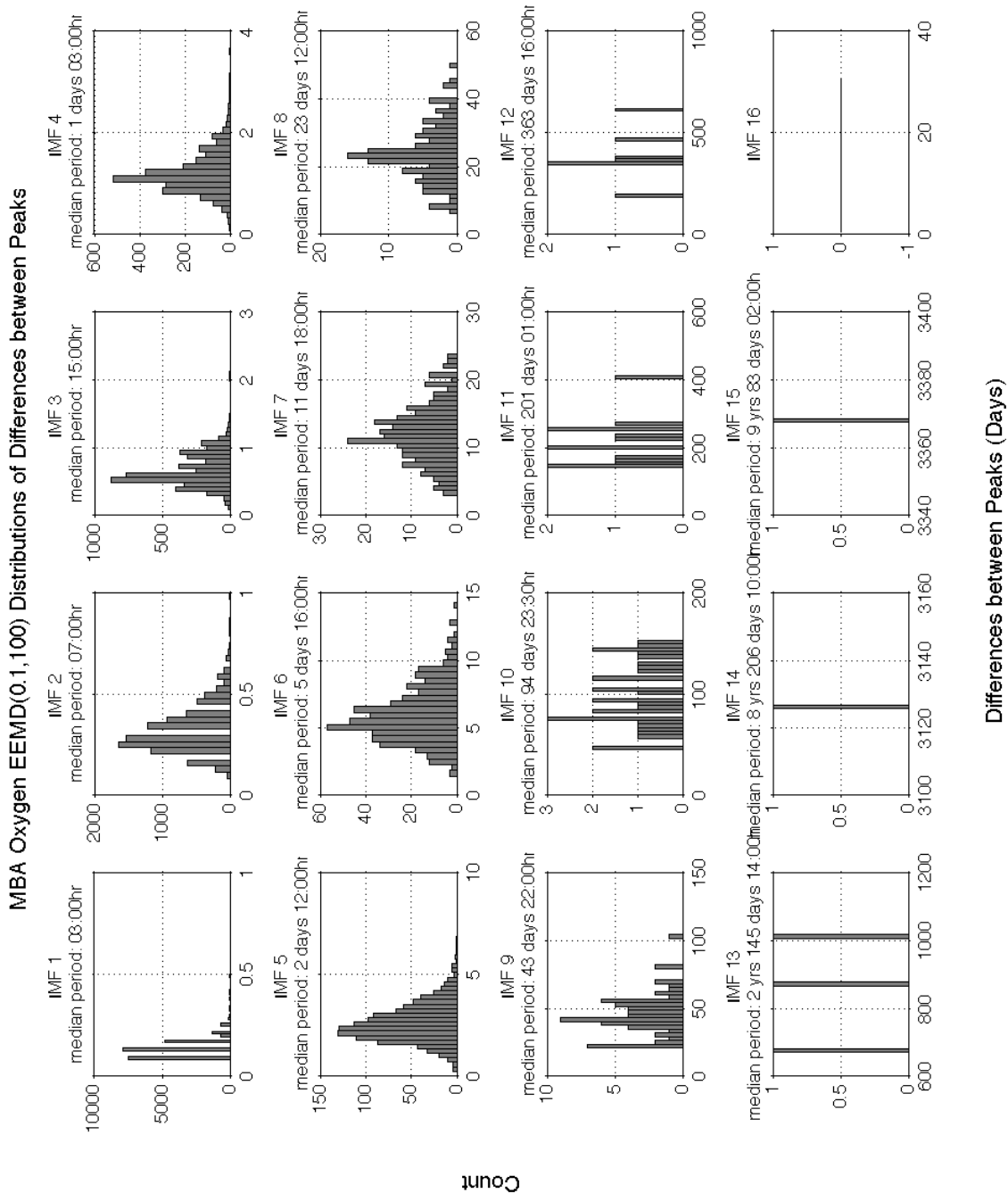


**Figure 55** Distribution of differences between peaks of each intrinsic mode function components (IMF) 1 through 15 from the ensemble empirical mode decomposition (EEMD) of dissolved oxygen at the Monterey Bay Aquarium. The median ‘period’ for each IMF is displayed above each distribution plot. The EEMD was run with a ratio of the standard deviation of the added noise of 0.1 and an ensemble number of 100.

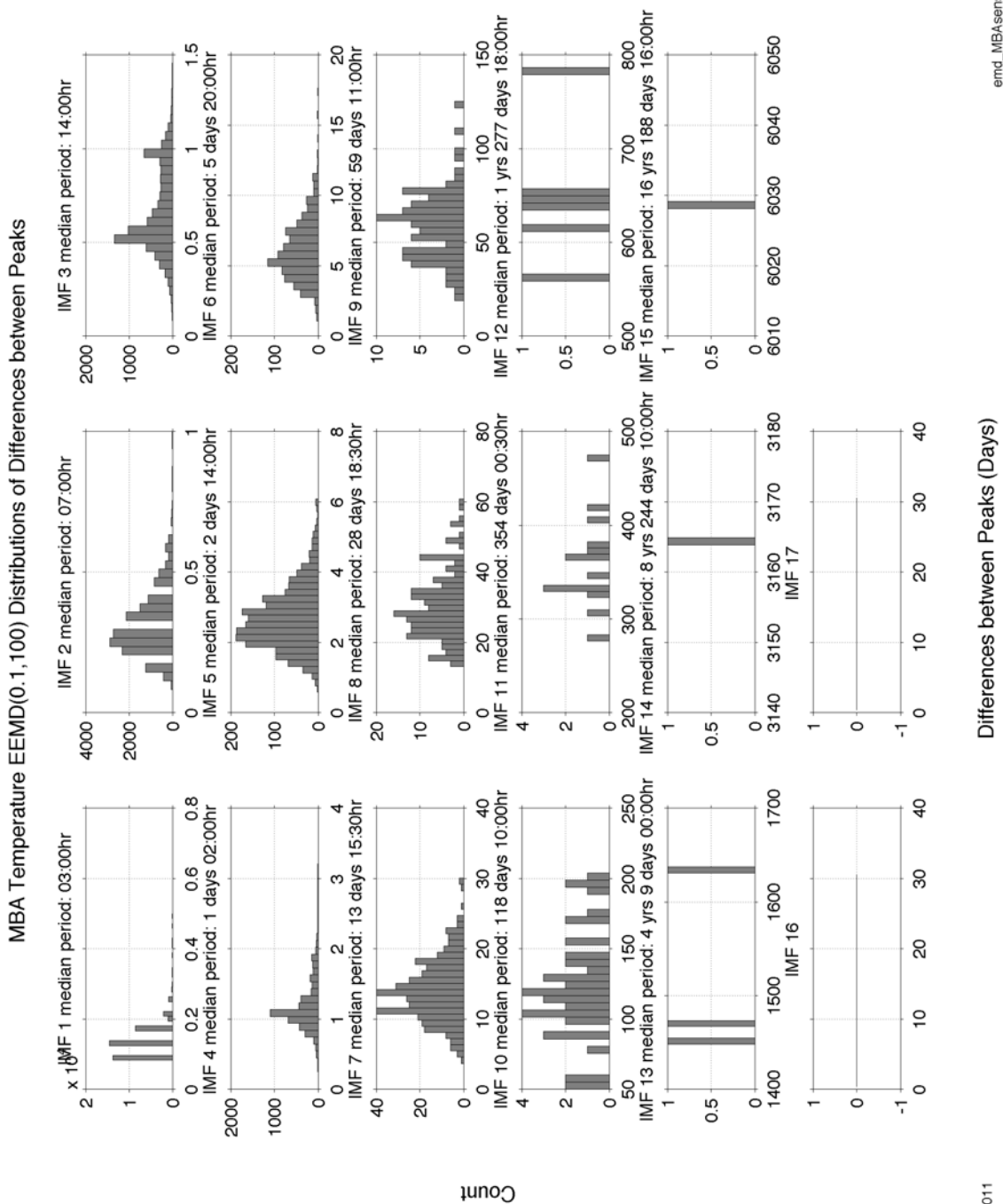


**Figure 56** Distribution of differences between peaks of each intrinsic mode function components (IMF) 1 through 15 from the ensemble empirical mode decomposition (EEMD) of temperature at the Monterey Bay Aquarium. The median ‘period’ for each IMF is displayed above each distribution plot. The EEMD was run with a ratio of the standard deviation of the added noise of 0.1 and an ensemble number of 100.

## **MBA TEMPERATURE IMF 12 AND ENSO**

I tested the hypothesis that IMF 11 and 12 contained energy from the ENSO cycle by comparing them to NOAA's Oceanic Niño Index (ONI) found at the National Weather Service's Climate Prediction Center ([http://www.cpc.ncep.noaa.gov/products/analysis\\_monitoring/ensostuff/ensoyears.shtml](http://www.cpc.ncep.noaa.gov/products/analysis_monitoring/ensostuff/ensoyears.shtml)) and to the Northern Oscillation Index (NOI) ([http://www.pfeg.noaa.gov/products/PFEL/modeled/indices/NOIx/noix\\_download.html](http://www.pfeg.noaa.gov/products/PFEL/modeled/indices/NOIx/noix_download.html)). The ONI measures warm and cold episodes using a threshold of  $\pm 0.5^{\circ}\text{C}$  [3 month running mean of ERSST.v3b SST anomalies in the Niño 3.4 region ( $5^{\circ}\text{N}$ - $5^{\circ}\text{S}$ ,  $120^{\circ}$ - $170^{\circ}\text{W}$ )], based on the 1971-2000 base period. When IMF 11 and 12 were added and compared to the ONI using cross covariance analysis, there was a moderate positive correlation of (0.503) at a lag of 3 months (Figure 57). This lag is reasonable, considering the ONI is an indicator of the strength of the ENSO cycle near the equator and the signal would take time to propagate north to the Monterey Bay.

The NOI is an extratropical-based ENSO index and a counterpart to the established Southern Oscillation Index (SOI)(Schwing et al. 2002). It is computed from the National Centers for Environmental Prediction sea level pressure anomalies (monthly sea level pressure minus climatology) of the North Pacific High [ $35^{\circ}\text{N}$ , $130^{\circ}\text{W}$ ], and Darwin, Australia [ $10^{\circ}\text{S}$ , $130^{\circ}\text{E}$ ]. This index is well suited to characterize the climate of the Northeast Pacific. In the cross-covariance analysis, the MBA temperature IMF 11+12 had a maximum correlation at 2 month lag with a correlation coefficient of -0.404 (the NOI has the opposite sign to the ONI).

Both comparisons of the ONI and NOI showed strong evidence that temperature at MBA was influenced by ENSO and that the MBA temperature IMF 11 and 12 captured the ENSO scale variability. These results are consistent with Breaker (2005) on the importance of mid-latitude ENSO forcing.

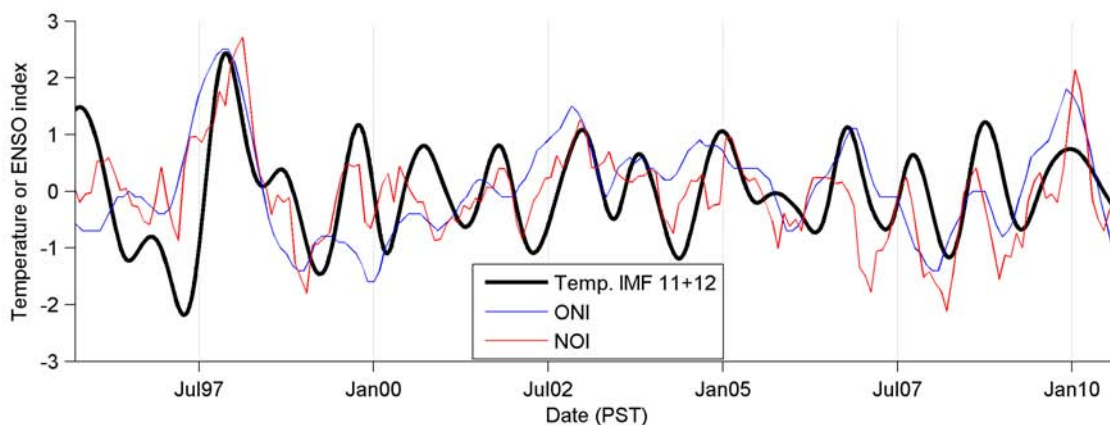


**Figure 57 MBA Temperature IMF 11+12, Oceanic Niño Index (ONI) and Northern Oscillation Index (NOI) comparison. IMF 11 + 12 over time overlaid with ONI and NOI.**

### **LONG-TERM TRENDS AT MBA**

The final IMF of the EEMD analysis contains the residuals. This is often where long period oscillations and long-term trends are revealed. This technique was employed to answer the initial question: were there any long-term trends in any of the MBA time series? The variance in this mode of the MBA DO analysis was very small. After experimenting with different levels of added white noise ( $N_{std} = 0.05, 0.1, 0.2$ ), the shape of the line changed, suggesting that no long-period oscillations or long-term trends were resolved in the ten-year DO time series. The EEMD temperature residuals (IMF16) show a cooling trend (Figure 52). Manipulation of the noise ( $N_{std} = 0.05, 0.1, 0.2$ ) parameter did not change the shape of the residual line indicating a robust trend line. The rate was between  $-0.08$  and  $-0.1$  °C/year, consistent with the Pacific Decadal Oscillation (PDO) (Breaker and Ruzmaikin 2010).

### **COMPARISON BETWEEN AN UPWELLING INDEX AND MBA MEASUREMENTS**

I hypothesized that during strong upwelling events deep water would be shallow enough for internal tides to push it inshore, resulting in high variability in dissolved oxygen (DO), temperature and pH at the Monterey Bay Aquarium (MBA). Short-term event-based analyses showed high variability at MBA when offshore wind speed and direction (NDBC buoy #46042) were strong and favorable for upwelling with a lag of a few days. For example, Figure 58 shows that on January 16<sup>th</sup> southeastern blowing winds

increase (bottom panel) and thus the Bakun Upwelling Index (BUI) increases (fourth panel). On the 17<sup>th</sup>, DO, temperature and pH at MBA start to show strong fluctuations than continue for the next few days. As BUI increases so does the the variance in DO, temperature and pH, indicating that the bottom water advected inshore by internal tidal motions is deep, upwelled water.

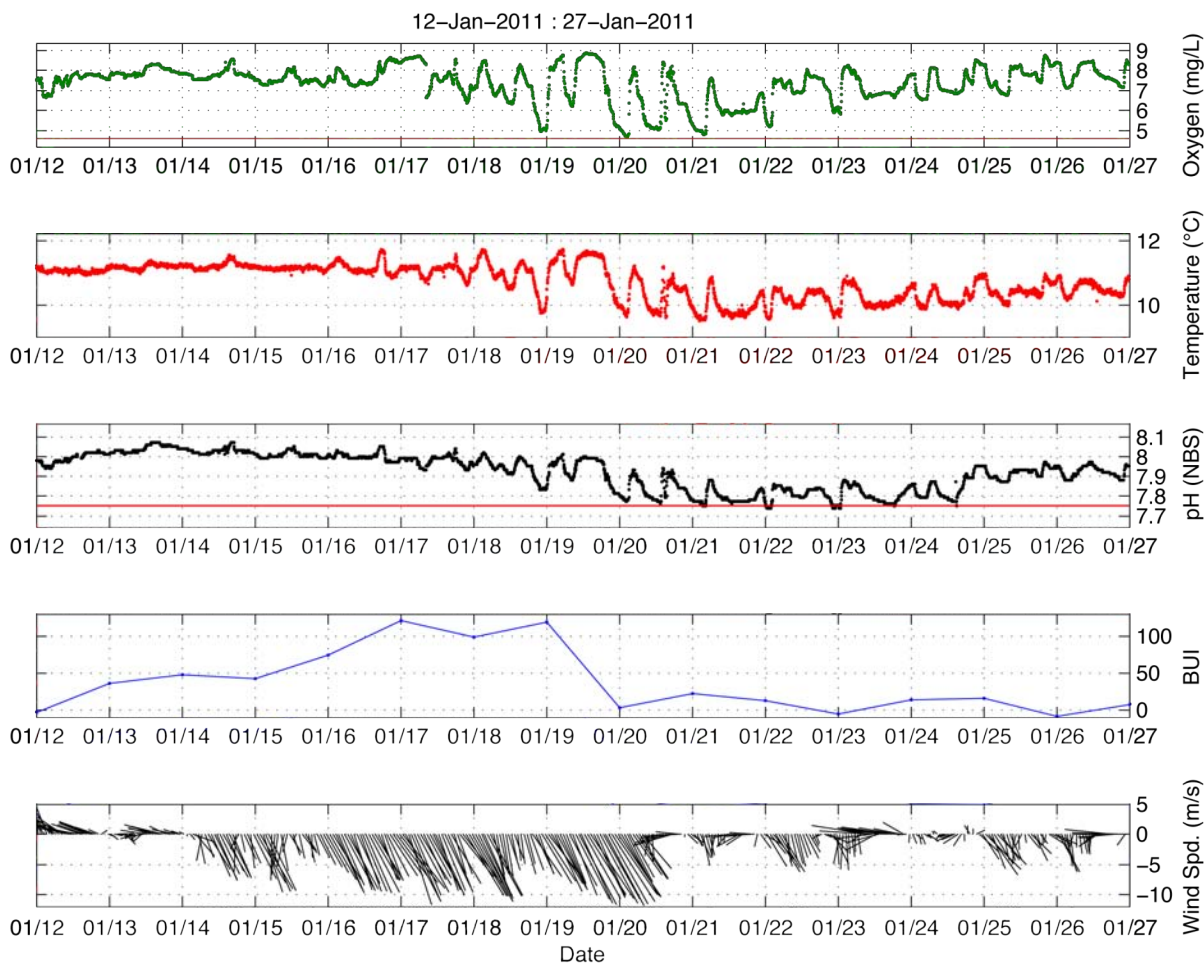


**Figure 58 Example of event based analysis of upwelling influence on oxygen, temperature and ph at the Monterey Bay Aquarium from January 12-27<sup>th</sup> 2011. The Bakun Upwelling Index (BUI) is plotted in blue (metric tons/sec/100m of coastline) and a vector plot of offshore wind from the NDBC buoy #46042 in black.**

To test this hypothesis, I compared the standard deviation of MBA DO to the NOAA Bakun Upwelling Index (BUI). Daily estimates of the Bakun Upwelling Index (BUI) were collected from NOAA's Pacific Fisheries Environmental Laboratory for 36°N, 122°W ([http://www.pfel.noaa.gov/products/PFEL/modeled/indices/upwelling/NA/data\\_download](http://www.pfel.noaa.gov/products/PFEL/modeled/indices/upwelling/NA/data_download))



d.html). The comparison resulted in a strong positive correlation (correlation coefficient = 0.458) at a lag of 3 days for the MBA DO time series dates of April 1, 2000 to March 30, 2011 (Figure 59). This relationship was persistent each year (Figure 60), with correlation coefficients as strong as 0.56 and lags between 2 and 5 days. This pattern did not change seasonally (mean of all monthly cross correlations = 3.2 days  $\pm$  2.6, n = 121) (Figure 61), indicating that this hypothesis was likely true. When daily minimums in DO were correlated with the BUI again there was a strong correlation (-0.52) at the lag of 3 days, however, when daily maximums were compared to the BUI there was a weak positive relationship (0.16) at a lag of 12 days. Monthly comparisons between daily maximums and BUI did not have consistent lags, correlation coefficients or seasonal pattern. These results suggest that the bottom-water DO and hypoxic events are forced by the advection of deep waters and that surface DO is inconsistently linked to surface production but on a much longer time scale. A cross correlation between daily minimums and maximums in DO lagged up to 50 days showed a very weak correlation (0.12) at no lag and no consistent pattern when compared monthly. If local surface productivity were being decomposed locally, one would expect to see super saturation of surface waters followed by hypoxic bottom waters more than 12 days later, which is not consistent with the results.

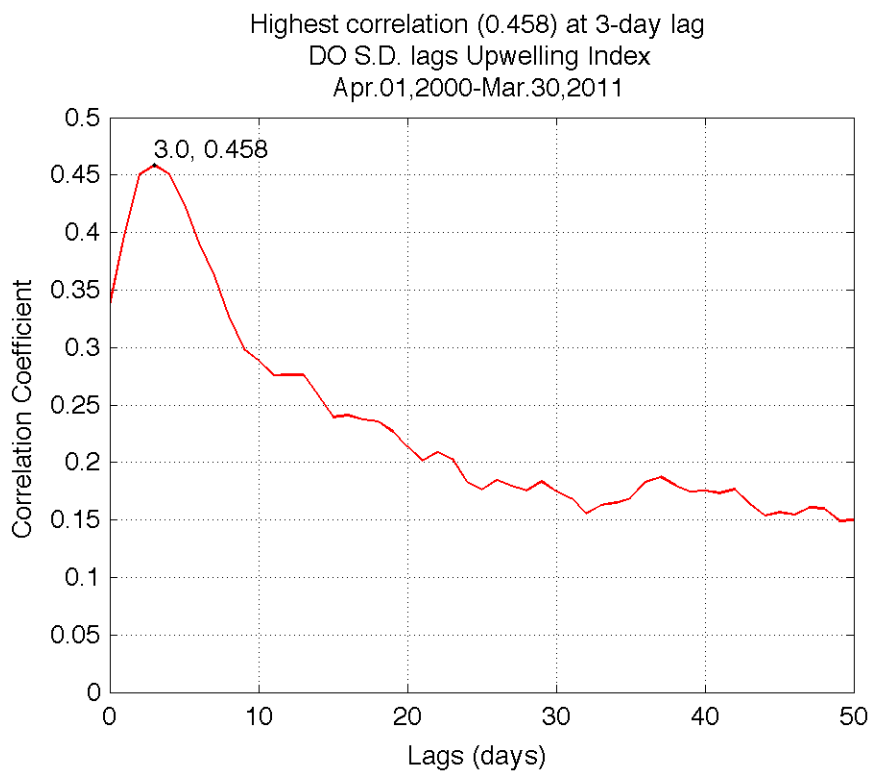


**Figure 59 Cross covariance results comparing the daily standard deviation of Monterey Bay Aquarium (MBA) dissolved oxygen (DO) to the NOAA Bakun Upwelling Index (BUI). Black dot and labels indicate lag time (days) at strongest correlation coefficient.**

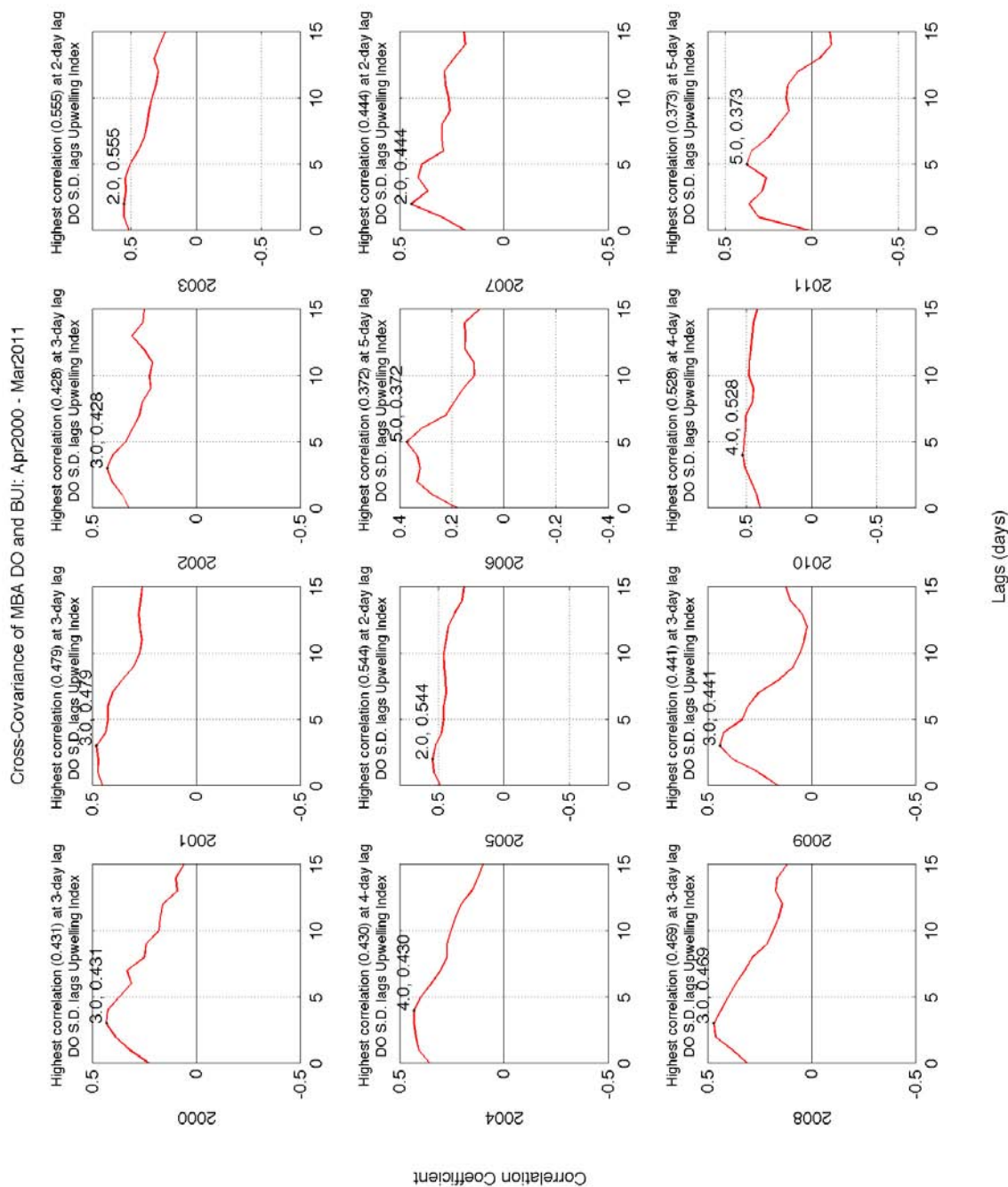


**Figure 60** Yearly cross covariance analysis results comparing the daily standard deviation of Monterey Bay Aquarium (MBA) dissolved oxygen (DO) to the NOAA Bakun Upwelling Index (BUl). Black dots and labels indicate lag time (days) at strongest correlation coefficient.

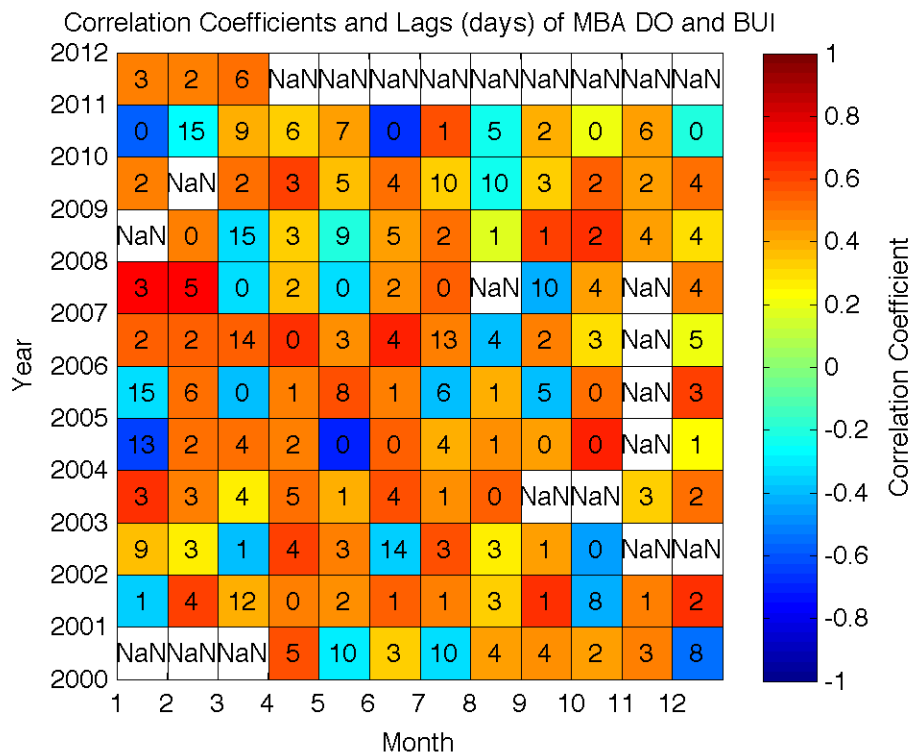


**Figure 61 Matrix of monthly correlation coefficients (color) and lags (numbers in boxes) for cross covariance analyses between the daily standard deviation of Monterey Bay Aquarium (MBA) dissolved oxygen (DO) and the Bakun Upwelling Index (BUI) for each year, 2000-2011. White indicates insufficient data.**

#### DEPTH OF ADVECTED OFFSHORE SOURCE WATERS

Due to the strong evidence that dissolved oxygen and pH variability is forced by upwelling modulated by internal tidal motions advecting a vertical gradient, the next question was: What is the depth of advected source water? The depth was estimated by comparing the temperature measurements at the Monterey Bay Aquarium (MBA) to temperature at different depths at a mooring in the center of Monterey Bay in approximately 1000 m of water (36.75° N, -122.03° W, M1 in Figure 4). Hourly temperature at 1, 10, 20, 40, 60, 80, 100, 150, 200, 250 and 300 m was downloaded from the Monterey Bay Aquarium Research Institution (MBARI) public data site (<http://dods.mbari.org/data/ssdsdata/deployments/previous.html>) from the M1 mooring from the deployment of October 20, 2009 through October 27, 2010. The MBA temperature showed the same seasonal pattern as temperature at M1. The MBA time series had a strong positive correlation (0.626) to temperature at 40 m at the M1 mooring

at a lag of 5 hours. Spectral analysis (see next section for explanation of technique) of temperature at all depths down to 300 m at M1 indicated that internal tidal heaving was felt all the way down to 300 m depth throughout the year (Figure 62). Peaks occurred at the semidiurnal ( $M_2$  and  $S_2$ ) and diurnal ( $K_1$ ) tidal frequencies at all depths. Depths of 100 m and below showed a peak at the  $O_1$  tidal constituent unlike at MBA and MLML (Figure 74). Throughout the year, the lowest daily temperatures corresponded to offshore temperatures at depths of 80 m and occasionally to 100 m (Figure 63). These results indicate that internal wave energy is present all year round and down to at least 300 m depth. When the temperature time series from the Moss Landing Marine Laboratories (MLML) sea water intake ( $\sim 20$  m) was compared to the M1 temperature-depth data, MLML measurements often reached levels associated with 200 m. Also noteworthy was that density at 300 m (deepest sensor) increased during the upwelling season indicating that upwelling was shoaling water from even deeper than 300 m.

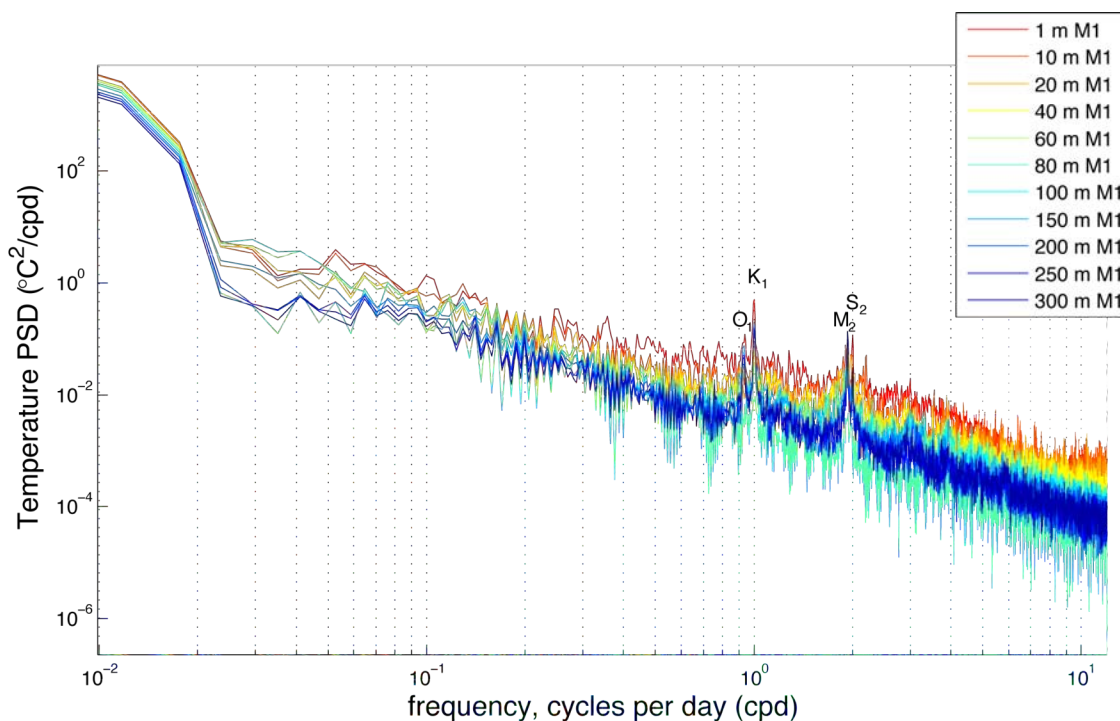


**Figure 62 Auto-spectra of temperature measurements recorded from October 20, 2009 through October 27, 2010 at different depths along the Monterey Bay Aquarium Research Institution's M1 mooring (colored lines). Dominant tidal constituents are labeled. Plotted in log-log space, frequency in cycles per day (cpd).**

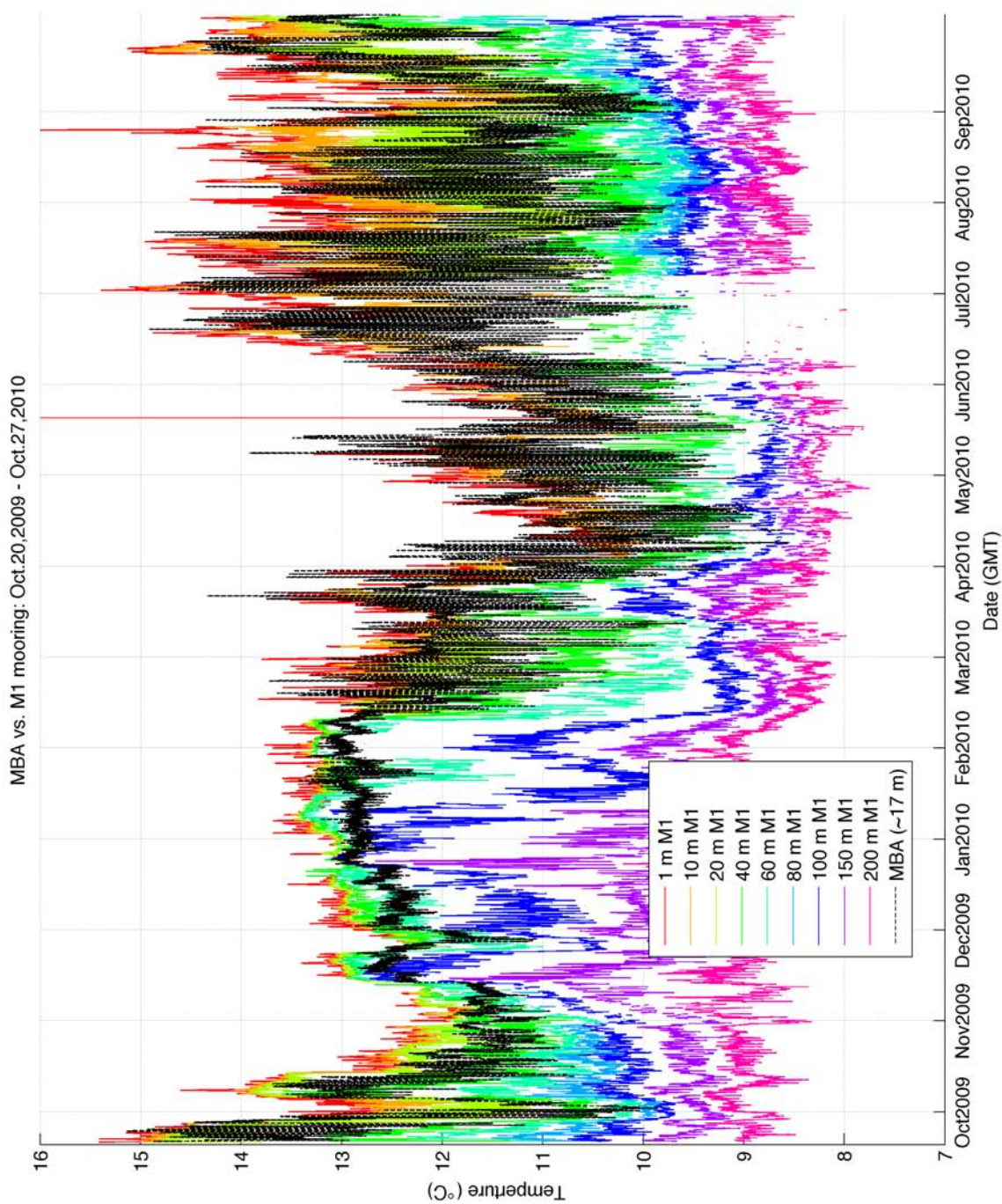


**Figure 63** Temperature measurements recorded from October 20, 2009 through October 27, 2010 at the Monterey Bay Aquarium seawater intake (black dashed line) and at different depths along the Monterey Bay Aquarium Research Institution’s M1 mooring (colored lines).

## **ARE THERE DIFFERENCES BETWEEN SOUTHERN AND CENTRAL MONTEREY BAY? AND IF SO, WHY?**

### **Methods Review**

The Moss Landing Marine Laboratories (MLML) has a seawater intake system at the head of the Monterey Canyon, 22.5 km northeast of the Monterey Bay Aquarium. This system draws water from ~20 m depth and is strongly influenced by an internal tide (Petruncio et al. 1998; Carroll 2008) due to the proximity of the Monterey Canyon.

Recall from the general methods section that the MLML temperature has been measured as part of the industrial monitoring system since December of 2002. Dissolved oxygen (DO) from the industrial system was not maintained to an acceptable level of accuracy, and in September 2010, a scientific monitoring system was installed and system maintenance was improved. Currently, there are three DO sensors in the MLML monitoring system (see general methods section for instrumentation), but only measurements from the scientific system were used, as this was the most trusted instrument.

### **Analysis and Results**

#### **TEMPERATURE AND DISSOLVED OXYGEN AT MBA AND MLML SEAWATER INTAKES**

One of the most obvious differences between the MBA and MLML temperature time series is that the variance at MLML is much higher (Figure 64). A cross covariance between 10-minute averaged MBA and MLML temperature, December 2002 to October 2010, lagging up to 12 hours (720 minutes) gave a maximum correlation coefficient of 0.624 with MBA lagged MLML by 6.5 hours (Figure 65). Minor correlation coefficient peaks were seen approximately 12.4 hours before and after the strongest peak, indicative of the semidiurnal tidal signal seen at both MBA and MLML.



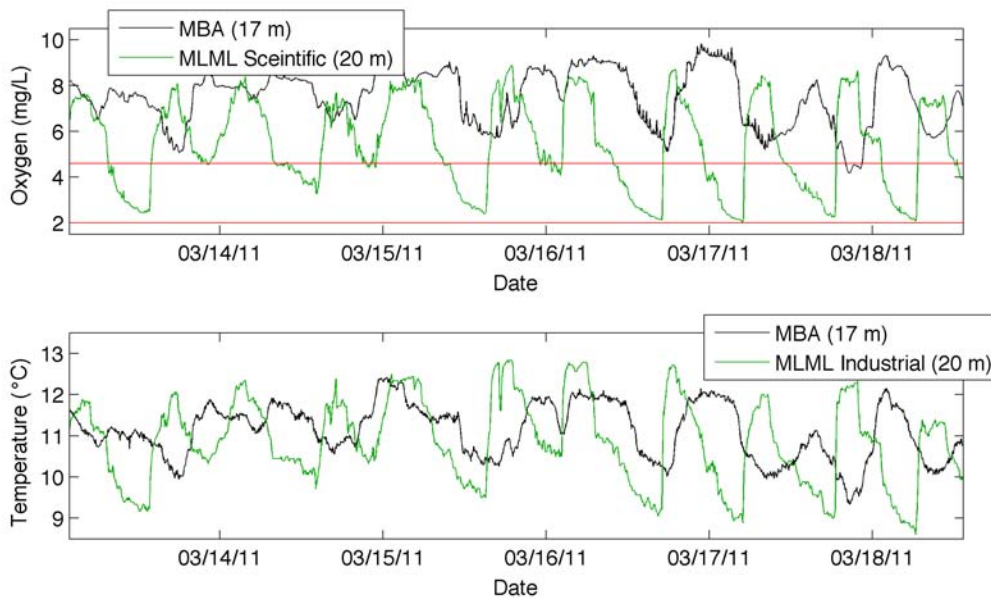


**Figure 64 Example Monterey Bay Aquarium (black) and Moss Landing Marine Laboratories (green) dissolved oxygen (top panel) and temperature (bottom panel) over several days in March 2011.**

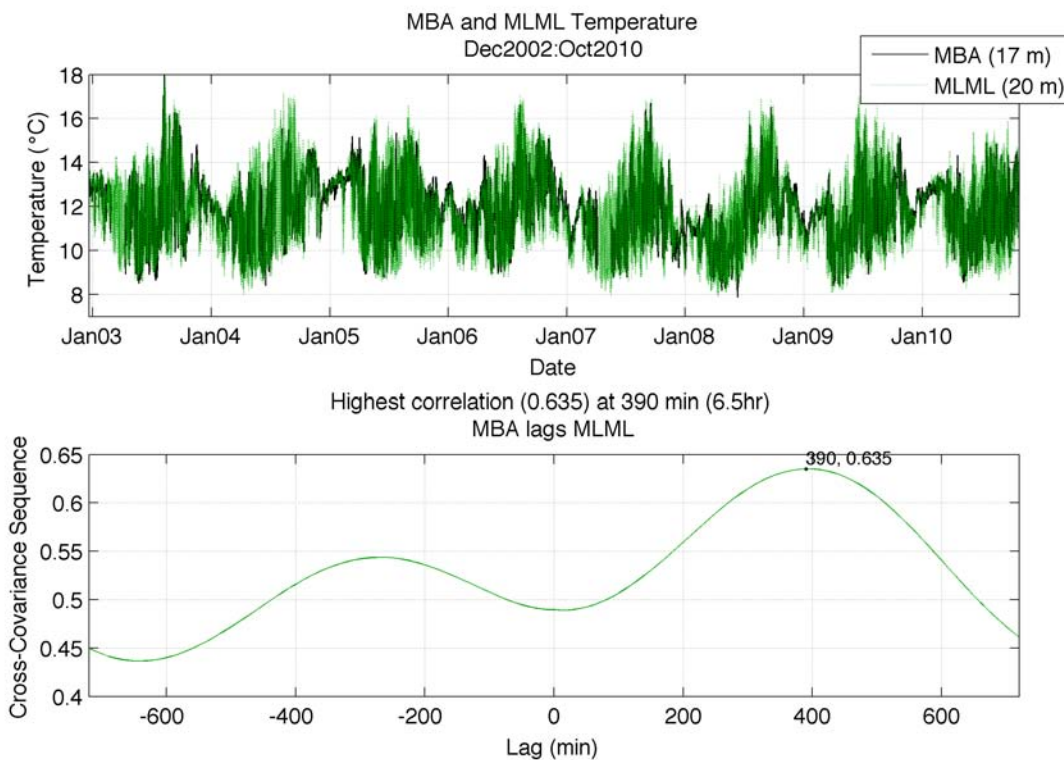




**Figure 65 Top panel, time series of Monterey Bay Aquarium (black) and Moss Landing Marine Laboratories (green) temperature. Bottom panel, A cross covariance between DO and temperature over the entire time series, December 2002 to October 2010.**

When all years are compared in both locations to look as seasonal patterns, the onset of high variance in early March is the same, as predicted since this is attributed to the beginning of the upwelling season (Figure 66). Another feature both locations share is a peak in early November that is persistent each year and may be associated with the onset of winter storms. Unlike temperature at MBA, MLML shows a peak in variability near the end of the upwelling season in August and higher variability during the winter (December through February).

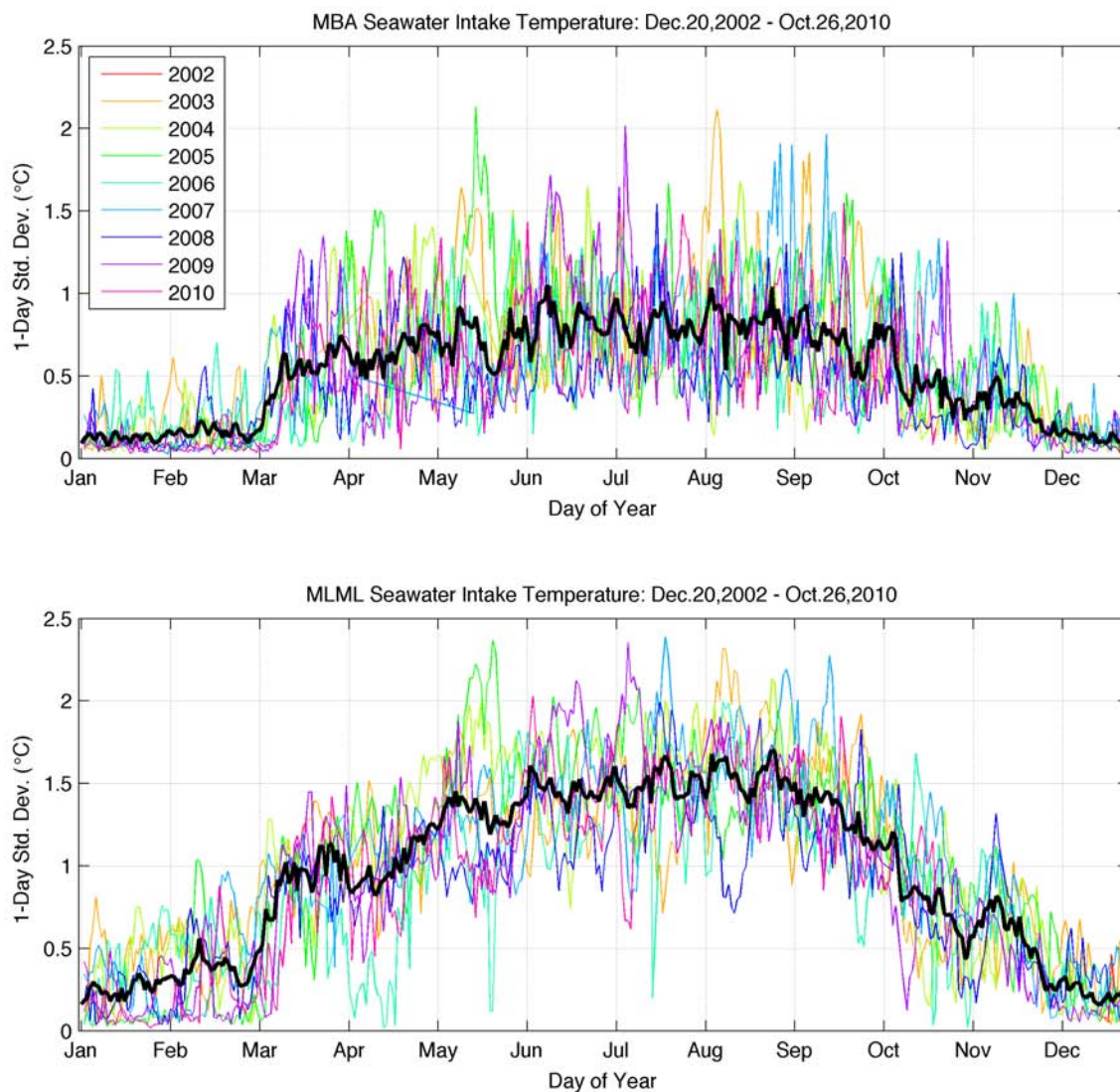


**Figure 66 Running 1-day standard deviation of temperature at Monterey Bay Aquarium (top panel) and Moss Landing Marine Laboratories (bottom panel). All years are overlaid (colored lines) and day of year average over all years (black line).**

Dissolved oxygen data from the MLML scientific system showed significant amounts of time below the 4.6 and 2 mg L<sup>-1</sup> hypoxia thresholds, even during the winter (Figure 67). As with temperature, DO variance was higher at MLML than at MBA. The result of a cross covariance analysis of 10-minute averaged MBA and MLML scientific was a correlation coefficient of 0.36 with MBA lagging MLML by 5.8 hours.

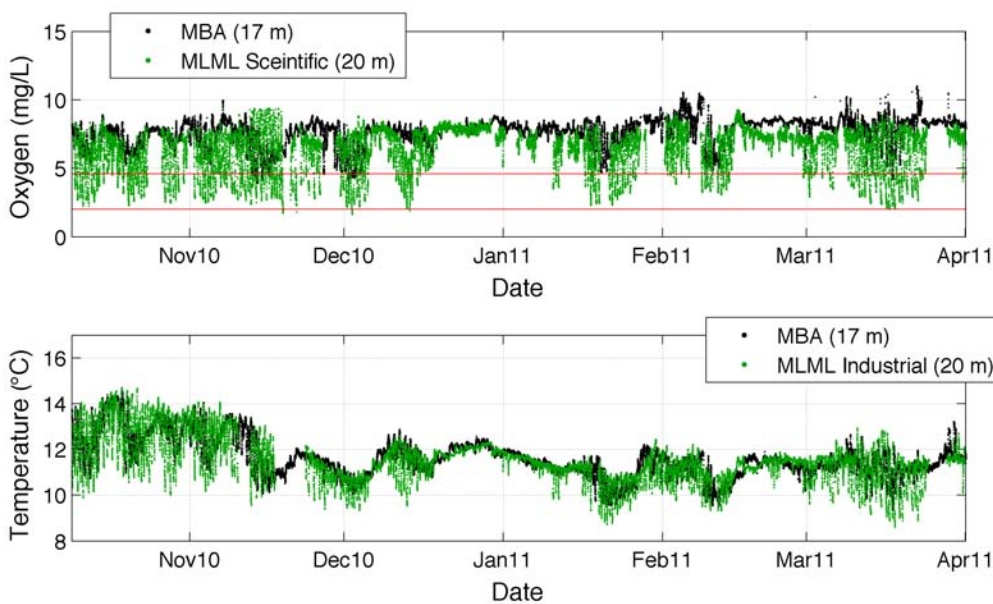


**Figure 67 Monterey Bay Aquarium (black) and Moss Landing Marine Laboratories (green) dissolved oxygen and temperature time series, October 9, 2010 to May 1, 2011. Oxygen sublethal (4.6 mg L<sup>-1</sup>) and lethal (2 mg L<sup>-1</sup>) thresholds are shown in red.**

#### EEMD OF MLML TEMPERATURE

The 5-minute MLML temperature time series from the “industrial” monitoring system (December 2002 – October 2010) was averaged to 1 hour and then tested for normality and skewness to determine if the time series was nonlinear (Figure 68). A Lilliefors’ composite goodness-of-fit test found that the data were not normally distributed ( $p = 0.001$ ). The data were positively skewed at +0.23. Both tests indicated that the MLML temperature time series was nonlinear, consistent with our choice of analysis technique.

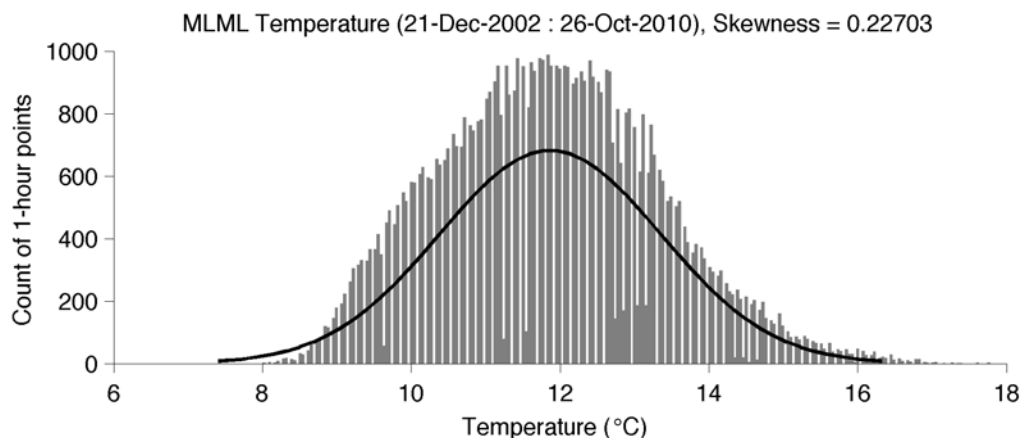


**Figure 68** Distribution of measurements of MLML temperature (vertical grey bars) superimposed with a fitted normal distribution (black lines).

An EEMD analysis using a ratio of the standard deviation of the added noise (Nstd) of 0.7 and an ensemble number (NE) of 100 was run on hourly MLML temperature time series resulting in sixteen IMFs, the last being the residual. A higher ratio of the standard deviation of added noise was used (0.7, compared to 0.1 used to process the MBA time series) because considerable mode mixing was occurring at lower IMFs around the semidiurnal period, which may have been due to the strong rectification of the semidiurnal tidal signal. High variance in IMF 2 and 3 corresponded to the semidiurnal tidal signal, which may have been separated into two IMFs due to the asymmetry of the signal (Figure 69, Figure 71, Figure 72) (Breaker et al. 2007). The ebb portion of the semidiurnal signal at MLML was often much longer than the flood with a hump half way down (see example March 16<sup>th</sup>-17<sup>th</sup> 2011 in Figure 64). The diurnal tidal signal (IMF 4) was much weaker than at the MBA site, confirming spectral analysis results discussed in next section (Figure 73). Similar to the MBA time series EEMD results, IMF 7, 8 and 9 had periods and bursts in variance associated with the Madden Julian Oscillation (M-J, Figure 71). Breaker et al. (2001) showed the intermittent nature of the M-J oscillations at mid-latitudes along the California coast. IMF 11 had periods associated with the annual signal and high variance, consistent with the results of Breaker (2005). The time series was too short to compare to an ENSO index. The residuals had a robust cooling trend of -0.1 to -0.12 °C per year, depending on the white noise added (Nstd = 0.05, 0.1 and 0.2), consistent with the cooling trend seen in the residuals of the MBA temperature time series EEMD results. Also similar to the MBA temperature time

series, the MLML temperature did not seem to be strongly influenced by drivers with periods in the synoptic weather band (IMF 6).

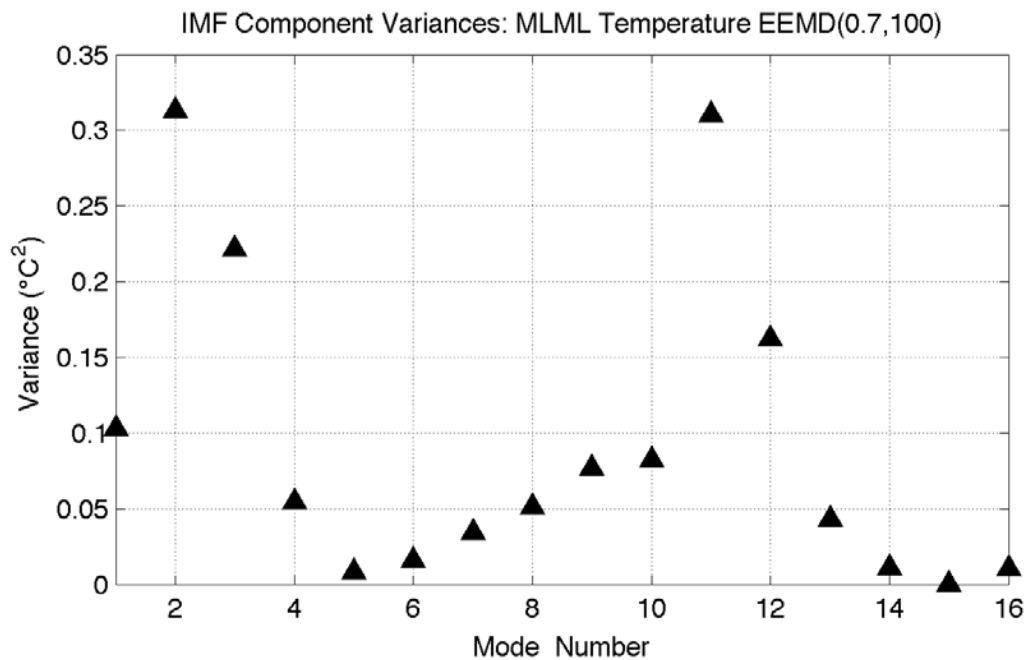


**Figure 69** The variance of each intrinsic mode function components (IMF) 1 through 16 (units of  $(^{\circ}\text{C})^2$ ) from the ensemble empirical mode decomposition (EEMD) of temperature at the Moss Landing Marine Laboratories (MLML). The EEMD was run with a ratio of the standard deviation of the added noise of 0.7 and an ensemble number of 100.

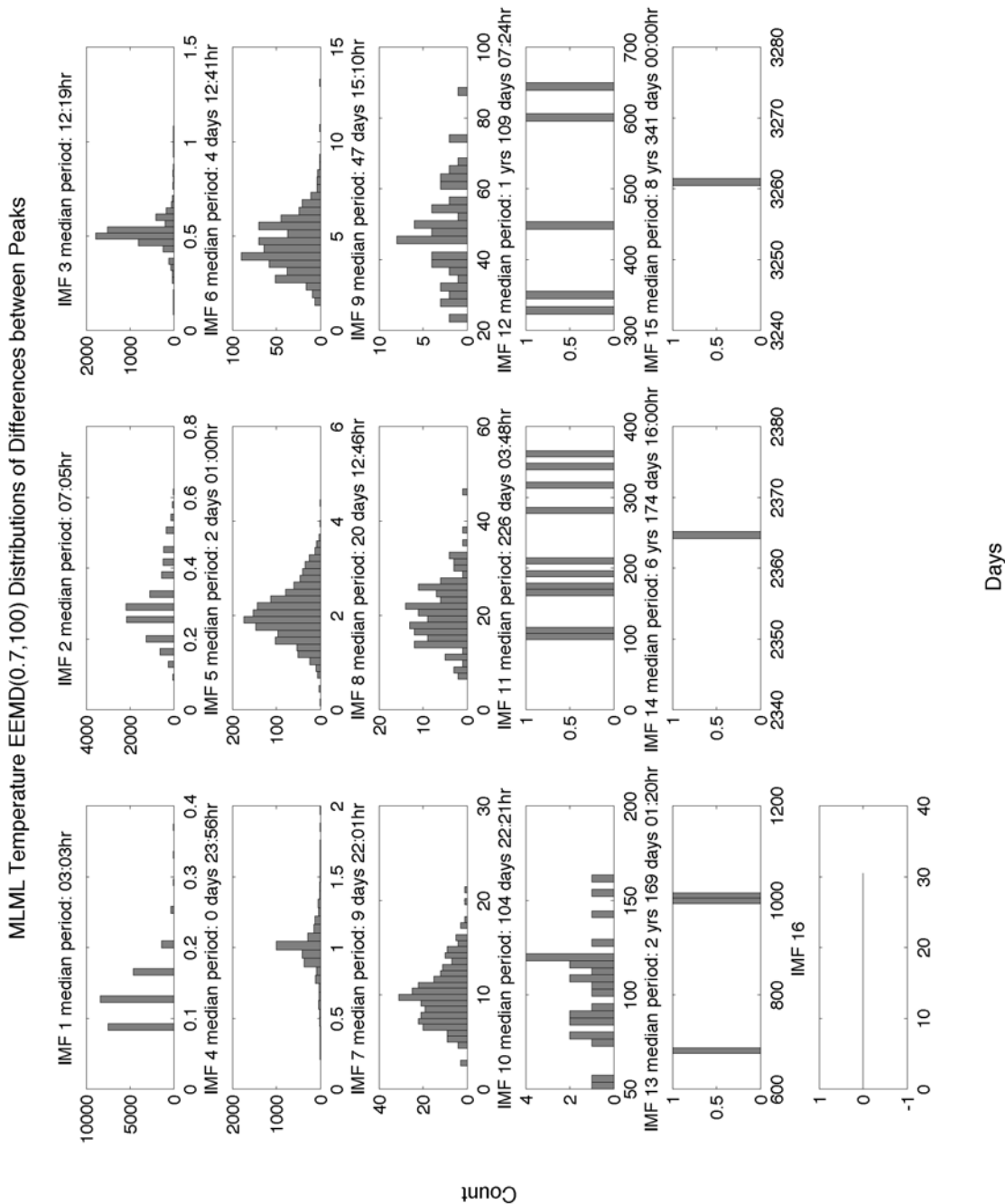


**Figure 70** Distribution of differences between peaks of each intrinsic mode function components (IMF) 1 through 16 from the ensemble empirical mode decomposition (EEMD) of temperature at the Moss Landing Marine Laboratories (MLML). The EEMD was run with a ratio of the standard deviation of the added noise of 0.7 and an ensemble number of 100. The median ‘period’ for each IMF is displayed above each distribution plot.

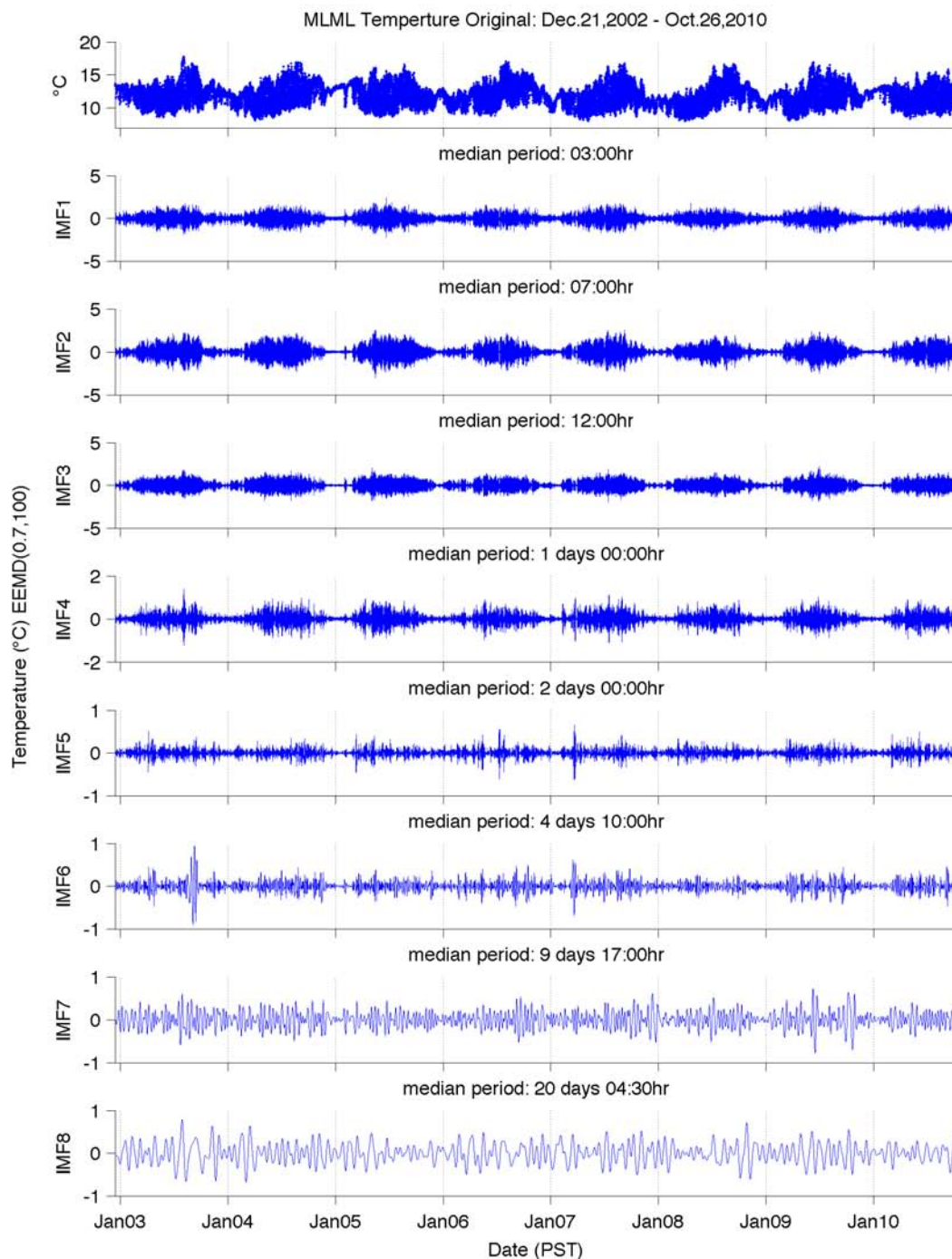


**Figure 71** The intrinsic mode function components (IMF) from the ensemble empirical mode decomposition (EEMD) of temperature at the Moss Landing Marine Laboratories (MLML) December 2002 – October 2010. Top panel, the original temperature (°C) time series. Bottom panels, IMF 1 through 7 in °C over time. See next figure for IMF 9-16. The EEMD was run with a ratio of the standard deviation of the added noise of 0.7 and an ensemble number of 100.



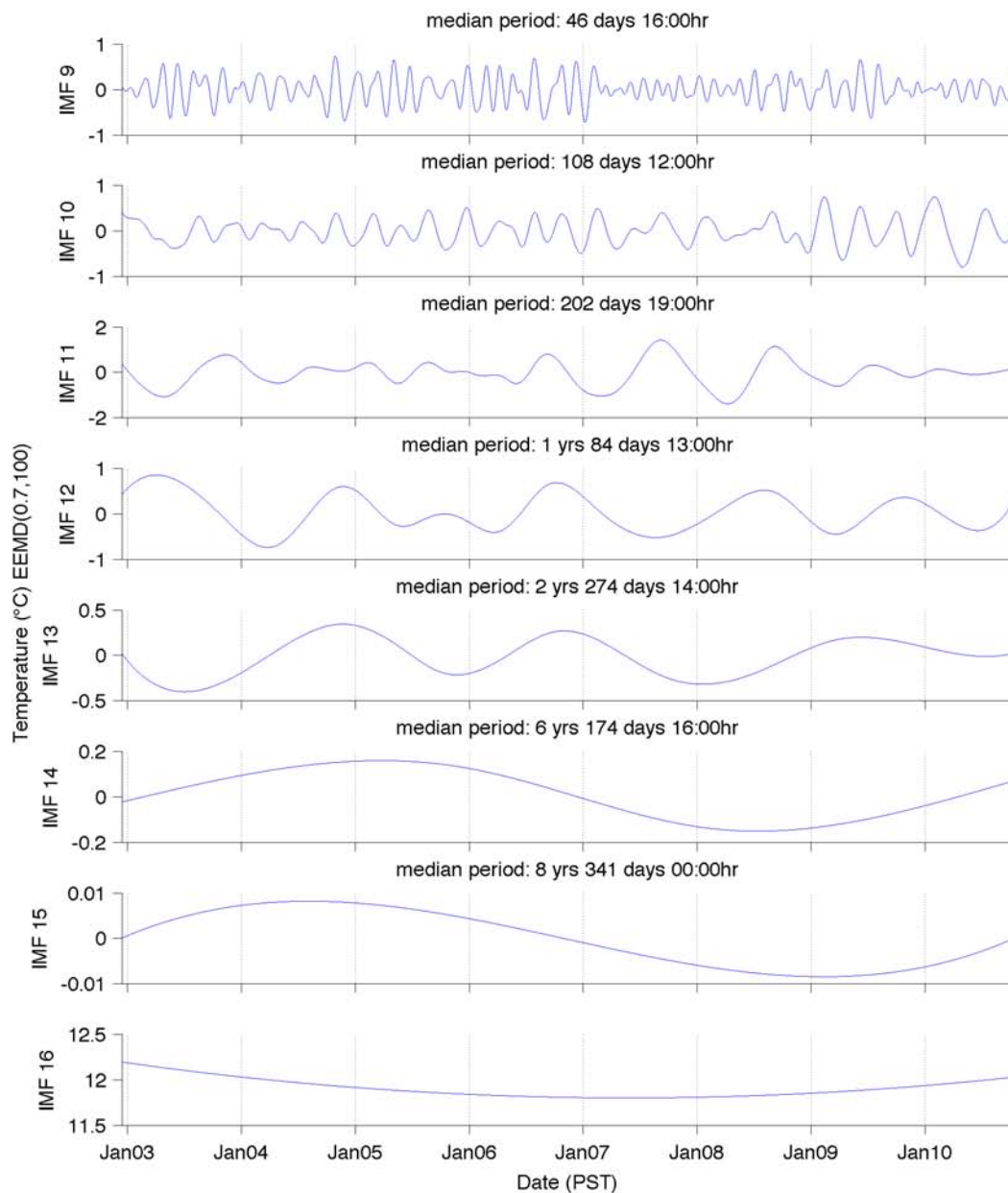


**Figure 72** The intrinsic mode function components (IMF) 8 through 14 ( $^{\circ}\text{C}$ ) from the ensemble empirical mode decomposition (EEMD) of temperature at the Moss Landing Marine Laboratories (MLML) December 2002 – October 2010. The final IMF (16) is the residual of the analysis. See previous figure for IMF 1-7. The EEMD was run with a ratio of the standard deviation of the added noise of 0.7 and an ensemble number of 100.

#### *Auto-spectra of MBA and MLML temperature time series*

Spectral analyses of the MBA and MLML temperature time series were performed using both a short and long window length in order to resolve peaks at high

and low frequencies. A smoothed power spectrum was produced by Welch's method of averaging replicate spectra calculated on a series of 50% overlapping 85-day sections of the data to look at tidal band frequencies and 7.5-year for seasonal peaks. The time series resolution was interpolated to 1 hour resulting in a maximum resolvable period of 2 hours (Nyquist frequency =  $(2 \cdot \Delta t)^{-1}$ ). Both short and long windowing methods produced dominant peaks at 1.00 and 1.93 cycles per day, the diurnal and semidiurnal tidal frequencies ( $K_1$  and  $M_2$ ), corresponding to periods of 24.0 and 12.4 hours in both DO and temperature (Figure 73, left panels, red circles). The powers at the semidiurnal frequency were equivalent at both MBA (3.82  $^{\circ}\text{C}^2 \text{cpd}^{-1}$ ) and MLML (4.20  $^{\circ}\text{C}^2 \text{cpd}^{-1}$ ) while the semidiurnal power at MLML (26.77  $^{\circ}\text{C}^2 \text{cpd}^{-1}$ ) was 21 times higher than at MBA (1.27  $^{\circ}\text{C}^2 \text{cpd}^{-1}$ ). The energy at the semidiurnal frequency also produced several harmonics at higher frequencies (Figure 73, left bottom panel). Such strong energy at the semidiurnal frequencies and harmonics are likely related to the proximity to the nearby Monterey Submarine Canyon (Carroll 2008).

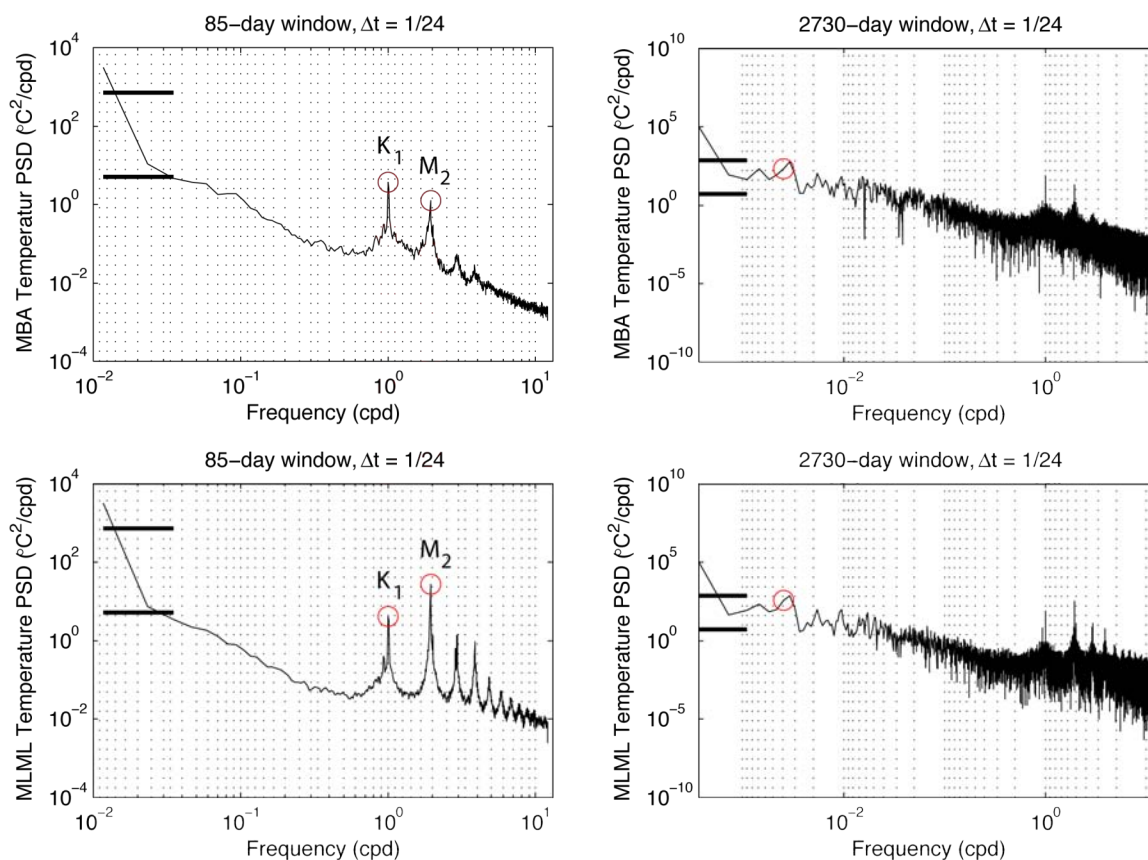




**Figure 73 Auto-spectra of Monterey Bay Aquarium (MBA, top panels) and Moss Landing Marine Laboratories (MLML) temperature (bottom panels) using a smaller (left panels) and larger (right panels) window size used to resolve diurnal/semidiurnal and seasonal frequency peaks, respectively. Peaks of interest are circled in red. Time step = 1hour.**

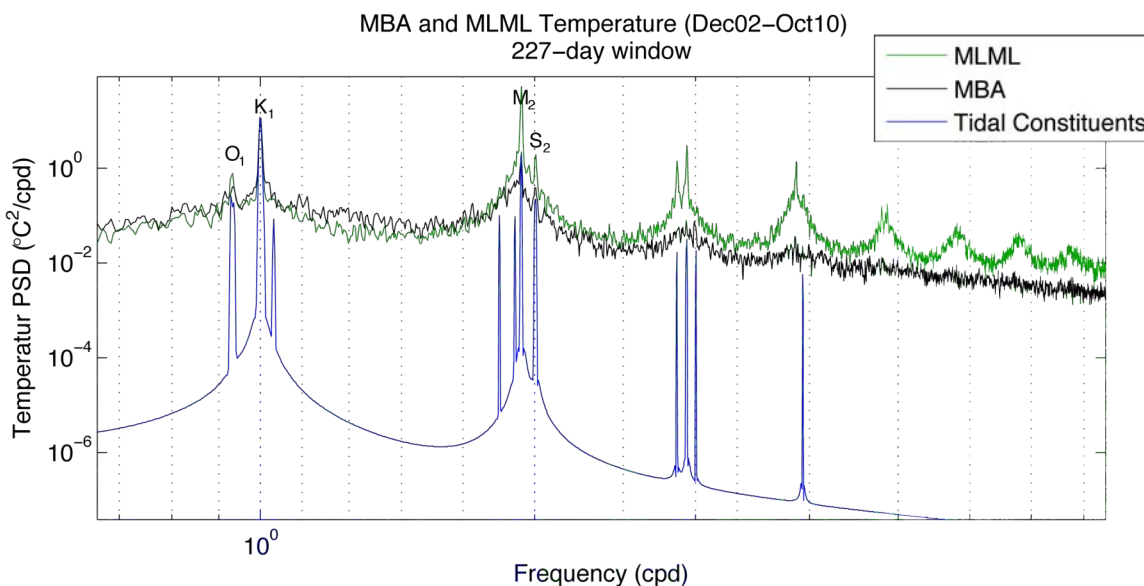


**Figure 74 Auto-spectra of Monterey Bay Aquarium (MBA, black) and Moss Landing Marine Laboratories (MLML, green) temperature and tidal constituents (blue). Plotted in log-log space, frequency is in cycles per day (cpd). Selected tidal constituents are labeled.**

#### *Cross-spectra of MBA and MLML temperature*

Both MBA and MLML temperature data were divided into three 227-day sub-windows with a 50% overlap, and multiplied by a Hanning window to compute cross power density using a time step of 5 minutes. There were dominant peaks at the diurnal and semidiurnal frequencies and several harmonics (Figure 75), meaning that both series had energy at tidal frequencies, as expected.

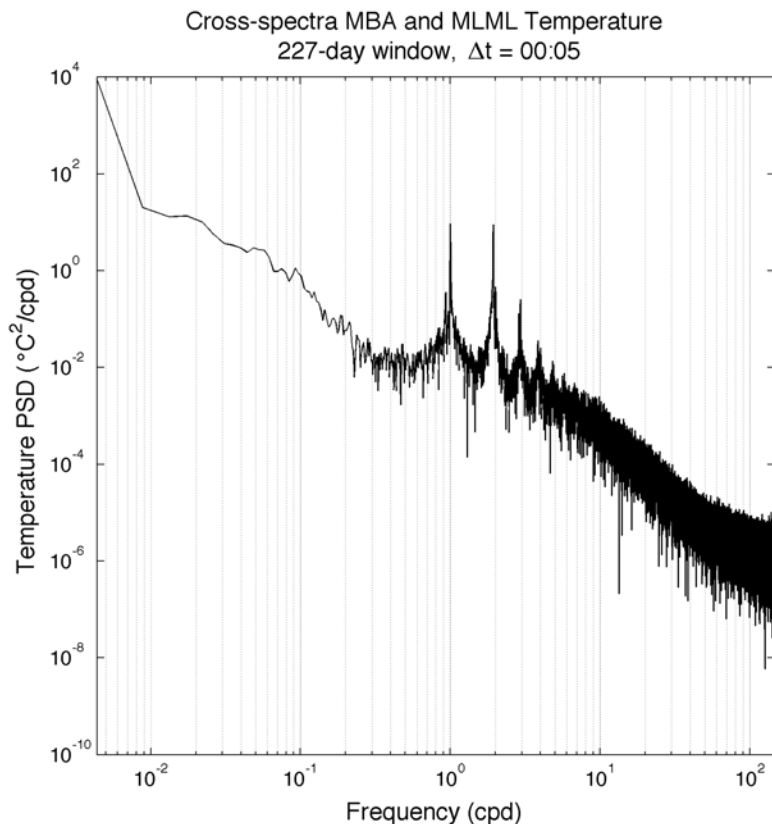


**Figure 75 Cross power spectra between Monterey Bay Aquarium (MBA) and Moss Landing Marine Laboratories (MLML) temperature.**

Coherence and phase were calculated between MBA and MLML temperature, again using an 85-day window. There was high coherence at the diurnal and the semidiurnal frequencies (Figure 76, top panel). The phase at the diurnal frequency was approximately  $-70^\circ$ , corresponding to MBA lagging MLML by 4.6 hours. At the semidiurnal frequency, there was a phase shift of approximately  $-32^\circ$  translating to MBA lagging MLML by 1.1 hour (Figure 76, bottom panel).

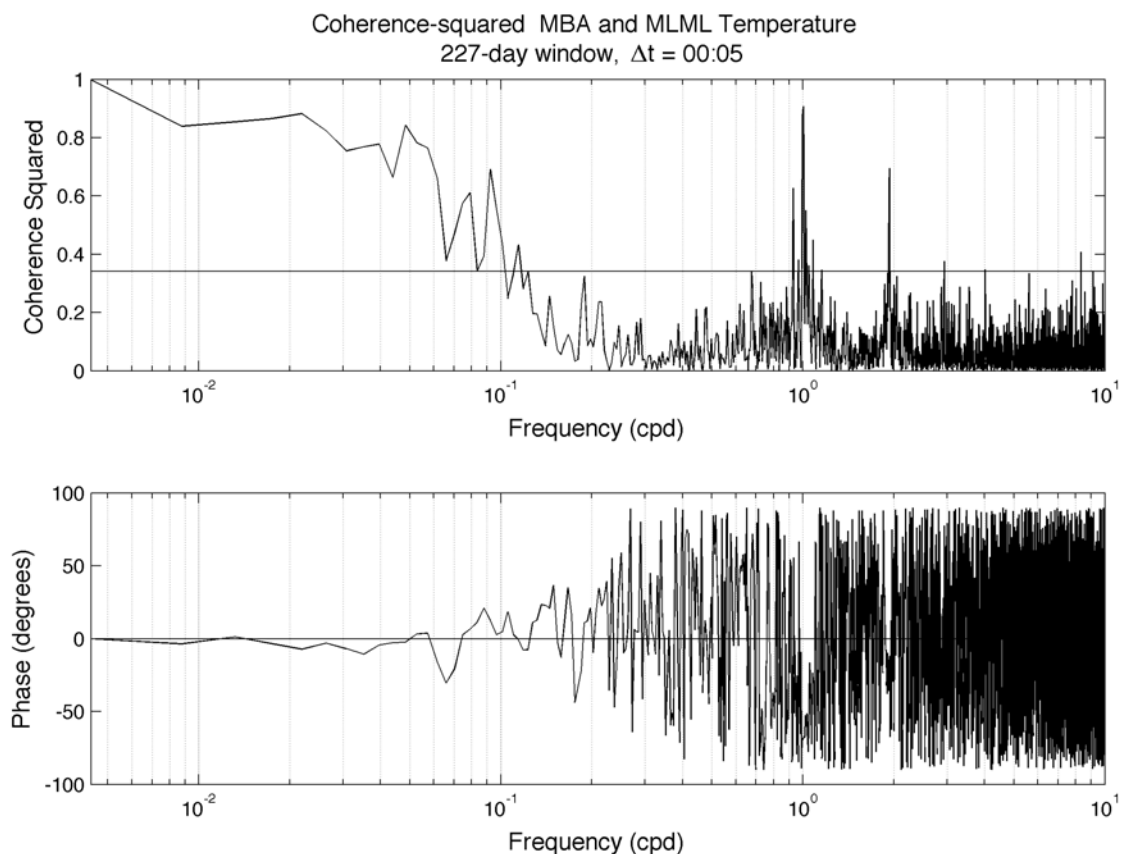


**Figure 76 Coherence (top panel) and phase (bottom panel) plots for Monterey Bay Aquarium (MBA) and Moss Landing Marine Laboratories (MLML) temperature. Top panel, horizontal line is level of 99% significance. Bottom panel, horizontal line is at a phase of  $0^\circ$ .**

## CONCLUSIONS AND DISCUSSION

The purpose of this project was to examine opportunistic time series collected at two locations in the Monterey Bay, California and attempt to identify possible drives of oxygen and pH variability. High frequency fluctuations in temperature have been shown to be ubiquitous in coastal California, caused by the advection of temperature gradients (primarily vertical since the dominate temperature gradient is vertical, but horizontal advection can play a secondary role) (Carroll 2008; Cudaback and McPhee-Shaw 2009; Carter 2010), however, these internal tides have not been examined in as much detail in oxygen or pH. Although the water monitoring programs at the Monterey Bay Aquarium (MBA) and the Moss Landing Marine Laboratories (MLML) were not initially designed for scientific environmental monitoring and thus have a certain amount of unquantifiable

error, there is enough certainty to draw some important conclusions. Let us now return to the original questions and summarize the conclusions.

- What has been the state of oxygen, pH and temperature in the nearshore environment of the southern Monterey Bay over the past decade? Do oxygen and pH levels drop to biologically stressful levels?
- What are the dominant time scales of high variability in oxygen and pH? What are the relationships between the measured variables and underlying drivers of system variability? Are there any trends in the time series?
- Are there differences between southern and central Monterey Bay? And if so, why?

At both nearshore locations, I found considerable variability in temperature, which was expected from previous studies on internal waves in the Monterey Bay (Storlazzi et al. 2003; Woodson et al. 2007; Carroll 2008). A more surprising result was the high variance in both dissolved oxygen (DO) and pH, and the extremely low values that both parameters often reached. Dissolved oxygen often broach biologically threatening thresholds, below 4.6 and 2 mg L<sup>-1</sup>, for multiple hours each day during the upwelling season. Since the Vaquer-Sunyer and Duarte (2008) DO thresholds (4.6 and 2 mg L<sup>-1</sup>) were not based on nearshore species in upwelling environments, it raises the question: how are nearshore species in eastern boundary current ecosystems adapted to low oxygen? The results presented here from the MBA and MLML time series will be important in designing realistic physiological exposure experiments as well as fitting into marine hypoxia and acidification modeling and management.

Due to the dominant internal tide forcing of this system, low DO events often occur once or twice a day several days after a strong upwelling event at the MBA site, and usually twice a day at the MLML site due to the strong diurnal forcing there. Multiple studies have described stronger internal tides closer to the Monterey Canyon (Kunze et al. 2002; Jachec et al. 2006; Carroll 2008; Carter 2010). At MBA, mild hypoxic events ( $\leq 4.6$  mg L<sup>-1</sup>) last on average 2.4 hours ( $\pm 3.6$  S.D.,  $n = 1817$ ) with a maximum duration of 40.1 hours and severe hypoxic events ( $\leq 2$  mg L<sup>-1</sup>) last on average 1.4 hours ( $\pm 1.1$  S.D.,  $n = 12$ ) with a maximum of 3.3 hours (Figure 77). At the head of the Monterey Canyon at the MLML site, mild hypoxia was not confined to the upwelling

season and on average would last 2.1 hours ( $\pm 2.3$  S.D.,  $n = 397$ ). Durations of severely hypoxic events were on average 1.0 hour ( $\pm 1.1$  S.D.,  $n = 56$ ) at MLML. Hypoxic event durations were similar at both sites but events occurred much more often at the MLML site. Diurnal and semidiurnal baroclinic oscillations have been identified as an important nutrient delivery system to transport deep-water into the nearshore (Shea and Broenkow 1982; Carroll 2008). This nutrient-rich water is also low in DO and pH, and thus brings potential physiological stressors along with the productive coastal ecosystem.

Average and maximum hypoxic/low pH event durations nearshore Monterey Bay (17m depth), upwelling season

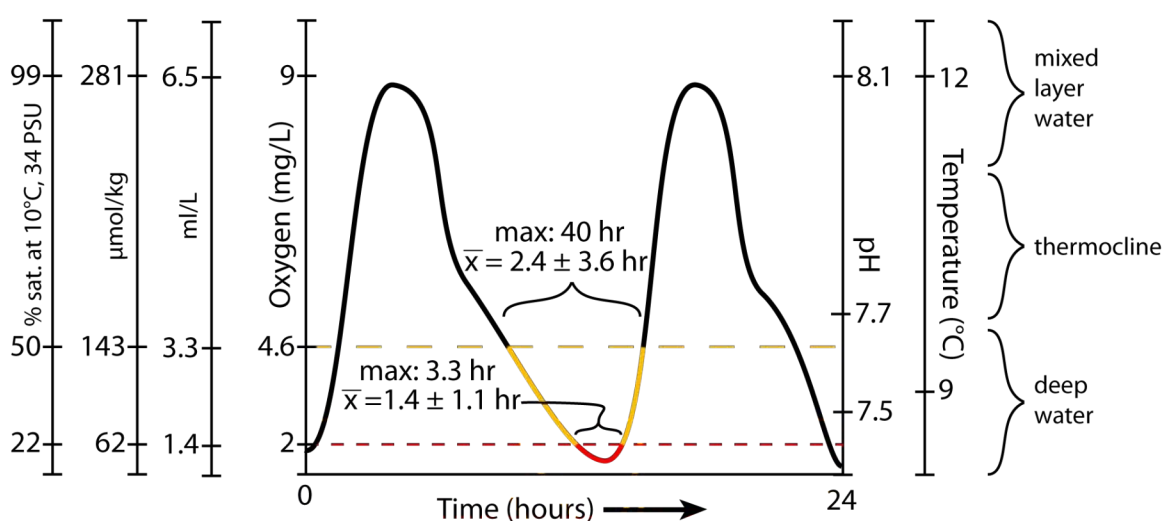


**Figure 77 Schematic of average low DO/ low pH event in the nearshore of southern Monterey Bay (Monterey Bay Aquarium) over a 24 hour period at ~17 m depth. Center plot shows the DO/pH/temperature signal fluctuating with the semidiurnal internal tide. Additional axes indicated different oxygen units and the associated pH and temperature ranges. Far right labels show origin of the water sampled.**

Upwelling events precede pulses of increased variance in DO and low DO events throughout the record. The Bakun Upwelling Index was able explain up to 56% of the variance in the daily standard deviation of DO with a 2-5 day lag. Comparisons with temperature data taken at various depths at an offshore mooring indicate that internal tidal motions are persistent all year round down to 300 m, and water is regularly being advected from 100-200 m depth into the nearshore. Upwelling modulated by tidal fluctuations is the main driver of hypoxic and low pH events, pushing water from ~100 m depth up to MBA and up from ~200 m at the MLML site. When coastal upwelling occurs

the mixed layer is compressed and moved offshore, replaced by denser water, and then baroclinic tidal motions transport the deep water inshore (Figure 78). These results are consistent with the heaving up of deep-water seen by Carroll (2008) and Shea and Broenkow (1982). When there is low variability seen at either intake, the thermocline is likely either too deep or the water column is mixed, as is typical in winter.

Also worth noting is that density data from the offshore mooring indicate that upwelling must draw water up from deeper than 300 m (deepest thermistor on mooring). Density increases were seen at the 300 m sensors during the upwelling season and coupling with internal tidal motions could bring water up into nearshore ecosystems from much deeper than previous estimates of 50 to 100 m (Schwing et al. 1996).

Other possible physical and biological drivers were considered, but the short-term variability in temperature, DO and pH at the MBA site seem to be almost entirely driven by advective processes. Alternative hypotheses involving acute effects of algal or bacterial respiration are not consistent with observed properties of the events; temperature and DO were tightly correlated with no lag. Short term DO variability did not correlate strongly with photosynthetically available radiation (PAR) or the surface barotropic tide. Changes in DO saturation associated with temperature fluctuations did not cause hypoxic or super saturation events. Oxygen super-saturation events are likely forced by surface productivity. Correlations between daily maximums in DO and an upwelling index showed a weak positive relationship after a 12-day lag, which was not seasonally consistent. When this is compared to a strong correlation at a 3-day lag between the upwelling index and daily DO standard deviations and minimums, it suggests that that upwelling stratifies the water column and brings low oxygen water, while the DO of the surface water is only very mildly effected by surface productivity through the introduction of upwelled nutrients. Local surface productivity (super saturation events) did not precede hypoxic events. The annual cycle in DO was associated with the upwelling season and was out of phase with the rainy season that would have brought terrestrial nutrient input to the system. In contrast to the East and Gulf coasts of the United States (Diaz and Rosenberg 2008), terrestrial nutrient input plays a minor role off the California coast compared to the mass introduced through upwelling and internal

waves (McPhee-Shaw et al. 2007; Carroll 2008) and is likely not important in inducing hypoxia.

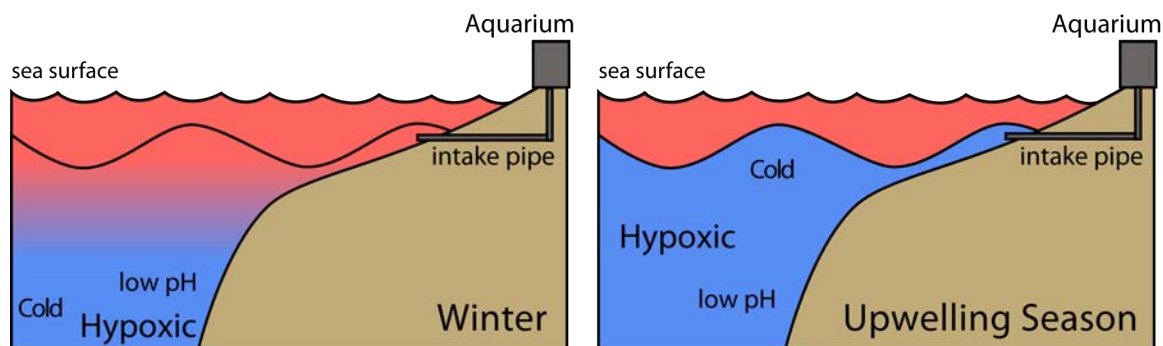


**Figure 78 Schematic of cold, hypoxic and low pH water transport into nearshore. Right panel illustrates the winter, non-upwelling season when hypoxic water is deep and the mixed layer is deep. The water advected inshore by internal tidal motions is similar to surface waters. The left panel, shows upwelling conditions where deep cold, hypoxic water is shallow enough for the internal tide to transport it inshore.**

The long duration of these water-monitoring programs made it possible to look at long-period oscillations, but the sampling period was not long enough to detect any trends on a decadal scale that might be related to climate change (Breaker and Ruzmaikin 2010). Ensemble empirical mode decomposition was well designed to handle a long, nonlinear time series. In using this analysis some more subtle drivers and trends were seen in the longer monitoring programs: MBA DO (10 years) and temperature (15 years), and MLML temperature (8 years). Several modes in all three time series showed influences from the Madden-Julian oscillation, consistent with similar observation by (Breaker 2005), and indicate that both temperature and DO are influenced by large scale atmospheric and oceanic perturbations. The long temperature time series from MBA correlated with El Niño/Southern Oscillation indices with a several month lag (lagged Oceanic Niño Index (ONI) by 3 months and Northern Oscillation Index (NOI) by 2 months). Temperature at both sites showed a residual decrease consistent with the Pacific Decadal Oscillation and the results of (Breaker and Ruzmaikin 2010). The decrease was -0.08 to -0.1 °C/year at MBA and -0.1 to -0.12 °C/year at MLML.

In this system DO appears to act primarily as a conservative tracer unlike the well-studied low DO events off the Oregon and Washington coast, where local biological activity on a wide continental shelf further depletes upwelled waters that are already

hypoxic (Grantham et al. 2004; Connolly et al. 2010). Evidence that local oxygen depletion on the shelf in Monterey Bay is not occurring is supported by the comparisons to the offshore M1 mooring that indicate internal tidal forcing pushes water up from ~100 m (MBA) and ~200 m (MLML) throughout the year, but during the upwelling season water heaved up from even deeper origin. Most hypoxic events at MBA occur when upwelling is at its strongest (April-May) not after local super saturation events or at the end of the summer when the cumulative depletion of oxygen fed by a summer of production would be at its peak (Grantham et al. 2004; Hales et al. 2006; Connolly et al. 2010). If local depletion were occurring, the internal tides would sweep this water up the shelf as it does all year round (Carter 2010). The seasonally skewed distribution of DO indicates a system dominated by advection. These results along with the Ensemble Empirical Mode Decomposition (EEMD) results show that longer scale variability is controlled by large-scale basin-wide oscillations and perturbations, not local forcings like storm runoff or algal production and decomposition.

pH was measured weekly since 1996 and every 5 minutes for over a year at the MBA intake site. The 5-minute flow-through measurements showed a range of 7.46 to 8.45. Levels often fell below 7.75, which was identified by Feely et al. (2008) to be associated with a saturation state of aragonite ( $\Omega_{\text{arag}}$ ) of 1 in offshore waters (aragonite being the more soluble form of calcium carbonate). At MBA, the  $\Omega_{\text{arag}}$  was often recorded below 1 in the weekly measurements taken between May 2010 and April 2011. The  $\Omega_{\text{arag}}$  data had a moderate positive relationship with pH but did not correspond to only pH levels below 7.75. These results are surprising considering how much time was below 1 and how detrimental these levels can be to calcifying organisms (Fabry et al. 2008; Hauri et al. 2009), however, analytical and human error could be high here.

Traditionally, researchers have investigated stressful environmental conditions like hypoxia and low pH in isolation, but, as we see from the MBA time series, these two stressors can be closely linked. During the observed intrusions, both oxygen and proton concentrations reached levels that are generally considered to be threatening, and dual exposure to hypoxia and low pH may have synergistic physiological and ecological consequences that are difficult to predict (Pane and Barry 2007; Fabry et al. 2008). Low pH not only alters calcification rates, but can also directly influence biochemical reaction



rates and binding of substrates. For example, a pH-induced decrease in oxygen-binding affinity of hemocyanin, an important respiratory protein in the blood of many marine invertebrates, could severely stress aerobic respiration when combined with low ambient DO (Rosa and Seibel 2008).

The results of this research will be important for designing realistic exposure regimes for physiological studies on nearshore organisms from eastern boundary current systems. Research needs to be done on these organisms, which have not been included in reviews of hypoxia tolerances (Vaquer-Sunyer and Duarte 2008). Physiological impacts of hypoxia on Pacific Coast organisms have been limited deeper waters near the OMZ (Levin, 2003; Levin et al. 2009). Animals in the benthic nearshore may be uniquely susceptible to these hypoxic/low pH inundations if deepwater chemistry changes faster than surface waters (Brewer and Peltzer 2009) and changing baselines exceed physiological tolerances. Future work needs to be done to synthesize hypoxia and acidification research for the entire California Current Large Marine Ecosystem, near shore and off shore. The coast has a spectrum of drivers of system variability and it will be important to identify the most important ones in different areas and if the drivers are shifting in their influence. This work will be furthered by modeling large-scale hypoxia and acidification and the results presented here will help quantify nearshore dynamics that are traditionally ignored in large-scale models.

## REFERENCES

- Andersson AJ, Mackenzie FT, Bates NR. 2008. Contribution to the Theme Section "Effects of ocean acidification on marine ecosystems" Life on the margin: implications of ocean acidification on Mg-calcite, high latitude and cold-water marine calcifiers. *Marine Ecology Progress Series* 373:265-273.
- Aydin M, Top Z, Olson DB. 2004. Exchange processes and watermass modifications along the subarctic front in the North Pacific: Oxygen consumption rates and net carbon flux. *Journal of Marine Research* 62:153-167.
- Bakun A. 1990. Global climate change and intensification of coastal ocean upwelling. *Science* 247(4939):198-201.
- Bograd SJ, Castro CG, Di Lorenzo E, Palacios DM, Bailey H, Gilly W, Chavez Francisco P. 2008. Oxygen declines and the shoaling of the hypoxic boundary in the California Current. *Geophysical Research Letters* 35(12):L12607.
- Bograd SJ, Schroeder I, Sarkar N, Qiu X, Sydeman WJ, Schwing FB. 2009. Phenology of coastal upwelling in the California Current. *Geophysical Research Letters* 36(1):L01602.
- Bopp L, Quéré CL, Heimann M, Manning AC, Monfray P. 2002. Climate-induced oceanic oxygen fluxes: Implications for the contemporary carbon budget. *Global Biogeochemical Cycles* 16(2):13.
- Breaker LC, Broenkow WW, Watson WE, Jo Y-H. 2007. Tidal and Nontidal Oscillations in Elkhorn Slough, CA. *Estuaries and Coasts* 31(2):239-257.
- Breaker LC, Liu PC, Torrence C. 2001. Intraseasonal oscillations in sea surface temperature, wind stress, and sea level off the central California coast. *Continental Shelf Research* 21(6-7):727-750.
- Breaker LC, Ruzmaikin A. 2010. The 154-year record of sea level at San Francisco: extracting the long-term trend, recent changes, and other tidbits. *Climate Dynamics* 36(3):545-559.
- Breaker LC. 2005. What's happening in Monterey Bay on seasonal to interdecadal time scales. *Continental Shelf Research* 25(10):1159-1193.
- Breitburg D. 2002. Effects of hypoxia, and the balance between hypoxia and enrichment, on coastal fishes and fisheries. *Estuaries and Coasts* 25(4):767-781.
- Brewer PG, Peltzer ET. 2009. Limits to Marine Life. *Science* 324(5925):347-348.

- Caldeira K, Wickett ME. 2003. Anthropogenic carbon and ocean pH. *Nature* 425(6956):365.
- Carroll D. 2008. Carmel Bay: Oceanographic dynamics and nutrient transport in a small embayment of the central California coast. [M.S. thesis]. Moss Landing, CA: Moss Landing Marine Laboratories, California State Universities. 136 p.
- Carter GS. 2010. Barotropic and Baroclinic M2 Tides in the Monterey Bay Region. *Journal of Physical Oceanography* 40(8):1766-1783.
- Chan F., Barth J. A., Lubchenco J., Kirincich A, Weeks H, Peterson WT, Menge B. A. 2008. Emergence of Anoxia in the California Current Large Marine Ecosystem. *Science* 319(5865):920.
- Connolly TP, Hickey BM, Geier SL, Cochlan WP. 2010. Processes influencing seasonal hypoxia in the northern California Current System. *Journal of geophysical research* 115:C03021-C03021.
- Crabbe KL. 2007. Directional Characteristics of Inner Shelf Internal Tides. Directional Characteristics of Inner Shelf Internal Tides Monterey, CA: Naval Postgraduate School. 94 p.
- Cudaback CN, McPhee-Shaw EE. 2009. Diurnal-period internal waves near point conception, California. *Estuarine, Coastal and Shelf Science* 83(3):349-359.
- Diaz RJ, Rosenberg R. 2008. Spreading Dead Zones and Consequences for Marine Ecosystems. *Science* 321(5891):926-929.
- Diaz RJ, Solow A. 1999. Ecological and economic consequences of hypoxia: Topic 2 Report for the integrated assessment of hypoxia in the Gulf of Mexico. Silver Springs (MD): NOAA Coastal Ocean Program
- Diaz RJ. 2001. Overview of hypoxia around the world. *Journal of Environmental Quality* 30(2):275-281.
- Dickson AG, Millero F.J. 1987. A comparison of the equilibrium constants for the dissociation of carbonic acid in seawater media. *Deep Sea Research Part A. Oceanographic Research Papers* 34(10):1733-1743.
- Doney SC. 2010. The Growing Human Footprint on Coastal and Open-Ocean Biogeochemistry. *Science* 328(5985):1512 -1516.
- Emerson S, Watanabe Y, Ono Tsuneo, Mecking S. 2004. Temporal Trends in Apparent Oxygen Utilization in the Upper Pycnocline of the North Pacific: 1980–2000. *Journal of Oceanography* 60(1):139-147.
- Escribano R, Schneider W. 2007. The structure and functioning of the coastal upwelling system off central/southern Chile. *Progress in Oceanography* 75:343-347.

- Fabry VJ, Seibel BA, Feely RA, Orr JC. 2008. Impacts of ocean acidification on marine fauna and ecosystem processes. *ICES Journal of Marine Science* 65(3):414-432.
- Feely RA, Sabine CL, Hernandez-Ayon JM, Ianson D, Hales B. 2008. Evidence for Upwelling of Corrosive “Acidified” Water onto the Continental Shelf. *Science* 320(5882):1490-1492.
- Feely RA, Sabine CL, Lee K, Berelson W, Kleypas J, Fabry VJ, Millero Frank J. 2004. Impact of Anthropogenic CO<sub>2</sub> on the CaCO<sub>3</sub> System in the Oceans. *Science* 305(5682):362-366.
- Feely RA, Sabine CL, Schlitzer R, Bullister J, Mecking S, Greeley D. 2004. Oxygen Utilization and Organic Carbon Remineralization in the Upper Water Column of the Pacific Ocean. *Journal of Oceanography* 60(1):45-52.
- Field JC, Baltz K, Phillips AJ, Walker WA. 2007. Range expansion and trophic interactions of the jumbo squid, *Dosidicus gigas*, in the California Current. *California Cooperative Oceanic Fisheries Investigations (CalCOFI) Reports* 48:131-146.
- Friederich GE, Walz PM, Burczynski MG, Chavez F. P. 2002. Inorganic carbon in the central California upwelling system during the 1997-1999 El Niño-La Niña event. *Progress In Oceanography* 54(1-4):185-203.
- García-Reyes M, Largier J. 2010. Observations of increased wind-driven coastal upwelling off central California. *Journal of Geophysical Research* 115:8.
- Gazeau F, Quiblier C, Jansen JM, Gattuso J-P, Middelburg JJ, Heip CHR. 2007. Impact of elevated CO<sub>2</sub> on shellfish calcification. *Geophysical Research Letters* 34:5.
- Gilly W, Markaida U, Baxter CH, Block BA, Boustany A, Zeidberg L, Reisenbichler K, Robison B, Bazzino G, Salinas C. 2006. Vertical and horizontal migrations by the jumbo squid *Dosidicus gigas* revealed by electronic tagging. *Marine Ecology Progress Series* 324:1-17.
- Golyandina N, Nekrutkin VV, Zhiglavskii AA. 2001. Analysis of time series structure: SSA and related techniques. Boca Raton, FL: CRC Press
- Grantham BA, Chan Francis, Nielsen KJ, Fox DS, Barth John A., Huyer A, Lubchenco Jane, Menge Bruce A. 2004. Upwelling-driven nearshore hypoxia signals ecosystem and oceanographic changes in the northeast Pacific. *Nature* 429(6993):749-754.
- Gray JS, Wu RS, Or YY. 2002. Effects of hypoxia and organic enrichment on the coastal marine environment. *Marine Ecology Progress Series* 238:249-279.
- Hales B, Karp-Boss L, Perlin A, Wheeler Patricia A. 2006. Oxygen production and carbon sequestration in an upwelling coastal margin. *Global Biogeochemical Cycles* 20(3):GB3001.

- Hauri C, Gruber N., Plattner G.-K., Alin S, Feely RA, Hales B, Wheeler P. A. 2009. Ocean acidification in the California Current System. *Oceanography* 22(4):60-71.
- Helly JJ, Levin LA. 2004. Global distribution of naturally occurring marine hypoxia on continental margins. *Deep Sea Research Part I: Oceanographic Research Papers* 51(9):1159-1168.
- Huang N, Shen Z, Long S, Wu M, Shih H, Zheng Q, Yen N-C, Tung C, Liu H. 1998. The empirical mode decomposition and the Hilbert spectrum for nonlinear and non-stationary time series analysis. *Proceedings of the Royal Society of London. Series A: Mathematical, Physical and Engineering Sciences* 454(1971):903-995.
- Jachec SM, Fringer OB, Gerritsen MG, Street RL. 2006. Numerical simulation of internal tides and the resulting energetics within Monterey Bay and the surrounding area. *Geophysical Research Letters* 33:4.
- Johnson KS. 2010. Simultaneous measurements of nitrate, oxygen, and carbon dioxide on oceanographic moorings: Observing the Redfield Ratio in real time. *Limnology and Oceanography* 55(2):615-627.
- Keeling RF, Garcia HE. 2002. The change in oceanic O<sub>2</sub> inventory associated with recent global warming. *Proceedings of the National Academy of Sciences of the United States of America* 99(12):7848-7853.
- Kunze E, Rosenfeld LK, Carter GS, Gregg MC. 2002. Internal Waves in Monterey Submarine Canyon. *Journal of Physical Oceanography* 32:1890-1913.
- Levin LA, Ekau W, Gooday AJ, Jorissen F, Middelburg J. J, Naqvi W, Neira C, Rabalais N. N, Zhang J. 2009. Effects of natural and human-induced hypoxia on coastal benthos. *Biogeosciences* 6:2063-2098.
- Levin LA. 2003. Oxygen Minimum Zone Benthos: Adaptation and Community Response to Hypoxia. *Oceanography and Marine Biology: An Annual Review* 41:1-45.
- Lewis E, Wallace DWR. 1998. Program Developed for CO<sub>2</sub> System Calculations. Oak Ridge (TN): Carbon Dioxide Information Analysis Centre
- Madden RA, Julian PR. 1994. Observations of the 40-50-day tropical oscillation - a review. *Monthly Weather Review* 122(5):814-837.
- Matear R, Hirst AC. 2003. Long-term changes in dissolved oxygen concentrations in the ocean caused by protracted global warming. *Global Biogeochemical Cycles* 17:20.
- McGregor HV, Dima M, Fischer HW, Mulitza S. 2007. Rapid 20th-Century Increase in Coastal Upwelling off Northwest Africa. *Science* 315(5812):637-639.
- McPhee-Shaw EE, Siegel DA, Washburn Libe, Brzezinski MA, Jones JL, Leydecker A, Melack J. 2007. Mechanisms for nutrient delivery to the inner shelf: Observations from

- the Santa Barbara Channel. *American Society of Limnology and Oceanography* 52(2):1748–1766.
- McPhee-Shaw EE, Sternberg RW, Mullenbach B, Ogston AS. 2004. Observations of intermediate nepheloid layers on the northern California continental margin. *Continental Shelf Research* 24(6):693-720.
- Mehrbach C, Culbertson CH, Hawley JE, Pytkowicz RM. 1973. Measurement of the Apparent Dissociation Constants of Carbonic Acid in Seawater at Atmospheric Pressure. *Limnology and Oceanography* 18(6):897-907.
- Orr JC, Fabry VJ, Aumont O, Bopp L, Doney SC, Feely RA, Gnanadesikan A, Gruber Nicolas, Ishida A, Joos F, et al. 2005. Anthropogenic ocean acidification over the twenty-first century and its impact on calcifying organisms. *Nature* 437(7059):681-686.
- Pane EF, Barry JP. 2007. Extracellular acid–base regulation during short-term hypercapnia is effective in a shallow-water crab, but ineffective in a deep-sea crab. *Marine Ecology Progress Series* 334:1-9.
- Paulmier A, Ruiz-Pino D. 2009. Oxygen minimum zones (OMZs) in the modern ocean. *Progress In Oceanography* 80(3-4):113-128.
- Pawlowicz R, Beardsley B, Lentz S. 2002. Classical tidal harmonic analysis including error estimates in MATLAB using T\_TIDE. *Computers & Geosciences* 28(8):929-937.
- Petruncio ET, Rosenfeld LK, Paduan JD. 1998. Observations of the Internal Tide in Monterey Canyon. *Journal of Physical Oceanography* 28:1873-1903.
- Pörtner HO, Langenbuch M, Michaelidis B. 2005. Synergistic effects of temperature extremes, hypoxia, and increases in CO<sub>2</sub> on marine animals: From Earth history to global change. *Journal of Geophysical Research* 110:C15.
- Pörtner HO, Langenbuch M, Reipschläger A. 2004. Biological Impact of Elevated Ocean CO<sub>2</sub> Concentrations: Lessons from Animal Physiology and Earth History. *Journal of Oceanography* 60(4):705-718.
- Pörtner HO. 2008. Contribution to the Theme Section “Effects of ocean acidification on marine ecosystems” Ecosystem effects of ocean acidification in times of ocean warming: a physiologist’s view. *Marine Ecology Progress Series* 373:203-217.
- Prince ED, Goodyear CP. 2006. Hypoxia-based habitat compression of tropical pelagic fishes. *Fisheries Oceanography* 15(6):451-464.
- Rabalais NN, Turner RE, Jr. WJW. 2002. Gulf of Mexico Hypoxia, a.k.a. “The Dead Zone.” *Annual Review of Ecology and Systematics* 33:235-263.
- Rao AR, Hsu E-C. 2008. Hilbert-Huang Transform Analysis of Hydrological and Environmental Time Series. Berlin: Springer.

Rosa R, Seibel BA. 2008. Metabolic physiology of the Humboldt squid, *Dosidicus gigas*: Implications for vertical migration in a pronounced oxygen minimum zone. *Progress In Oceanography* 86(1-2):72-80.

Sabine CL, Feely RA, Gruber Nicolas, Key RM, Lee K, Bullister JL, Wanninkhof R, Wong CS, Wallace DWR, Tilbrook B, et al. 2004. The Oceanic Sink for Anthropogenic CO<sub>2</sub>. *Science* 305(5682):367 -371.

Sanchez G, Calienes R, Zuta S. 1999. The 1997-98 El Nino and its effects on the coastal marine ecosystem off Peru. *Reports of California Cooperative Oceanic Fisheries Investigations* 41:62-86.

Sarmiento JL, Herbert TD, Toggweiler JR. 1988. Causes of anoxia in the world ocean. *Global Biogeochemical Cycles* 2(2):115-128.

Schwing FB, Murphree T, Green PM. 2002. The Northern Oscillation Index (NOI): a new climate index for the northeast Pacific. *Progress In Oceanography* 53(2-4):115-139.

Schwing FB, O'Farrel M, Steger JM, Baltz K. 1996. Coastal Upwelling Indices West Coast of North America 1946-1995. NOAA Technical Memorandum NMFS.

Seibel BA. (manuscript in preparation) Critical oxygen levels and metabolic suppression in oceanic animals: Implications for energetics and ecology in expanding oxygen minimum zones. *Journal of Experimental Biology*.

Shaffer G, Olsen SM, Pedersen JOP. 2009. Long-term ocean oxygen depletion in response to carbon dioxide emissions from fossil fuels. *Nature Geoscience* 2:105-109.

Shea RE, Broenkow WW. 1982. The role of internal tides in the nutrient enrichment of Monterey Bay, California. *Estuarine, Coastal and Shelf Science* 15(1):57-66.

Snyder MA, Sloan LC, Diffenbaugh NS, Bell JL. 2003. Future climate change and upwelling in the California Current. *Geophysical Research Letters* 30:C4.

Spillane MC, Enfield DB, Allen JS. 1987. Intraseasonal Oscillations in Sea Level along the West Coast of the Americas. *Journal of Physical Oceanography* 17(3):313-325.

Storlazzi CD, McManus MA, Figurski JD. 2003. Long-term, high-frequency current and temperature measurements along central California: insights into upwelling/relaxation and internal waves on the inner shelf. *Continental Shelf Research* 23(9):901-918.

Stramma L, Johnson GC, Sprintall J, Mohrholz V. 2008. Expanding oxygen-minimum zones in the tropical oceans. *Science* 320(5876):655-658.

Stramma L, Schmidtko S, Levin LA, Johnson GC. 2010. Ocean oxygen minima expansions and their biological impacts. *Deep Sea Research Part I: Oceanographic Research Papers* 57(4):587-595.

- Vaquer-Sunyer R, Duarte CM. 2008. Thresholds of hypoxia for marine biodiversity. *105(40):15452-15457.*
- Watanabe Y, Ono T., Shimamoto A, Sugimoto T, Wakita M, Watanabe S. 2001. Probability of a reduction in the formation rate of the subsurface water in the North Pacific during the 1980s and 1990s. *Geophysical Research Letters 28(17):3289–3292.*
- Western Regional Climate Center. 2011. Monterey, California - Climate Summary 1/7/1949 to 12/31/2005. Available from: <http://www.wrcc.dri.edu/cgi-bin/cliMAIN.pl?camtry+nca>
- Whitney FA, Freeland HJ, Robert M. 2007. Persistently declining oxygen levels in the interior waters of the eastern subarctic Pacific. *Progress In Oceanography 75(2):179-199.*
- Woodson CB, Barth J. A., Cheriton OM, McManus MA, Ryan JP, Washburn L., Carden KN, Cheng BS, Fernandes J, Garske LE, et al. 2011. Observations of internal wave packets propagating along-shelf in northern Monterey Bay. *Geophysical Research Letters 38:6.*
- Woodson CB, Eerkes-Medrano DI, Flores-Morales A, Foley MM, Henkel SK, Hession-Lewis M, Jacinto D, Needles L, Nishizaki MT, O’Leary J, et al. 2007. Local diurnal upwelling driven by sea breezes in northern Monterey Bay. *Continental Shelf Research 27(18):2289-2302.*
- Wootton JT, Pfister CA, Forester JD. 2008. Dynamic patterns and ecological impacts of declining ocean pH in a high-resolution multi-year dataset. *Proceedings of the National Academy of Sciences 105(48):18848-18853.*
- Wu Z, Huang NE. 2009. Ensemble empirical mode decomposition: A noise-assisted data analysis method. *Advances in Adaptive Data Analysis 01(01):1.*
- Wyrski K. 1962. The oxygen minima in relation to ocean circulation. *Deep Sea Research and Oceanographic Abstracts 9(1-2):11-23.*
- Zhang C. 2005. Madden-Julian Oscillation. *Reviews of Geophysics 43:36.*



